2012

Measurement And Modeling Of Isocyanic Acid (Hnco) In The Troposphere

Anthony Kozeque Cochran
North Carolina Agricultural and Technical State University

Recommended Citation

Cochran, Anthony Kozeque, "Measurement And Modeling Of Isocyanic Acid (Hnco) In The Troposphere" (2012). *Dissertations*. 33.
https://digital.library.ncat.edu/dissertations/33

Measurement and Modeling of Isocyanic Acid (HNCO) in the Troposphere

Anthony Kozeque Cochran

North Carolina A&T State University

A dissertation submitted to the graduate faculty
in partial fulfillment of the requirements for the degree of
DOCTOR OF PHILOSOPHY
Department: Energy & Environmental Systems
Major: Energy and Environmental Systems
Major Professor: Dr. Solomon Bililign
Greensboro, North Carolina
2012

School of Graduate Studies
North Carolina Agricultural and Technical State University

This is to certify that the Doctoral Dissertation of

Anthony Kozeque Cochran

has met the thesis requirements of
North Carolina Agricultural and Technical State University

Greensboro, North Carolina
2012

Approved by:

Solomon Bililign, Ph.D. Major Professor	James Roberts, Ph.D. Committee Member
Zerihun Assefa, Ph.D. Committee Member	Keith A. Schimmel, Ph.D. Committee Member and Department Chairperson

Sanjiv Sarin, Ph.D.
Associate Vice Chancellor for Research and
Dean of Graduate Studies

Dedication

To my grandmother Ionia Webb Smith and my grandfather L. C. Cochran, for the energy and gifts you left me with after you left this earth.

Biographical Sketch

Anthony Cochran earned his B.S. degree at Chicago State University in 1996 and then moved on to Baton Rouge, LA to work on the M.S. degree in particle physics at Southern University to search for evidence of neutrino oscillations at Los Alamos National Laboratory's linear accelerator. After finishing the M.S. degree in 1998, he moved on to Hampton University to work on a Ph.D. in nuclear physics. He was privileged to have collaborated on several experiments in Halls A and C at the Jefferson Lab accelerator before completing his experiment on quasi-elastic electron scattering from He-4. Taking a break from his Ph.D. efforts in 2001-2003, he accepted two research fellowships at the New Brunswick Laboratory for nuclear standards and Argonne National Laboratory, both in Argonne Illinois. He continued his Ph.D. pursuit in systems science at Clark Atlanta University where he worked in surface physics research. He was awarded a research fellowship to work at one of the NSF's STCs. He chose to work at the Nanobiotechnology Center at Cornell University from 2004-2005 using microfabrication techniques to develop an optical nanobiosensor. Finally, after a 2006 decision to start his career as patent examiner in X-ray CT systems with the US Patent and Trademark Office, he joined Dr. Solomon Bililign's group at North Carolina A&T State University to complete his Ph.D. in Energy and Environmental Systems. His current work involves the study and characterization of trace gases emitted by biomass burning in the atmosphere.

Acknowledgments

Thanking first my parents Margaret A. and Willie L. Cochran for bringing me here. They did what they could to build a solid and well-rounded foundation in a child amidst the struggles of the big city of Chicago. Thanks to my sister LaMonica Cochran-Ray, for having such perfect timing, to join our family when we really needed her the most, and some 30 or so years later, being the person that I needed to talk to in order to take my mind off of science and distractions just long enough to get back to work. Thanks also to my sister for making me the one and only “Uncle Hoss” to Jeremiah Anthony Ray.

Thanks to Dr. Elliott Treadwell for recognizing some of the gifts that I had in physics as an undergraduate and showing me the path to real research. Thanks to Dr. Ali R. Fazely and Dr. Larry Henry and Diola Bagayoko for helping me carve a way to the master’s degree.

Thanks to my mentor Dr. Margaret E. M. Tolbert for the relentless support in my endeavors, motivation in the face of the seemingly impossible and her general advice which shaped me into a true professional. Thanks also to my spiritual mentor and brother RoAnne for the powerful insight, wisdom, and knowing that so few are just gifted with.

Thanks to my current advisor Dr. Solomon Bililign for all of the financial support and experimental opportunities coordinated that allowed me to put together a solid dissertation and for the opportunities to travel abroad which were most rewarding and helped me to put life into a global perspective. Also thanks to my co-advisor Dr. James Roberts and (graduate student at the time) Dr. Patrick Veres, for welcoming me into their laboratory at NOAA ESRL CSD in order to conduct portions of my doctoral research and sharing techniques of conducting chemical ionization mass spectrometry. Thanks also to the rest of the CSD scientists for making the work and my stays in Boulder so much fun.

It is impossible to describe and no one would comprehend how many people kept me on the path, motivated, and striving throughout this process through conversation, opinion, good advice, advice, bad advice, or just plain old encouragement when needed . . . so this goes out to you. I will not be able to name all of the friends and associates, but there are a few that are special for reasons that they will know so I list them individually in no special order: Auntie Helen, Dora Ann Dyson, Br. Dejuan Hood, Tamiko James, Melva Smith, Pamela Bivens-Pippen, Dr. Mark Harvey, Alisha Williams, Dr. Tara Wade, Carmen Jones (rest peacefully), Dakia Jones, Dina George, Br. Willie Harrington, Cedric Moore ("hey big guy"), Karen Davis, Babette Stevens (for the name "Dr. Southside").

Table of Contents

List of Figures

List of Tables

Abstract

A recent study of biomass fires and some field measurements have revealed that isocyanic acid can reach levels as high as 600 ppbv near fires and up to 200 pptv in ambient air. After the solubility was measured for the first time, it was then possible for any potential human health effects of HNCO to be evaluated. HNCO is highly soluble in the human body given that the physiological pH is 7.4, and there exists an increased risk for atherosclerosis, cataracts, and rheumatoid arthritis via protein carbamylation. Based on preliminary experimental results conducted at a pH of 3.0 ± 0.1 and room temperature (T = 25 ± 1°C), Henry's coefficient was found to be 21.1 ± 2.7 M/atm with the first order loss rate $k = (6.3 \pm 1.6) \times 10^{-4}\ s^{-1}$ (in solution). This solubility measurement made it possible for HNCO atmospheric sensitivity and in-cloud lifetimes to be estimated using a numerical cloud box model. It is revealed that it is essential for the cloud pH to be calculated at every timestep rather than prescribing a constant pH value. The model shows that the elevation, liquid water content, droplet size, and gas-phase nitric and isocyanic acid concentrations are critical in characterizing HNCO in clouds and the -cloud lifetime of HNCO which is estimated to range from approximately 6.156 ± 0.007 to 82.435 ± 0.188 hours. It is also noteworthy to mention that the lower liquid water content of a cloud such as fog or haze (approximately .05 g/m^3), the better the chance of reducing the HNCO concentration. We also demonstrate that the idea of making a numerical cloud chemistry estimate with a static pH leads to completely inaccurate results. A dynamic cloud acidity calculation is determined to be essential.

CHAPTER 1

Scope of the Work

1.1. Background

One major source of trace airborne contamination and aerosols is from biomass burning (BB). BB is widespread, especially in the tropics and it serves to clear land for shifting cultivation, to make forests to agriculturally productive, and to remove dry vegetation in order to promote the growth of higher yield grasses. BB is a major source of many trace gases especially the emissions of CO, CH_4 and other hydrocarbons, NO, HCN, CH_3CN, and CH_3C1 are of the greatest importance (Bowman et al., 2009; Crutzen & Andreae, 1990). BB influences global ecosystem patterns and processes including the carbon cycle and climate. Andreae and Merlot (2001) derived global estimates of pyrogenic emissions for several species emitted by the various types of biomass burning from savannah fires.

Recent investigations into the impact that biomass burning emissions have on our air quality (Roberts et al., 2010) have yielded new information about the extent of organic and inorganic acids concentrations in the troposphere. That investigation verified the elevated levels of organic acids and, more specifically, carboxylic acids were as expected, but also revealed that there were unexpectedly high levels of inorganic acids produced such as nitrous acid (HONO) and hydrochloric (HCl). The properties and impacts of trace acids, along with the cutting edge methods, modeling, and instrumentation used to detect, quantify, and analyze them are the focuses of this dissertation.

The composition and chemistry of the atmosphere is of importance for several reasons, but primarily because of the potential negative health effect and ecological hazards from interactions between the atmosphere and living organisms (Mahecha et al., 2007). The climate can also be affected through the increase and/or decrease in chemical concentrations which can alter the albedo. There is also value in providing parameters for more accurate atmospheric modeling in order to determine fate and transport of different contaminants. The composition of the Earth's atmosphere changes due to natural (Kesselmeier et al., 2002) and man-made (Novakov & Penner, 1993) influences and some of these changes may be harmful to human health, crops, and ecosystems.

Two of the more important constituents of the atmosphere are volatile organic compounds (VOC) (de Gouw & Warneke, 2007) and secondary organic aerosols (SOA) (Tsigaridis & Kanakidou, 2007). Global models have been developed to investigate the SOA response to changes in biogenic volatile organic compound emissions in the future atmosphere and how important SOA will be relative to sulfate (SO_4^{-2}) which is often the major anthropogenic aerosol component. Examples of VOCs are aldehydes, ketones, and other light hydrocarbons. They are categorized as organic chemical compounds that have high enough vapor pressures under normal conditions to significantly vaporize and enter the atmosphere. The United States Environmental Protection Agency (EPA) defines a VOC as any compound of carbon, excluding carbon monoxide, carbon dioxide, carbonic acid, metallic carbides or carbonates, and ammonium carbonate, which participates in atmospheric photochemical reactions (40 CFR 51.100(s) as of 2/9/2007). VOCs are key participants in the formation of ozone and aerosols. They play a significant role in determining regional air quality, the chemistry of the global troposphere, and the global carbon cycle (Warneke & de Gouw, 2001; Warneke et al., 2005).

A subgroup of VOCs is organic acids and the method and instrumentation described later is fast and sensitive to many of the organic acids, particularly carboxylic acids (formic, acetic, pyruvic, etc.). Organic acids are extremely important as they are trace gases that contribute significantly to the acidity of atmospheric condensed phase and precipitation (Keene, Galloway, & Holden, 1983). In addition, analysis by aerosol mass spectrometry (AMS) suggests that a significant fraction of SOA consists of organic acids (Takegawa, Miyakawa, Kawamura, & Kondo, 2007). As an example of how organic acids have an influence on chemical processes in cloud droplets, the liquid-phase oxidation of SO_2 by H_2O_2 depends critically on the pH value of cloud droplets (Viidanoja, Reiner, & Arnold, 1998). This heterogeneous interface (gas to liquid phase) is a relatively active area of research due to the difficulty in garnering good agreement between measurements given that the experimental error is very high. Given that products of biomass burning (Roberts et al., 2010) are the focus of this work, carboxylic acids and inorganic acids (isocyanic, nitrous, hydrochloric, etc.) will be studied in detail. Isocyanic acid will be singled out for additional characterization due to the unexpectedly high concentrations observed in pyrolysis and its suspected negative impact to human health.

1.2. Experimental Goals

Emissions from 34 laboratory biomass fires were investigated at the combustion facility of the U.S. Department of Agriculture Fire Sciences Laboratory in Missoula, Montana (Veres et al., 2010). Gas phase organic and inorganic acids were quantified using negative ion proton-transfer chemical-ionization mass spectrometry (NI-PT-CIMS), open-path Fourier transform infrared spectroscopy (OP-FTIR), and proton-transfer reaction mass spectrometry (PTR-MS).

The fire sciences lab studies led to the decision to measure organic and inorganic acids the CalNex 2010 field campaign (NOAA Earth Systems Research Laboratory, 2009) with the mass spectrometric method of negative ion proton transfer chemical ionization (NI-PT-CIMS), which will be described in detail later. A description of a similar laboratory based experiment, that attempted to make the same measurements using a time-of-flight method, will also be discussed. The mission of the CalNex 2010 campaign was to study the important issues at the nexus of the air quality and climate change problems, and to provide scientific information regarding the trade-offs faced by decision makers when trying to address these issues simultaneously. This work was an opportunity to verify controlled burn measurements, if there were any wild fires in the vicinity during the experiment. This leads to another focus of this dissertation, which is to address the kinetics at the gas-liquid interface known as "heterogeneous uptake" (Molina, Molina, & Kolb, 1996). It is achieved directly by using a dynamic method (Kames & Schurath, 1995) to make kinetic and solubility measurements. This is extremely valuable work as it not only characterizes an exotic chemical that is rarely studied, not well characterized in terms of kinetics, and had not been widely recognized as an important constituent of biomass burning emissions, but also measures its solubility which has never been done. This work opens the door for a simple method to provide solubilities for numerous other exotic and reactive species.

The advent of this first solubility measurement of HNCO enables it to be modeled as it traverses the troposphere through cloud and aerosol interactions. Given the ubiquity of aqueous phase material in the atmosphere (especially the lower troposphere and planetary boundary layer) it is imperative to understand the chemistry and kinetics of HNCO with clouds and also aerosols in order to assess the extent of and associated health risk involved.

1.3. Modeling Goals

A cloud chemistry numerical model (Barth et al., 2003; Lelieveld & Crutzen, 1991) was run to complement the experimental work with the goal of making predictions about the lifetimes HNCO under different conditions of cloud acidity, droplet size, liquid water content, and temperature. The model was also converted to simulate HNCO interactions with aerosol surfaces. This would be a thorough study of HNCO interactions with the condensed phase (aerosol and water). As will be detailed later, HNCO is extremely sensitive to acidity and the model was modified to calculate the pH of the condensed phase as it changes over time due to equilibrium reactions. Finally, HNCO kinetics in supercooled and pyrocumulus cloud will also be explored in order to better characterize HNCO loss in the true troposphere.

This dissertation is organized as follows: following the goals and the motivation for this work in the scope of the work, Chapter 2 details the experimental and theoretical methods and equipment involved in this work and the scientific background. The final chapter describes the numerical cloud modeling work done to help better understand and characterize the fate of HNCO in the troposphere. Finally, results and conclusions will be presented.

CHAPTER 2

Experimental Characterization of Isocyanic Acid: A Product of Biomass Burning

2.1. Overview

The trace gas products of biomass burning are presently being investigated on a grand scale (Veres et al., 2011; Vicente et al., 2011) and very sophisticated and extremely sensitive instrumentation is required to make measurements at the trace level (100 pptv and lower). The method of (positive ion) proton transfer mass spectrometry (PTR-MS) has proven to be an excellent method to probe for gas concentrations at this trace levels both in the laboratory and the field (de Gouw et al., 2003) (de Gouw & Warneke, 2007). A more specialized version of this instrument, designed specifically for trace acid measurements, is known as the negative ion proton transfer chemical ionization mass spectrometry (NI-PT-CIMS) and is ideal for field measurements in that it can make rapid, sensitive, and selective measurements of acidic species (Veres et al., 2008). It was deployed recently for the specific intent of measuring the amount of trace organic and inorganic acids resulting from biomass burning (Veres et al., 2010). It was also used to measure isocyanic acid uptake in water solutions yielding the first laboratory measurement of the Henry's Law solubility constant (H) for HNCO and its first order loss rate (k). The resulting solubility measurement was used to estimate the lifetime of HNCO in a recent paper by Roberts et al. (2011). As part of this dissertation research, the measurement was also used in a cloud microphysics numerical model in order to better understand the uptake and evolution of HNCO in the condensed phase (aerosol and cloud water). An introduction to the model and cloud microphysics is given later in Chapter 3.

Reflectron time-of-flight (RTOF) mass spectrometry was tested in attempt to make complementary and more thorough measurements of the Henry's Law constant at several pH values as a function of temperature but unfortunately sensitivity limitations proved to be insurmountable. The RTOF experiments and observations will be discussed in the experimental section in an effort to aid future related experiments. The kinetic and lifetime information obtained will be vital in understanding the fate and transport of these trace gas contaminants from biomass burning. This section will provide the summary of the state of knowledge in this area and background information on chemical kinetics, chemical thermodynamics, heterogeneous uptake, and selected instrumentation involved in making trace gas measurements. Since this study deals with organic and inorganic acids in the atmosphere resulting from biomass burning, a brief summary on biomass burning is also provided.

2.2. Biomass Burning

Considerable progress has been made over the last decade in the effort to determine emissions from biomass burning(Andreae & Merlet, 2001). Evaluation of the available data (Streets et al., 2003) indicates that a vast number of chemical species have been identified in biomass burning smoke and that reliable emission information exists for most of the key species, at least for savanna fires. There remain, however, serious gaps for important species, including ones that could be valuable atmospheric tracers, such as HCN and acetonitrile (Andreae & Merlet, 2001). The species HNCO presented in this work was observed but not expected in such a large abundance.

Soot deposits in the lungs of 5000 year old mummies is an excellent way to portray just how long the pollution from biomass fires has had an impact to human health (Pabst & Hofer, 1998). Although biomass burning is one of the most ancient forms of anthropogenic atmospheric pollution, its importance on the chemistry of the atmosphere has only been recognized since the late seventies. (Crutzen, Heidt, Krasnec, Pollock, & Seiler, 1979; Radke, Stith, Hegg, & Hobbs, 1978). Interest in this topic grew during the 1980's, when several studies suggested that biomass burning emissions are as important as fossil fuel emissions (Andreae, 1983; Fishman, Watson, Larsen, & Logan, 1990) and that these emissions needed much better characterization due to not only their direct health concerns, but also to their impact on climate change, since they, have an impact on the radiation budget via light scattering and complex microphysical processes (Crutzen & Andreae, 1990; Penner, Dickinson, & Oneill, 1992).

It is estimated that 90% of biomass fires are anthropogenic and in the United States from 1991 to 2008, the annual average number of wild fires was approximately 80,000 and the number of prescribed fires was 14,000 (Burling et al., 2010) . In 2001 an excellent review was conducted by Andreae and Merlet (Andreae & Merlet, 2001) where they accumulated and evaluated the large body of biomass burning emission data available at the time to derive global estimates of pyrogenic emissions. They then derived global estimates of pyrogenic emissions for important species emitted by various types of biomass burning (grasslands, tropical forests, charcoal burning, etc) and compared their estimates with results from inverse modeling studies. They concluded that further study was needed in biofuel production such as charcoal, and that the global emission estimate of biomass burning needed to be validated.

Biomass burning results from forest clearing for agricultural and grazing purposes, weed and other vegetation control, and elimination of agricultural waste and stubble after harvest. Biomass fuels are also used for heating, cooking, and producing charcoal (Crutzen & Andreae, 1990). Burning of savannas has been the focus of several studies and is thought be a 40% contribution to the total yearly carbon released by biomass burning. Other processes (i.e. boreal forest burning) can also contribute at certain times of the year (Levine, Cofer, Cahoon, & Winstead, 1995).

Following well-publicized large fire catastrophes in recent years and intensive scientific efforts over the last decade, the general public as well as the scientific community is now aware that emissions from biomass burning represent a large perturbation to global atmospheric chemistry, especially in the tropics. Whether it is due to either ‘natural’ wildfires or in relation to anthropogenic land-clearance activity, biomass burning is an important land surface disturbance agent and a key process in changing the composition of the atmosphere through the release of carbon, trace gases, and aerosols. Figure 2.1 (Finneran, 2010) is an image from NASA’s MODSIS sensor that shows some burning focal points across the planet.

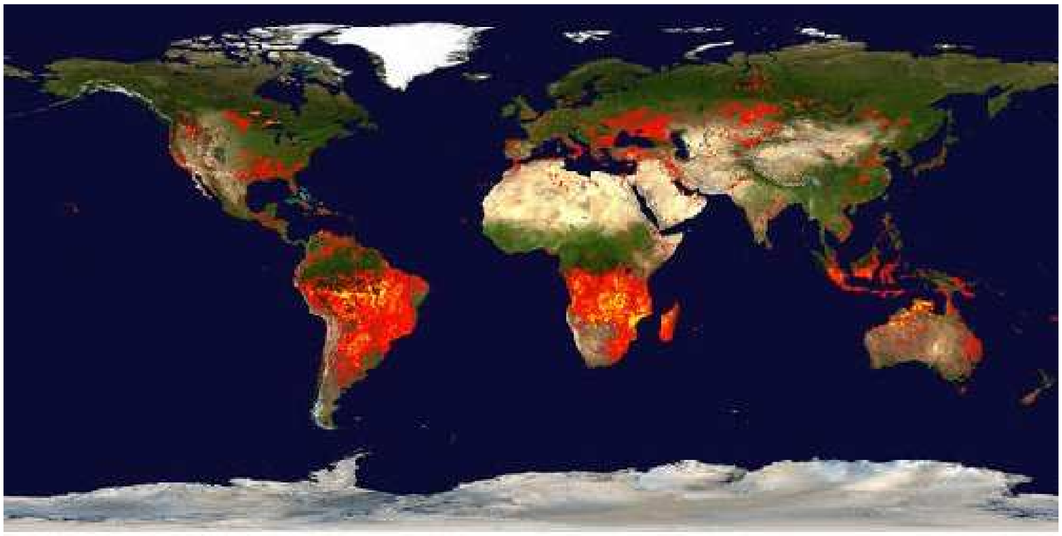

Figure 2.1. Global biomass burning from NASA’s MODSIS sensor (Finneran, 2010)

Trace gas emissions and aerosols from biomass burning represent a significant part of total gas emissions. Table 2.1 (Finlayson-Pitts & Pitts, 2000a) shows some estimated emissions from biomass burning. Water vapor, carbon dioxide, carbon monoxide, tropospheric ozone, and organic aerosol are among products with the higher contributions from burning, but also include significant amounts of many other compounds such as nitric oxide (NO), nitrogen dioxide (NO_2), methane (CH_4), ammonia (NH_3), and a multitude of non-methane organic compounds (NMOC) and oxygenated volatile organic compounds (OVOC) comprise a large fraction of the NMOCs (Christian et al., 2003).

There have been measurements made recently that indicate that there are elevated levels of trace organic acids and some inorganic acids present in the burning/pyrolysis process (Roberts et al., 2010; Veres et al., 2010). It was determined that the expected organic acid gases were present, but there were also elevated inorganic acids as well (nitrous and isocyanic acid). The focus of this thesis is on a subgroup of organic acids called carboxylic acids and the exotic isocyanic acid (HNCO). Biomass burning emissions have an effect on regional air quality, and depending on the emission product and elevation of the source, can also be transported over large distances to impact regions far from the source (Warneke et al., 2009).

Table 2.1

Biomass burning products (Finlayson-Pitts & Pitts, 2000a)

Species	**Biomass burning (Tg of element/yr)**	**All sources (Tg of element/yr)**	**Biomass burning (%)**
Carbon Dioxide (gross from combustion)	3500	8700	40
Carbon Dioxide (net from deforestation)	1800	7000	26
Carbon Monoxide	350	1100	32
Methane	38	380	10
Nonmethane hydrocarbons[b]	24	100	24
Nitrous oxide	0.8	13	6
NO_x	8.5	40	21
Ammonia	5.3	44	12
Nitrous oxide	0.8	13	6
Sulfur gases	2.8	150	2
Carbonyl sulfide	0.09	1.4	6
Methyl chloride	0.51	2.3	22
Hydrogen	19	75	25
Tropospheric ozone[c]	420	1100	38

Table 2.1 *(cont.)*

Species	Biomass burning (Tg of element / yr)	All sources (Tg of element / yr)	Biomass burning (%)
Total particulate matter	104	1530	7
Particulate organic carbon	69	180	39
Elemental carbon (black soot)	19	<22	>86

[a] From Andreae (1991); see for original references

[b] Excluding isoprene and terpenes.

[c] Formed from reactions in air due to biomass burning.

To assess the atmospheric impact of biomass burning, and especially to represent it quantitatively in models of atmospheric transport and chemistry, accurate data on the fates, lifetimes, and reaction rates of trace gases and aerosols from biomass fires are required. The work here contributes to this effort.

2.3. Organic Acids in the Troposphere

2.3.1. Introduction. Sources of atmospheric organic acids can be direct and indirect as well as natural and manmade. Direct sources include emissions from the biosphere, biomass burning, and motor vehicle exhaust (Talbot, Andreae, Berresheim, Jacob, & Beecher, 1990). Secondary sources include production via photochemical oxidation of atmospheric hydrocarbons (Fisseha et al.; Madronich et al., 1990). Formic and acetic acid are the two most abundant of the carboxylic acids (Chapman, Kenny, Busness, Thorp, & Spicer, 1995; Madronich et al., 1990) and are both formed via reactions of biogenic and anthropogenic alkenes with ozone, while acetic acid can also be formed by reactions of peroxy acetyl radicals ($CH_3C(O)O_2$) with HO_2 and organic peroxy radicals, particularly CH_3O_2 (Madronich & Calvert, 1990; Moortgat, Veyret, & Lesclaux, 1989).

2.3.2. Carboxylic acids: An important subgroup of organic acids. Carboxylic acids, RC(O)OH play a central role in the VOC chemistry of the troposphere. They are key intermediate species in the photooxidation of organic compounds and undergo interesting and important chemistry in both the gas phase and particle phases. Sources of small carboxylic acids include plant and soil biogenic sources, gas phase chemistry involving; O_3-alkene chemistry, RC(O)OO + HO_2 chemistry, RC(O)OO + aqueous droplets, and particle phase oxidation of organic compounds involving OH and O_3 (Altshuller, 1991). The particulate phase behavior of carboxylic acids is of particular interest since these compounds are important constituents of organic secondary organic aerosol (SOA) (Alfarra et al., 2006; de Gouw et al., 2005; Gelencser & Varga, 2005; Yang, Ray, & Yu, 2008). This link between photochemical production of SOA and gas phase organic acids opens the door for the possibility of using gas phase measurements of organic acids as a marker of SOA chemistry. The occurrence, sources, and sinks of carboxylic acids is reviewed by Chebbi and Carlier (Chebbi & Carlier, 1996).

Formic and acetic acids are the most abundant and ubiquitous trace acids in ambient air, but their sources are not yet fully understood. They originate from photochemical oxidation of VOCs. Formic acid is the simplest of the carboxylic acids and retains virtually no information concerning the carbon backbone that produced it. There are numerous other relatively volatile carboxylic acids that contain more chemical information on clustering, solubility and acidity (Graul, Schnute, & Squires, 1990). The C_2-C_3 simple and oxygenated carboxylic acids have origins that range from general (acetic, propionic, and oxalic acids) (Strobel, 2001), to biogenic (glycolic, glyoxylic, pyruvic, methacrylic acids) (Ai & Ohdan, 1997), to petrochemical or industrial (acrylic acid) (Ghilarducci & Tjeerdema, 1995). In addition, there are acids that have special roles that are potential pollutants such as trifluoroacetic and trichloroacetic acids in peptide synthesis (King, Fields, & Fields, 1990) and macromolecule precipitation (Sun & Dent, 1980) (respectively).

Organic acids in the troposphere have become an issue of growing concern since low molecular weight carboxylic acids such as formic and acetic acids are major components in the troposphere and can lead affect the climate (Caldwell, Renneboog, & Kebarle, 1989; Graul et al., 1990). Carboxylic acids are water soluble and represent a major fraction of the total organic carbon in fog and cloud water and in precipitation and also have the ability to increase cloud acidity depending on the gas phase concentration (Chebbi & Carlier, 1996). They may also be involved in potentially important atmospheric transformations such as heterogeneous uptake from the gas to aqueous phase (Chameides & Davis, 1983). It has been shown that carboxylic acids contribute to the acidity of precipitation (Fornaro & Gutz, 2003; Kawamura, Steinberg, & Kaplan, 1996). It was estimated that carboxylic acids, particularly formic and acetic acids, may contribute between 16% and 35% of the free acidity of precipitation in the United States. The contribution of these acids to the free acidity of precipitation may be as high as 65% in some remote areas (Keene et al., 1983). Table 2.2 lists numerous carboxylic acids and their gas-phase acidities (ΔG) that make some of them favorable for detection by mass spectrometry (discussed later in the chapter) (Veres et al., 2008).

The elementary and complex interaction of these acids with other species in the troposphere is the key to understanding their fates, lifetimes, and how they transport through across the globe. There are also broader questions involving other acids species in the troposphere that are active areas of research. Examples of such questions include the importance of nitrous acid (HONO) as a source of radicals (Calvert, Yarwood, & Dunker, 1994) and the origin and fate of inorganic acids, such as the Bronsted acids (HCl, HBr, and HI). A method for the sensitive and rapid measurement of those species would represent a significant improvement in the tools available for understanding that chemistry.

Table 2.2

Gas-phase acidities, anion masses, and anion abundances of common acids (Veres et al., 2008)

Compound	Formula	AG (kcal/mol)	Anion Observed (m/z)	Detectable Species
Hydrochloric acid	HCl	328.15	35 (76%), 37 (24%)	-
Formic acid	CH_2O_2	338.2	45	yes
Nitrous acid	HNO_2	333.7	46	-
Acetic acid	$C_2H_4O_2$	341.5	59	N/A
Nitric acid	HNO_3	317.8	62	-
Acrylic acid	$C_3H_4O_2$	337.2	27 (8%), 71 (92%)	yes
Propionic acid	$C_3H_6O_2$	340.1	73	yes
Glycolic acid	$C_2H_4O_3$	327.8	75	yes
Hydrobromic acid	HBr	317.9	79 (51%), 81 (49%)	-
Methacrylic acid	$C_4H_6O_2$	337.1	85	yes
Butyric acid	$C_4H_8O_2$	339.1	87	yes
Pyruvic acid	$C_3H_4O_3$	326.5	43 (1%), 87 (99%)	yes
Oxalic acid	$C_2H_2O_4$	N/A[a]	89	no
Lactic acid	$C_3H_6O_3$	330.3	89	yes
Methanesulfonic acid	CH_4O_3S	315.5	95	-
Sulfuric acid	H_2SO_4	300.0	91	-
Malonic acid	$C_3H_4O_4$	N/A[a]	103	no
Trifluoroacetic acid	$C_2HF_3O_2$	316.3	113	-
Benzoic acid	$C_7H_6O_2$	333.0	121	yes
Hydroiodic acid	HI	308.98	127	-
Nitrophenols	$C_6H_5NO_3$	320.9–329.5	138	yes
Trichloroacetic acid	$C_2HCl_3O_2$	N/A[b]	161	-
Pentafluoropropionic acid	$C_3HF_5O_2$	N/A[b]	19 (3%), 119 (67%), 163 (30%)	yes

Species that are measurable on the NI-PT-CIMS are denoted with ‘yes,’ unmeasurable species are denoted as such with a ‘no,’ and species which have not yet been studied are marked with ‘-.’

[a] Data not readily available. However, the first proton of these diacids is much more acidic in solution that the mono carboxylic acids

[b] Data not readily available. The strong electron withdrawing nature of halogen substituents should shift gas phase acidities to much lower values than corresponding hydrocarbon acids. Our observations are consistent with this assumption

2.3.3. Isocyanic acid (HNCO): A unique organic acid from biomass burning. People are constantly exposed to smoke, whether it be from wildfires, tobacco, biomass burning, or coal combustion used in cooking and heating (Crutzen & Andreae, 1990). Pyrolysis research of biomaterials has shown that various volatile and semi volatile organic compounds (SVOCs) are produced (Andreae & Merlet, 2001; Burling et al., 2010). The extent of the human impact of these products needs to be understood for obvious health effect reasons on both the regional and global scale. Cataracts, cardiovascular impairment, and chronic diseases such as rheumatoid arthritis are human health effects that have already been identified as smoke related risks (Scott, Wolfe, & Huizinga, 2010). Inflammatory response to protein carbamylation is a common biochemical pathway causing these health effects (Beswick & Harding, 1984).

Isocyanic acid has been known since 1830 and saw an increase in investigations in the 1950s and 1960s (Herzberg & Reid, 1950) (Ashby & Werner, 1965) through spectral analysis, but it had not previously been measured in the atmosphere. Cyanate salts are known to have the structure KOCN (potassium cyanate for example), but acidification of cyanate solutions are known to produce HNCO exclusively. Proton transfer reactions were used to measure the basicity and acidity of HNCO using an ion cyclotron resonance mass spectrometer (Wight & Beauchamp, 1980) .

HNCO is slightly acidic (pKa = 3.7) and unstable in pure form as it prefers to polymerize (D. J. Belson & A. N. Strachan, 1982) under normal conditions which makes it difficult to produce and measure in the laboratory. Fortunately it is stable and volatile at dilute concentrations (a few ppmv) in the gas-phase. In California, low limits for occupational exposure on the order of 0.5 ppbv for methyl isocyanate (California, 2001) and 5 ppbv for total isocyanates (Statute Book of the Swedish Work Environment Authority, 2005) have been established.

A sensitive negative-ion proton-transfer chemical ionization mass spectrometer (NI-PT-CIMS) was developed that offers a fast response measurement of HNCO and other acids in air (Roberts et al., 2010). In addition, the NI-PT-CIMS instrument can be used to measure the Henry’s Law solubility of HNCO. It was shown in work by Roberts et al. (2011) that smoke from biomass burning and other smoke related sources contains HNCO at concentrations that cause carbamylation at physiologically significant levels. Therefore it is imperative to understand the fate and transport of isocyanic acid and this is achieved in this thesis through modeling the cloud chemistry and microphysics of HNCO as well as its aerosol interactions.

2.4. Gas Phase Kinetics

Understanding the kinetics of reactions of trace gases in the atmosphere is important due to the need to assess their lifetimes and ultimately their atmospheric fates. It's useful to be able to predict factors that will affect the rate at which a chemical reaction proceeds. Knowing the reaction kinetics of classes of compounds such as organic acids with OH or even isocyanic acid (Jensen, 1958) allows one to estimate lifetimes under typical atmospheric conditions and hence to rule out those reactions that are too slow to be significant, allowing one to concentrate on the most important reactions.

There are several factors that can influence the rate of a chemical reaction. In general, a factor that increases the number of collisions between particles will increase the reaction rate and vice versa. A higher concentration of reactants leads to more effective collisions per unit time, which leads to an increasing reaction rate (except for zero order reactions). The process can be understood by applying the collision theory of gases and predicting the magnitude of the reaction rate coefficient. In basic collision theory, the collision rate is an upper limit to the actual reaction rate constant. In this work, we focus on bimolecular ion-molecule reactions. The most elementary approach to bimolecular reactions is based on the collision of "hard" spheres that have no structure. This was investigated theoretically by Kummerlöwe and Beyer (Kummerlöwe & Beyer, 2005) where they obtained rate estimates for collisions of ionic clusters with neutral reactant molecules using the hard-sphere approach.

NI-PT-CIMS is a negative ion proton transfer reaction (PTR) between ion species A^- (say acetate ions) and a neutral molecule B (say formic acid molecules) can be represented by the second-order reaction;

$$A^- + B \rightleftarrows C^- + D \tag{2.1}$$

where A is an ion and the products can be neutral molecules, ions or radicals, B is the neutral colliding partner. Since the equilibrium constant is given by Equation 2.2,

$$K_{eq} = \frac{[C^-][D]}{[A^-][B]} \tag{2.2}$$

measuring the rate constants in both directions and given that the reaction is at equilibrium, the value of the Gibbs free energy of reaction can be calculated from the relationship;

$$-\mathrm{RT}\,ln\mathrm{K}_{\mathrm{eq}} = \Delta\mathrm{G} = \Delta\mathrm{H} - \mathrm{T}\,\Delta\mathrm{S} \tag{2.3}$$

where R is the universal gas constant, T is the temperature in K, K_{eq} is the equilibrium constant, ΔG is Gibbs free energy change, ΔH is the enthalpy change, and ΔS is the entropy change associated with a given reaction.

In the reaction in Equation 2.1 where the neutral species is in much greater abundance than the ionic one, pseudo first order approximations are valid and it can be shown that

$$[A^-]_t = [A^-]_0\left(e^{-k[B]t}\right) \tag{2.4}$$

where $[A^-]_t$ is the concentration $[A^-]_0$ is the concentration at reaction time t = 0 and *k* is the bimolecular rate constant. Furthermore since,

$$\left[\mathrm{A}^-\right]_\mathrm{t} = \left[\mathrm{A}^-\right]_0 - \left[\mathrm{C}^-\right]_\mathrm{t} \tag{2.5}$$

Substituting Equation 2.5 into Equation 2.4, and assuming that the reaction involving the reagent ions is not significant enough to deplete the reagent ion concentration, i.e. the concentration is constant and large, it can be shown that

$$\left[C^-\right] = \left[A^-\right]_0 \exp\left(1 - k\left[B\right]t\right) \approx k\left[B\right]t \tag{2.6}$$

In this situation, the abundance of the product ion [C^-] is proportional to the concentration of its neutral precursor [B]. From (2.6) it is possible to obtain k in the forward direction:

$$k = \frac{\left[C^-\right]}{\left[A^-\right]\left[B\right]t} \tag{2.7}$$

where we can measure the ion intensities [C^-] and [A^-] using the mass spectrometer and the reaction time t can be obtained from flow velocity calculations for a given position where reaction takes place along the tube.

The primary initial goal of this work was to use the novel flow tube to extract kinetic information from the reaction of carboxylic acids and also measure the effect that water clustering had on the reaction kinetics. The lessons learned from this initial experiment and recommendations to improve the method will be discussed in much further detail in section 8 of this chapter.

2.5. Heterogeneous Chemical Kinetics: Gas Uptake

2.5.1. Resistance model of gas uptake. Given the gaseous nature of most of the primary and secondary pollutants of interest, the emphasis on kinetic studies of atmospheric reactions has typically been on gas-phase systems. It is now evident that reactions that occur in bulk liquid and on the surfaces of solids and liquids (collectively termed the condensed phase) have an impact on problems like stratospheric ozone depletion (Barth, Hess, & Madronich, 2002). A significant portion of this dissertation is dedicated to the understanding heterogeneous (gas-liquid phase) interactions in the troposphere. Biomass burning products in the gas phase have the potential to be taken up by the condensed phase (aerosol or water). These are known as heterogeneous interactions and review of the kinetics involved is given by Molina and coworkers (Molina et al., 1996) where they have compiled the results of laboratory measurements of rate parameters and presented current views on the physical and chemical foundation underlying the interpretation of the kinetic parameters. The aqueous phase that serves as a reaction medium in the atmosphere can be in the form of clouds, fogs, rain, and even particulate matter.

Interpreting the experimental results of gas-phase atmospheric chemical processes requires understanding of aqueous-phase reactions in cloud droplets and deliquesced aerosol particles. At heterogeneous equilibrium, Henry's law can be used to describe the distribution between the phases provided that the Henry's law coefficient is known.

There are four main aspects of heterogeneous kinetics of gases:

1) Diffusion of the gas to the surface of the condensed-phase medium
2) Transport of the gas across the interface (known as accommodation)
3) Diffusion of the absorbed gas into the bulk phase (solubility)
4) Reaction of the absorbed gas in the bulk phase

It should be noted that reactions that occur at the interface are complex and not addressed here, as it is not an important factor in the system under consideration.

Figure 2.2 (Finlayson-Pitts & Pitts, 2000a) shows the uptake process and is taken from the work of Finlayson-Pitts (Finlayson-Pitts & Pitts, 2000b) which also provides a very good description of the heterogeneous process under different conditions which determine the rate limiting processes (Kolb et al., 2010).

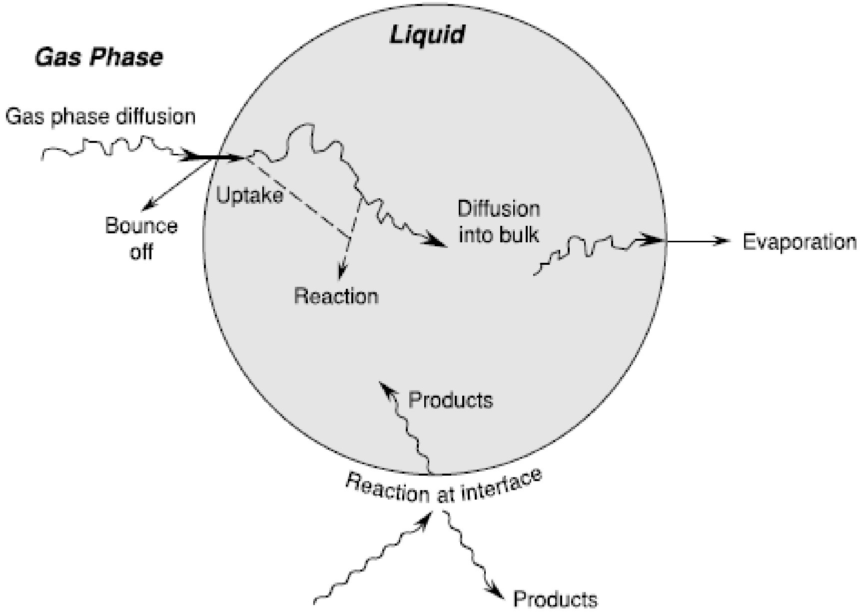

Figure 2.2. The heterogeneous uptake processes (Finlayson-Pitts & Pitts, 2000a)

Gases dissolve in the condensed phase to various degrees, depending on the characteristics of the gas and the solvent. As mentioned in Finnlayson-Pitts (Finlayson-Pitts & Pitts, 2000a), at a sufficient span of time, equilibrium can be established between the gas- and liquid-phase concentrations, which is described by Henry's law. Henry's law can be used to predict solution concentrations only under specific conditions. It assumes that there are no irreversible chemical reactions that are so fast that the equilibrium cannot be established. The other assumption is that the surface of the droplet is an unimpeded air/water interface, since some aerosols can have an organic covering on the surface (Husar & Shu, 1975).

In the liquid phase molecules are in close contact, with the space between molecules being ~10% of the distance between their centers. Thus, reactants have between 4 and 12 nearest neighbors that they can collide with. The reactants can then be thought of as existing in a solvent "cage,“ in which several collisions occur before breaking out of that "cage" environment. Relative to the gas phase, reactants take longer to diffuse together when in aqueous solution, but once they find themselves as nearest neighbors, they undergo a series of collisions rather than separating after one collision (Finlayson-Pitts & Pitts, 2000a). In other words, solution phase reactions tend to be slower because, in the gas phase, the reaction barriers are effectively lowered by the solvation energy. In solution, solvent molecules already interact with the reagent, whereas, in the gas phase, energy is produced upon intermolecular interactions between the two reagent molecules.

Figure 2.3 shows the "resistance model" as described in Molina et al. (Molina et al., 1996). The resistance model is a simplified representation based on electrical circuit analog, and it assumes that the uptake governing process are decoupled; each process is then expressed as a resistance term which represents its uptake limiting effect relative to the overall process. Therefore, treatment of systems in which gas-phase diffusion, mass accommodation, liquid phase diffusion, and reaction both in the bulk and at the interface must be taken into account can be characterized by Equation 2.8.

$$\frac{1}{\gamma}=\frac{1}{\Gamma_g}+\frac{1}{\alpha}+\frac{1}{\Gamma_{sol}+\Gamma_{rxn}} \tag{2.8}$$

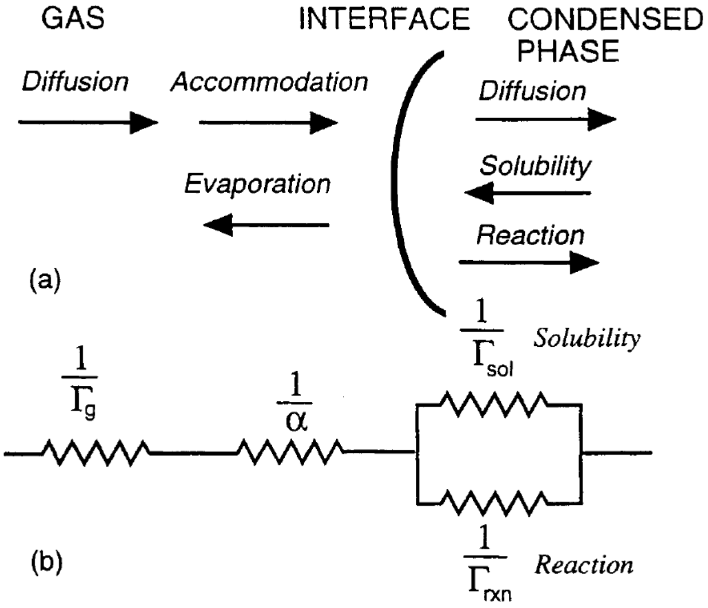

Figure 2.3. Resistance model of the heterogeneous process (Molina, Molina, & Kolb, 1996)

In the general case, Equation 2.8 describes the overall uptake process where γ is the uptake coefficient, Γ_g describes the gas-phase diffusion toward the liquid, the second term α describes the reaction at the interface, also known as accommodation and is the ratio of the number of gas molecules that make it into the bulk liquid to the total numbers of molecules that collide with the surface. The last terms are for the kinetics that occurs in the bulk and these are coupled since they occur simultaneously. Γ_{sol} is the liquid phase diffusion and solubility and Γ_{rxn} represents the liquid phase chemical reaction processes.

The uptake coefficients Γ_g, Γ_{sol} and Γ_{rxn} represent parameters normalized to the rates of gas-surface collisions and are unitless and can have values larger than 1. Therefore, in the limit of large Γ_g, Γ_{sol} and Γ_{rxn} their resistance becomes negligible and the maximum value of γ approaches α.

Often one process is rate limiting, simplifying the above representation. The time scale for gas-phase diffusion to particles is fast (on the order of seconds to a few minutes) depending on particle size and number. The time scales for losses of HNCO in the aqueous-phase (liquid, liquid aerosol, or cloud droplets) are much slower. Uptake of a modestly soluble and reactive trace gas by an aqueous droplet can depend on both its Henry's law constant, H and its aqueous phase reaction rate k_{hyd} and for species with a k_{hyd} small enough that liquid-phase diffusion does not act as a constraint on the reaction rate, the life time (τ) for loss of a trace gas to cloud droplets can be approximated by (Molina et al., 1996):

$$\tau = \frac{1}{HRTk_{hyd}L_cF_c} \tag{2.9}$$

where L_c is the liquid water content, F_c is the cloud volume fraction of liquid water (ranging from 10^{-12} for an aerosol of total surface area of 200 $\mu m^2/cm^3$, and .2 μm mean diameter, and up to 10^{-6} for fogs or clouds), and k_{hyd} is the first order rate constant for the aqueous-phase hydrolysis reaction. Thus the approximated lifetimes for HNCO then range from more than 10^4 years for reaction on an aerosol at pH 3, to approximately 12 hours for reaction in cloud or fog water of pH 5.5, k_{hyd} of 7.8×10^{-4} sec^{-1}, and the above liquid water content. The lifetime of HNCO is apparently limited by uptake on aerosols and clouds in the aqueous-phase. The lifetime of HNCO in clouds will be calculated from the current experimental work in the next chapter under various water content and pH values, but it will be seen that there is good agreement to the approximation of Equation 2.9.

2.5.2. Gas stripping and extracting equilibrium constants. Henry's Law constant is defined as the chemical concentration in the aqueous phase at equilibrium divided by the partial pressure of the chemical at infinite dilution. Gas stripping is the process of flowing gas through a liquid through an interface with porosity on the order of 10μm in order to maximize the gas to liquid surface reactions. One example of a successful gas stripping experiment used to determine Henry's coefficients for benzene, toluene, and several other VOCs is described by Mackay et al. (Mackay, Shiu, & Sutherland, 1979).

The equilibrium concentration of a dissolved gaseous species is proportional to the partial pressure of the gas, the proportionality constant being a property of the gas and a function of temperature, or;

$$C_{aq} = H \cdot P \tag{2.10}$$

where $[C_{aq}]$ is the aqueous equilibrium concentration (in mol/L or M), P is the gas-phase equilibrium pressure, and H(T) (typically reported in units of M/atm) is the Henry's law coefficient of the gas X in water at temperature T. The Henry's law coefficient is defined as the equilibrium constant for the heterogeneous reaction;

$$C_g \rightleftarrows C_{aq} \tag{2.11}$$

The kinetics of this concentration gradient can be thought of in terms of the mass transfer rate of gas-phase molecules into and out of the aqueous phase and chemical reaction at the surface or in solution. Any losses in the aqueous phase must be accounted for and conserved, therefore the change in concentration over time is a combination of solubility of the gas, which is governed by Henry's law, and the loss due to reaction in the condensed phase. The liquid concentration or cumulative analyte concentration at time t is C_{aq} and the rate of loss of liquid concentration dC_{aq}/dt can be expressed as a sum of the rate of loss due to dissolution (solvation) of (dC_{sol}/dt) and chemical reaction rates (dC_{rxn}/dt) that occur in solution (such as hydrolysis of acids). In the derivation that follows we use C instead of C_{aq} Therefore the first order concentration loss rate can be given as Equation 2.12.

$$\frac{dC}{dt} = \frac{dC_{sol}}{dt} + \frac{dC_{rxn}}{dt} \tag{2.12}$$

Since the solubility concentration can be expressed by Henry's law constant the relationship;

$$C_{sol} = H \cdot p \tag{2.13}$$

where C_{sol} is the aqueous phase concentration, H is Henry's coefficient, and p is the gas phase partial pressure of x. From the ideal gas law, PV = nRT, the concentration is;

$$C_g = C_{aq} = \frac{n}{V} = \frac{p}{RT} \tag{2.14}$$

and using Henry's relationship above;

$$\frac{P}{RT} = \frac{C_{sol}}{HRT} \tag{2.15}$$

and thus,

$$-\frac{dC_{sol}}{dt}=\frac{\Phi}{V}\frac{C}{HRT} \tag{2.16}$$

where C_{sol} is the aqueous phase concentration. Thus at equilibrium, the concentration in solution is time dependent and is governed by the rate of gas flow into solution Φ (cm^3s^{-1}) and the volume of solution V (cm^3). The ratio of Φ to V gives the gas uptake rate in inverse seconds. Multiplying this by the concentration expression gives the loss rate due to solubility.

The second component contributing to the concentration loss in solution is from chemical reactions that occur in solution. The first order loss rate is given as:

$$-\frac{dC_{rxn}}{dt}=kC \tag{2.17}$$

where k is the overall reaction rate constant and given in units of inverse minutes (m^{-1}). Pulling these two expressions together, we have the full expression for the first order loss.

$$-\frac{dC}{dt}=\frac{\Phi}{V}\frac{1}{HRT}C+kC \tag{2.18}$$

Integrating Equation 2.18 in order to solve for C, we get

$$\ln\frac{C_0}{C}=\left(\frac{\Phi}{V}\frac{1}{HRT}+k\right)t \tag{2.19}$$

Therefore C can be solved for easily by taking the exponential of both sides;

$$C=C_0e^{-\left(\frac{\Phi}{V}\frac{1}{HRT}+k\right)t} \tag{2.20}$$

where C_0 and C are the gas phase concentrations initially and at a time t respectively, Φ is the gas volume flow rate at ambient pressure, V is the liquid volume, H is Henry's coefficient, R is the ideal gas constant, T is the liquid temperature, k is the first order reaction rate constant. The stripping process assumes (i) the system is isothermal, (ii) the liquid phase is well mixed, (iii) the vapor behaves ideally, (iv) Henry's law is obeyed over the relevant concentration range, (v) the volume of liquid remains constant, (vi) the partial pressure of the solute is small compared to the total pressure, and (vii) the solute in the exit vapor is in equilibrium with the liquid.

If these assumptions hold, H and k can be experimentally extracted very easily by varying the flow rate and volume as described by Kames et al. (Kames & Schurath, 1995). This method is among a host of condensed phase uptake methods that have been recently reviewed (2010) by Kolb and coworkers (Kolb et al., 2010), where they identified the need for consistent definitions of the various parameters for the quantitative representation of the wide range of gas/condensed surface kinetic processes. Equation 2.20 will be used later in the calculation of the Henry's coefficient.

2.5.3. pH dependence of H. Another effect to consider when working with weak acids, as is the case in this work, is the pH of the system at equilibrium. For a generic acid HA in solution:

$$HA_{aq} \rightleftarrows A^{-} + H^{+} \tag{2.21}$$

$$K_a = \frac{[A^{-}][H^{+}]}{[HA_{aq}]} \tag{2.22}$$

where K_a is the equilibrium dissociation constant. The solubility of this acid is increased (additional $[A^{-}]/[HA_{aq}]$ which is the definition of Henry's law) due to this effect and is added to Henry's coefficient as

$$H_{eff} = \frac{[HA_{aq}] + [A^-]}{[HA_{gas}]} \tag{2.23}$$

$$[A^-] = \frac{K_a [HA_{aq}]}{[H^+]} \tag{2.24}$$

$$H_{eff} = H^* + H^* \frac{[A^-]}{[HA_{aq}]} \tag{2.25}$$

Using the equilibrium constant relationship above, H_{eff} can be simplified and expressed as

$$H_{eff} = H^* \left(1 + \frac{K_a}{[H^+]}\right) \tag{2.26}$$

In Equation 2.26, H^* is the intrinsic Henry's coefficient independent of any liquid phase equilibria. For this reason, the pH needs to be known and remain constant over the course of the experiment. To achieve this, an appropriately selected buffer is used for a given pH. The effective H can be plotted for any acid as a function of pH if the pK_a is known. A much more in-depth look at this is given by Sander (Sander, 1999). Measurement of this solubility would allow for the HNCO lifetime to be estimated and thus the exposure level can be assessed through modeling of its fate and transport.

2.6. Experimental Techniques: Mass Spectrometry in Biomass Burning

2.6.1. Background. Mass spectrometry is an age old method of elemental identification rooted in the work of J. J. Thompson in the late 1800s. More recently in the mid-1990s, a powerful instrument and method for studying gas-phase ion-molecule reactions is proton-transfer reaction mass spectrometry (PTR-MS) (Hansel et al., 1995; Jordan, Hansel, Holzinger, & Lindinger, 1995; Warneke et al., 1996). PTR-MS is a technique developed almost exclusively for the detection of gaseous organic compounds in air. PTR-MS allows real-time measurements of

VOCs in air with a high sensitivity and a fast time response. Comprehensive reviews of the recent progress that has been made in the field of PTR-MS include work by de Gouw, Warneke et al. (de Gouw & Warneke, 2007; de Gouw et al., 2003) which focused on VOC measurements and the development of instruments and methods. They state that PTR-MS has emerged as a fully useful tool to study the atmospheric chemistry of volatile organic compounds (VOCs) given its fast response time of 1 second and low detection limits in the range of 10 to 100 ppt.

A more recent review is by Blake et al. (Blake, Monks, & Ellis, 2009) in 2009 discusses applications of the PTR-MS method. It is concluded that more accurate determinations of the instrument response can be achieved by conducting calibrations using standard mixtures. They also conducted specificity studies of several PTR-MS instrument as well coupling their PTR-MS with a gas chromatograph (GC) for added flexibility.

Proton-transfer reaction mass spectrometry has its origins in the development of the “flowing afterglow” method for the study of ion-molecule reaction kinetics. It was first introduced in the 1960s by Ferguson and co-workers and involved the injection of ions into an inert buffer gas containing a small amount of neutral reactant to achieve reactions at thermal or near-thermal collision energies (Ferguson, Fehsenfeld, Schmeltekopf, Bates, & Immanuel, 1969). The study of ion-molecule reaction kinetics and thermodynamics was revolutionized by this flowing afterglow approach but a major weakness was that no ion selection was made before the chemical reaction. For more complex molecular ions, the possibility of producing a variety of secondary ions in the discharge source caused excessive complications in the product analysis and a means of ion selection prior to reaction was obviously necessary. This key step was tackled by Adams and Smith in a groundbreaking piece of work that led to the introduction of the selected ion flow tube (SIFT) technique (Adams & Smith, 1976). The basic components of a

SIFT instrument, that has improved selectivity over the flowing afterglow method, is the quadrupole filter that allows ions of only a specific mass-to-charge ratio (m/z) to pass into the flow tube thus limiting the reactions of unwanted reagent ions.

Proton-transfer-reaction mass spectrometry was developed by Lindinger et al. and the design is described in detail here (Lindinger, Hansel, & Jordan, 1998). It is a merger of the ideas of chemical ionization (CI) introduced by Munson and Field in 1966 (Munson & Field, 1966) with the swarm technique of flow-drift-tube type (FDT), invented by McFarland et al. in the early 1970s (McFarland, Albritton, Fehsenfeld, Ferguson, & Schmeltekopf, 1973). It significantly overcomes some of the disadvantages of GC methods but at the price of chemical detail and some compounds are not volatile enough for the GC. The GC has superb resolution but at the cost of long collection times (1/2 to 1 hr.). PTR-MS was particularly intended and favored for on-line measurements of VOCs during airborne field campaigns due to its rapid and sensitive performance, but there is a sacrifice in resolution achievable by a GC. The experimental realization of proton-transfer reaction mass spectrometry was refined by Hansel et al. (Hansel et al., 1995) with the drift tube reactor shown in Figure 2.4.

PTR-MS instruments used to date have utilized hollow cathode DC discharge ionization sources with drift tubes that suppress clustering, and quadruple mass analyzers that have limited mass resolution and mass range. The need for more flexibility and sensitivity led to the idea of chemical ionization and a thermal dissociation-chemical ionization mass spectrometry (TD-CIMS) technique for the simultaneous measurement of peroxyacyl nitrates (PAN) and dinitrogen pentoxide was introduced by Slusher et al. (Slusher, Huey, Tanner, Flocke, & Roberts, 2004) in 2004. A modified version of this of the Slusher CIMS is presented in the work by Veres et al. at the NOAA Earth Systems Research Laboratory (Veres et al., 2008) where negative ions are utilized in the proton transfer reaction (NI-PT-CIMS). Veres et al. have excellent reagent ion production on the order of 6 x 10^6 counts per second. This translated into a formic acid calibration with a sensitivity of 21 ± 4.3 counts per second per pptv and the detection limit for formic acid is approximately 80 to 90 pptv for a 1 s integration period. This well suited for on-line field campaign work, but the instrument is limited to only probing a few species per experiment, since each needs to be properly calibrated.

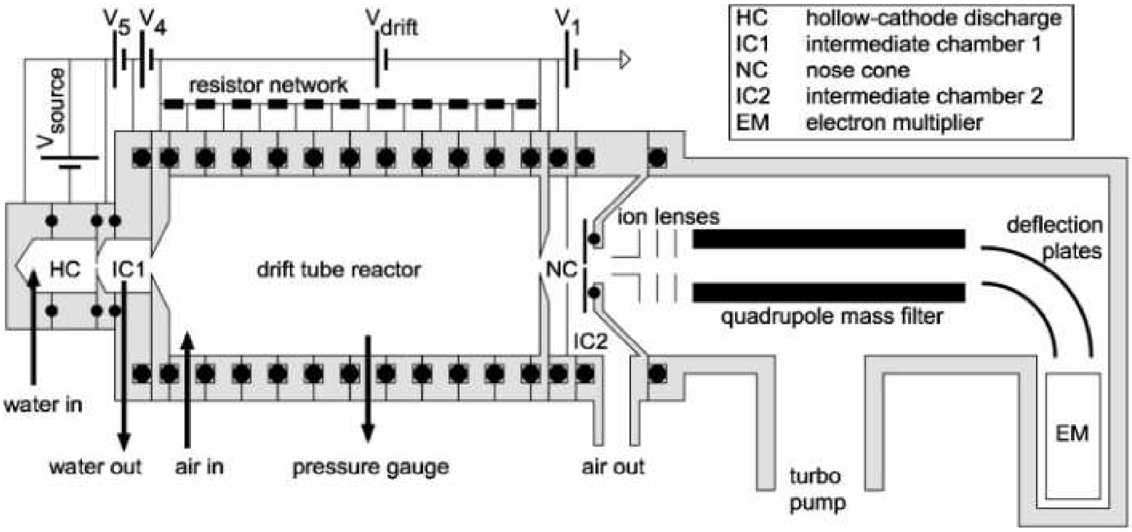

Figure 2.4. Original PTR-MS (Hansel et al., 1995)

Given its greater mass resolution, time-of-flight mass spectrometry has the potential to resolve isobaric species (those that have the same nominal mass). Blake et al. introduced the first time of flight instrument for PTR-MS study (Blake, Whyte, Hughes, Ellis, & Monks, 2004). The system possessed high mass resolution (m/Δm>1000) but had a low reagent ion production that was on the order of 10^4 counts per second, which was 2 orders of magnitude lower than the quadruple (PTR-QMS) instruments. Their reagent ions were produced by radioactive source (soft ionization), rather than the usual hollow cathode, which allows for the potential to measure clustering effect of the target molecule.

Ennis et al. (Ennis, Reynolds, Keely, & Carpenter, 2005) reported a reflectron PTR-TOFMS instrument coupled with a hollow cathode ion source demonstrating its portability and high mass resolution, though the sensitivity of this instrument was 5 to 10-fold less than that of PTR-QMS instruments. The instrument was capable of detecting trace gases as low as 1 ppbv on a timescale of between 10 and 60 s and with a sensitivity of 3.7 ncps ppbv^{-1} (normalized counts per second per parts per billion by volume) for toluene and 28 ncps ppbv^{-1} for acetone. This instrument is capable of high mass resolution, high mass accuracy (~300 ppm), and multiplexed spectral acquisition which leads to rapid and selective online analysis of trace components in complex gas mixtures.

A novel source was developed by Inomata et al. (Inomata, Tanimoto, Aoki, Hirokawa, & Sadanaga, 2006) that was capable of hydronium (H_3O^+) ion intensities at typically (5–7) x10^5 counts for a 1-min integration time with a duty cycle of 1%. Most recently, in 2009 Jordan et al. (A Jordan et al., 2009) reported on a high resolution and high sensitivity proton-transfer-reaction time-of-flight mass spectrometer. They report the development of a new version of PTR-MS using a time-of-flight mass spectrometer, which is capable of measuring VOCs at ultra-low concentrations (as low as a few pptv) under high mass resolution (as high as 6000 m/Δm in the so-called V-mode) with a mass range > 100,000 amu. This instrument was constructed by interfacing commercially available components such as the Ionicon hollow cathode ion source and drift tube section with a Tofwerk orthogonal acceleration reflectron time-of-flight mass spectrometer. In addition the instrument is highly sensitive (even for large masses yielding several tens of cps/ppbv) and features an extremely low detection limit on the order of a few pptv. This will make this instrument a useful and valuable tool for trace gas analysis in many fields, including atmospheric and environmental science, food and flavor science, medical applications, and industrial monitoring.

Our initial goal was to develop an instrument, method, and protocol for the sensitive and rapid measurement of gas-phase acidities of key carboxylic acids in the troposphere. Our improvement lies in the orthogonal coupling a novel flow reactor for the chemical reaction to a reflectron time-of-flight (TOF) mass analyzer to achieve a reasonably rapid time response and superior resolution as attempted by Tanimoto et al. (Tanimoto, Aoki, Inomata, Hirokawa, & Sadanaga, 2007) .

Our instrument is fitted with a novel flow tube that allows for higher pressure chemical reactions, which should increase the sensitivity due to the increased number density and reaction rate. Clustering is a drawback in a QMS tool because the presence of water clusters complicates the qualitative and quantitative information in the mass spectra. Since our spectrometer does not have an electrically biased drift tube, our instrument has the ability to observe and potentially characterize the reactivity of ion clusters. We also introduce the capability of easily detecting negative ions; a feature not commonly seen in TOF-MS. All of this coupled with the high resolution data collection of a reflectron TOF-MS should give our instrument the ability to measure thermochemical and kinetic data of negative ion proton transfer reaction of carboxylic acids with carboxylate ions and their hydrated states. Despite this, however, there are fundamental challenges associated with studying hydrated ion clusters that were not surmountable using this device, as detailed in section 2.6.4.

The next section describes the initial focus of this work. The initial project focused on two aspects that lead toward the development of NI-PTRMS: (1) the development of a clean, dependable source of acetate ions under different conditions of pressure, temperature and water vapor concentration, and (2) the determination of the gas-phase acidities of carboxylic acids of potential atmospheric interest. The following activities were attempted:

1) Optimizing the method of producing a clean, dependable source of acetate ions in the gas phase using ^{210}Po irradiation of acetic anhydride in nitrogen.
2) Determining the rate constants for forward and reverse proton transfer ion-molecule reactions
3) Determining the gas-phase acidities of carboxylic acids and other compounds of atmospheric interest

2.6.2. Equipment and methods. Studies of gas phase organic and inorganic acids in the troposphere from biomass burning require rapid, selective, and sensitive instrumentation far beyond the means of commercial instrumentation. The following chapter details the experimental apparatus that were used to obtain concentration, gas-phase kinetic, and heterogeneous kinetic information about HNCO, one of the biomass burning products which has attracted interest. The preferred apparatus for measuring the concentration and identity of gaseous molecules has been some version of the mass spectrometer (MS) and has been extensively covered and is generally well understood (Allan, 1999), thus it will only be described briefly here in order to describe the novelties of the instrumentation used in this work. The reflectron time-of-flight mass spectrometer (RTOF-MS) will be described first, as it was the initial focal point of the thesis, in an attempt to use negative ion chemical ionization in the study gas-phase kinetics. There are several novel aspects to the North Carolina A&T State University (NCAT) TOF system and they will be described in detail. The National Oceanic and Atmospheric Administration (NOAA) Earth Systems Research Laboratory (ESRL) negative ion proton transfer chemical ionization mass spectrometer (NI-PT-CIMS) is a companion system that has the versatility of being used both in the laboratory and the field. It has been described recently by Veres et al. (Veres et al., 2008) and only a brief description will be given here.

The final portion in this chapter is the heterogeneous uptake system (HUS) designed to produce and study the newly discovered biomass burning product, isocyanic acid (HNCO). The HUS can be used on either platform (RTOF or CIMS) in order to obtain solubility information on rarely studied biomass burning products. This HUS will prove to be a powerful and versatile method for extracting this information for not only HNCO, but several other uncharacterized biomass burning products to be identified as viable candidates for this method.

2.6.3. NCAT time-of-flight system. The complete RTOF-CIMS experimental setup at NCAT is a combination of several individual components coupled to the mass spectrometer. This work makes use of the time-of-flight (TOF) method of obtaining a mass spectrum as described thoroughly in the 2008 review by Mirsaleh-Kohan and coworkers (Mirsaleh-Kohan, Robertson, & Compton, 2008). This review is specific to the electron impact ionization method; however, this work attempts to use chemical ionization.

The basic principle of a time-of-flight (TOF) mass spectrometer is simple. At an initial time t = 0 ions are produced in a small volume. They are accelerated by a voltage V to a velocity $v = (2qV/m)^{1/2}$ where m is their mass and q their charge. The ions drift through a field-free region of length L before they are detected. Measuring the time delay between ion production at $t = 0$ and mass-dependent arrival time

$$t_m = \frac{L}{v} = \frac{L}{\sqrt{2qV/m}} \tag{2.27}$$

at the detector gives the mass m of the ion:

$$m = \frac{2qV}{L^2} t_m^2 \tag{2.28}$$

Though the acceleration voltage can be measured, it is typical that a compound with a known mass spectrum is used to relate arrival time to the mass to charge ratio (m/z). The mass resolution $m/\Delta m$ depends on the shortest time interval Δt that can still be resolved. From Equation 2.28 we obtain

$$\frac{\Delta m}{m} = \frac{2\Delta t}{t_m} \tag{2.29}$$

In practice a problem arises because the ions are not all produced at the same location, but within a finite volume. The electric field used to extract the ions varies over this volume and, therefore, the kinetic energy of the ions varies accordingly. Therefore, the velocities of ions, produced at different locations, are different which smears out the arrival times and limits the mass resolution.

The advantages of time-of-flight spectrometers are in that it is (a) possible to measure all mass components of a mixture of different species, (2) atoms or molecules with very large masses (for example biological molecules with $m/z > 10^4$) can be detected, and (c) the TOF design is simple and easy to construct.

Additional improvement in resolution of TOF are typically achieved by reflecting the ions at the end of the drift distance L by an electrostatic reflector, which consists of a stack of grids or rings at a positive voltage producing an electric field that repels the ions. The faster ions penetrate deeper into the reflecting field and therefore travel a larger distance, just compensating for an earlier arrival time at the reflecting field. This device, called a “reflectron” achieves the same total travel time for all ions within a velocity interval Δv.

A cross section scheme of the entire RTOF at NCAT is shown in Figure 2.5. It was built by Comstock Inc. (Oak Ridge, TN) and customized by Atom Sciences Inc. (Oak Ridge, TN) (Whitaker, 2004). Figure 2.5 shows the core of the system, with a source region where ion can be created and introduced into the "flight" region for mass separation. Ions are pulsed into the flight region by an electrostatic potential at a rate of 1500 to 2200 Hz. It is a reflectron time-of flight unit equipped with a standard 70 eV electron impact ionization source and is modified to allow for orthogonal injection of ion from chemical ionization.

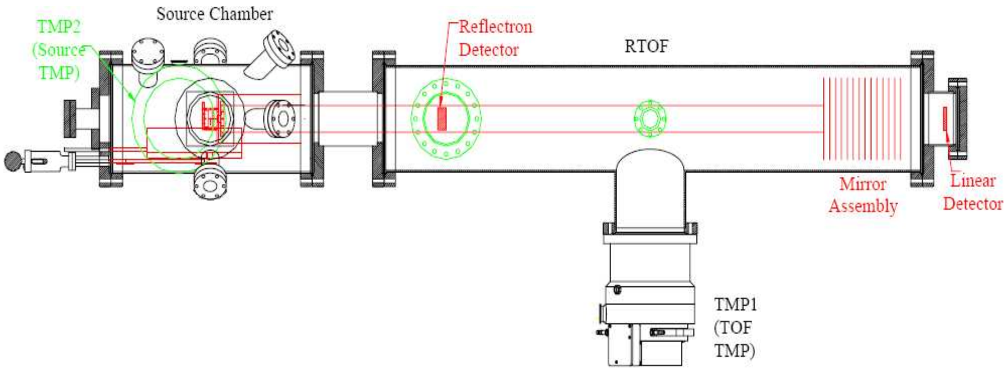

Figure 2.5. NCAT reflectron time of flight mass spectrometer

The source chamber is a custom 8" stainless steel tube with 10" Conflat flanges at each end and multiple 2-3/4" ports around it. The source chamber is described in detail in the Atom Sciences manual (Whitaker, 2004) so in brief, vacuum is provided by a Pfeiffer TMU 521 turbomolecular pump (~520 L/s) mounted horizontally (see TMP2 in Figure 2.6) with respect to the chamber and provides the main pumping for the source region. TMP2 is backed by a Pfeiffer DUO 5 rotary vane pump (not shown in Figure 2.6). The roughing pressure is monitored by an Edwards APG-M-NW25 Pirani ion gauge and the pressure in the source region is monitored by a Granville Phillips model 354 dual filament ion gauge which is mounted into one of the 2-3/4" ports. In one configuration, gaseous samples are introduced at a rate of 10 Hz by an R.M. Jordan C-211 pulsed valve mounted horizontally to the source region on a 6" flange, which is triggered by the computer. Ions are detected by a dual microchannel plate detector assembly and the resulting signal is amplified by a Minicircuits ZFL-500 wideband (0.05 to 500 MHz) amplifier. The resulting signal is raw time structured data that is converted into a digital signal via a time-to-digital converter (TDC) designed by PCB of London, England.

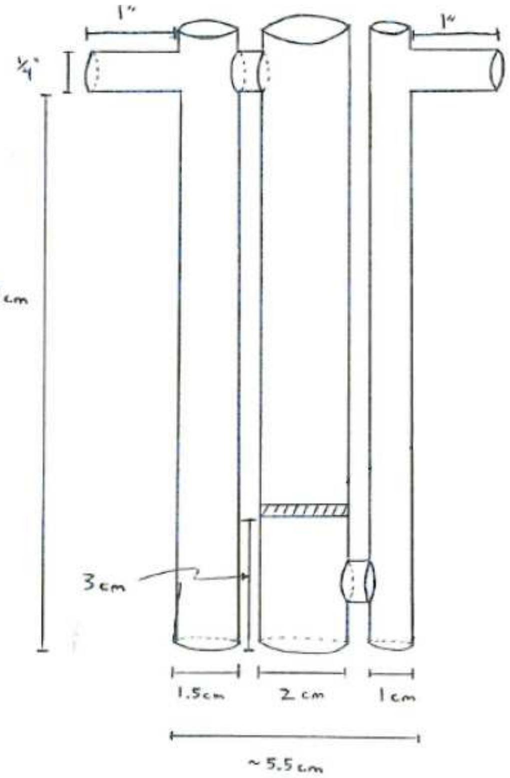

Figure 2.6. Glass bubbler with 10 μm porous frit

The converted data is managed by a direct memory access (DMA) system that allows certain hardware subsystems within the computer to access system memory independently of the central processor, and feeds data into LabView for analysis. Preprocessed data is used for online monitoring of signals and optimization. A final ascii data file containing the time, mass, and count intensity data can be saved for offline analysis at any time.

2.6.3.1. Chemical ionization. In order to obtain chemical kinetic and thermochemical information from gas phase reactions, a special ionization and ion transport method is needed that exploits the use of ions with favorable proton affinities which will allow for negative ion proton transfer reaction (see Table 2.2). The following is a description of the necessary components to achieve this and how they couple to the RTOF system.

The chemical ionization is achieved by first generating the reagent ions that then react with neutral molecules in what is termed "ion-molecule" reactions. Depending on the thermochemistry of the reactants, certain ion-molecule reactions are kinetically and/or thermodynamically favorable over others, which gives the method the necessary selectivity needed to ionize certain species and not others. The acetate ion is a suitable candidate for probing for many trace organic acids and particularly the carboxylic acids. The acetate ions are produced by bubbling about 200 standard cubic centimeters (sccm) of dry nitrogen through acetic anhydride ($C_4H_6O_3$, Fischer Scientific, 99.5%) via 1/8 inch PFA Teflon tubing (Fisher Scientific). The custom designed bubbler (Quark Glass Inc.) is shown in Figure 2.6. This creates a steady flow of acetic anhydride vapor which is then "soft" ionized by alpha particles from a Polonium-210 radioactive source (shown and described in greater detail below). The flow is controlled by Sierra Instruments, model 100CL mass flow controllers. The neutral reagent gas is produced and its concentration regulated by the custom diffusion cell (Quark Glass Inc.) shown in Figure 2.7.

The neutral reagent is carried by another 2 standard liters per minute (slpm) of nitrogen gas into a switching manifold (shown in Figure 2.8) where it can be controlled to inject the neutral species at 1 of 5 positions along a custom built flow tube. The manifold also has a second inlet where a third species may be added such as water vapor, allowing ion-molecule clustering effects to be measured.

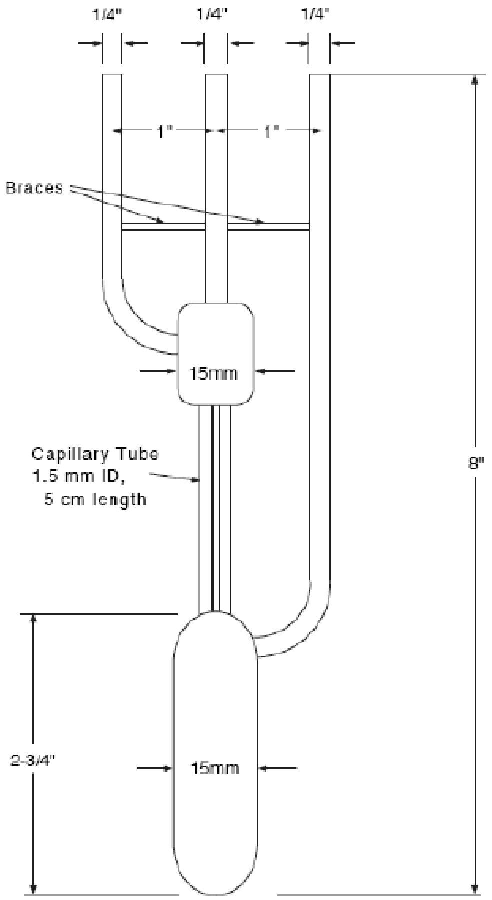

Figure 2.7. HNCO production cell

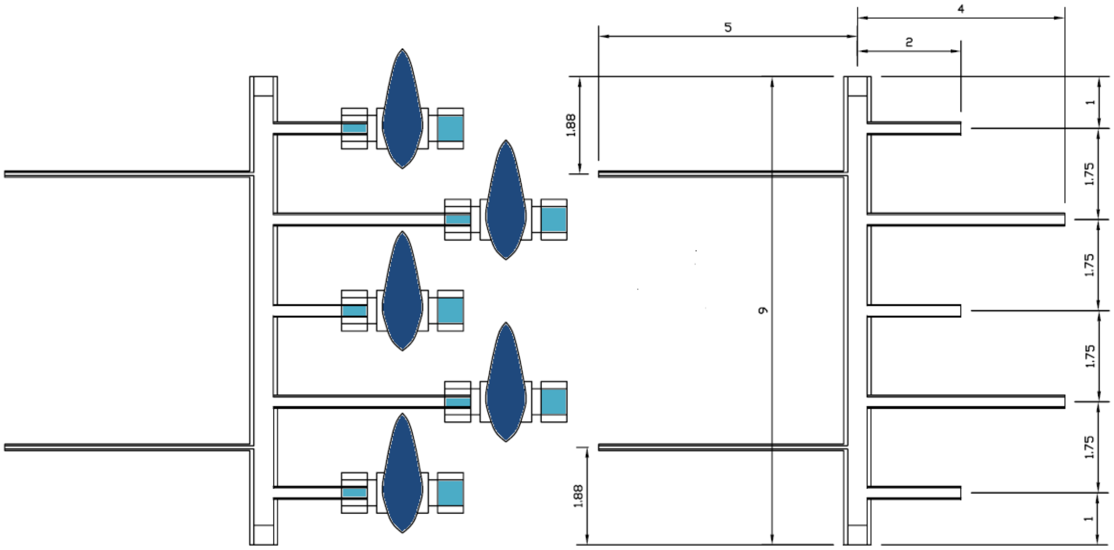

Figure 2.8. Gas switching manifold: The right side is the schematic (in inches) of the graphical image on the left

2.6.3.2. Soft ionization. The reagent ions are generated by flowing acetic anhydride ($C_4H_6O_3$) across a high energy alpha particle emitting source. The since the acetic anhydride is carried by nitrogen gas, dissociative electron attachment (Pariat & Allan, 1991) takes place after acetic anhydride bonds are broken (CH_3–C(O)–O–C(O)–CH_3). This yields the desired acetate ion, CH_3COO^-.

The alpha source is shown in Figure 2.9 and is a P-2031 Alpha ionizer (NRD Inc.) commercially used as a static removal product. The source of alpha particles is a polonium-210 (^{210}Po) embedded foil, which has an activity of 20 mCi (740 MBq) and a half-life of approximately 138 days. The P-2031 is designed to deliver high volumes of ionized compressed gases at near-ambient pressures and is placed in-line with the gas flow. The output flow of acetic anhydride vapor is coupled to the ionizer via ¼ -inch PFA Teflon tubing and a SS ¼ inch Swagelok to female NPT adapter. The output of the ionizer is connected to an NPT to KF-50 flange adapter (MDC, Inc.) at the entrance of the flow tube which is at the right side of Figure 2.10.

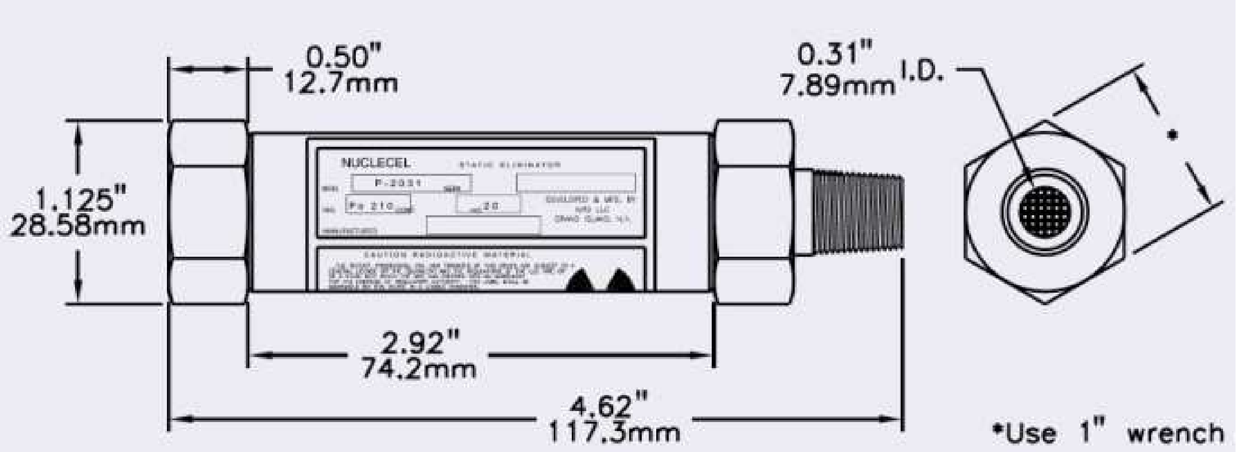

Figure 2.9. Polonium-210 ionization source and efficiency curve (image courtesy of NRD Inc.)

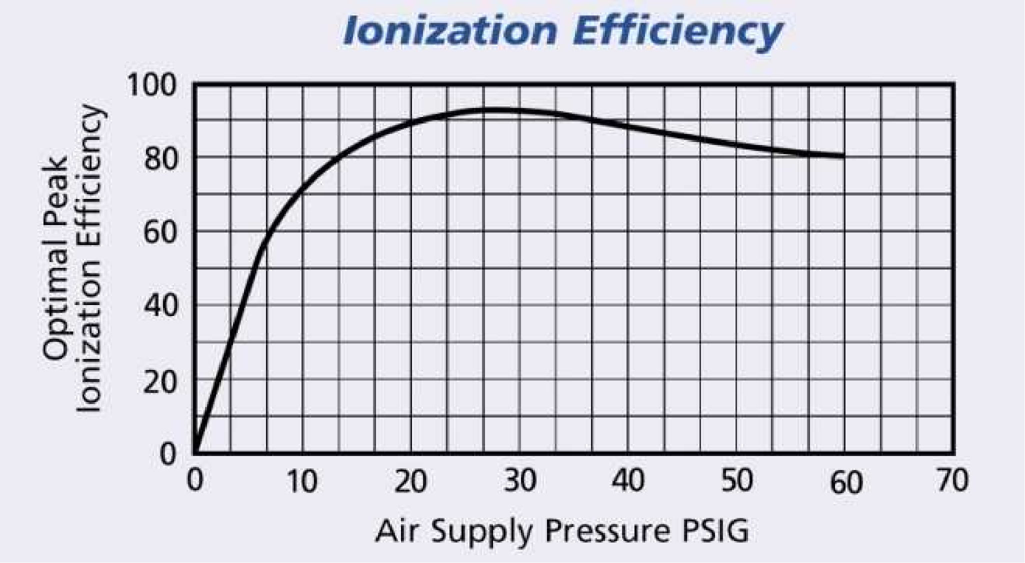

Figure 2.9. (cont.)

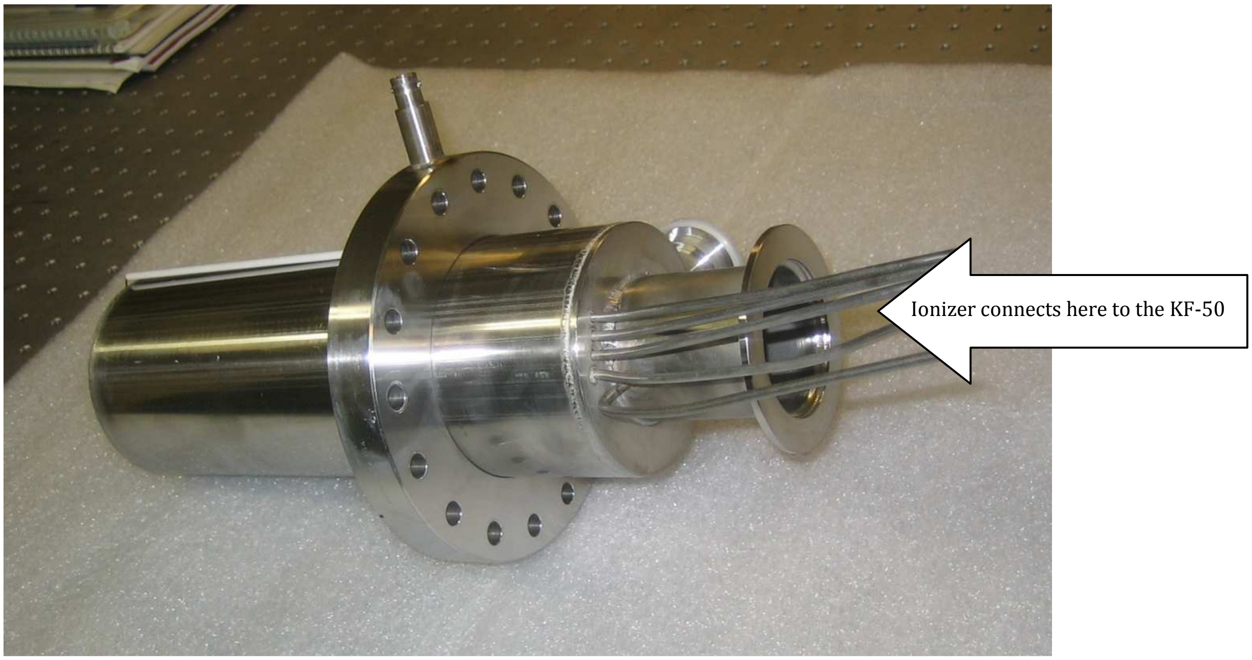

Figure 2.10. Custom-built flow tube reactor

2.6.3.3. Flow tube. The origin of the flow tube method is discussed by Carleton J. Howard (Howard, 1979). Howard also discusses the use of the flow tube in obtaining kinetic measurements. Our flow tube, pictured in Figure 2.10, is custom built (Atom Sciences, Inc.) and is designed to couple to the TOF MS (Figure 2.5) as close to the repeller region as possible. Ions which have undergone the proton transfer reaction within the flow tube are differentially pumped and focused into the first stage of the TOF using an Einzel lens, where the first element is the pinhole that provides the differential pumping.

The acetate ion and carrier gas is the main flow and enters the flow tube at the right in the center of the flange, while the neutral reagent gas enters one of 5 mixing inlet points along the flow tube. This allows for 5 different reaction times to be measured, which is the key to kinetic measurements.

The ion and carrier stream is the major component in the flow tube and thus serves to define the physical properties of the gas stream, e.g., pressure, flow velocity, heat capacity, thermal conductivity, viscosity, etc. The neutral species is only flowed in at about 10 sccm.

2.6.4. Results. After much troubleshooting and reconfiguration, the NCAT RTOF system was prepared for negative ion detection. In order to verify that the system was functioning in negative ion mode, electron impact ionization was used to generate the first negative ion spectrum from a sample of ambient air. The resulting spectrum is in red as shown in Figure 2.11 (the blue spectrum is the instrument background or negative ion baseline). This spectrum was not calibrated to specific masses, but several peaks can easily be seen in red that are well above the minimum pressure background level shown in blue. The background was of the same collection time and is negligible compared to the negative ion signal. This shows the excellent signal to noise ratio for electron impact in the negative ion mode. The peaks seen below 5 amu are not from ions but from electronic interference in the repeller due to a combination of voltage or time settings. Though it cannot be certain since no mass calibration could be performed, the most probable identity of the main peak is OH^- (m/z =17).

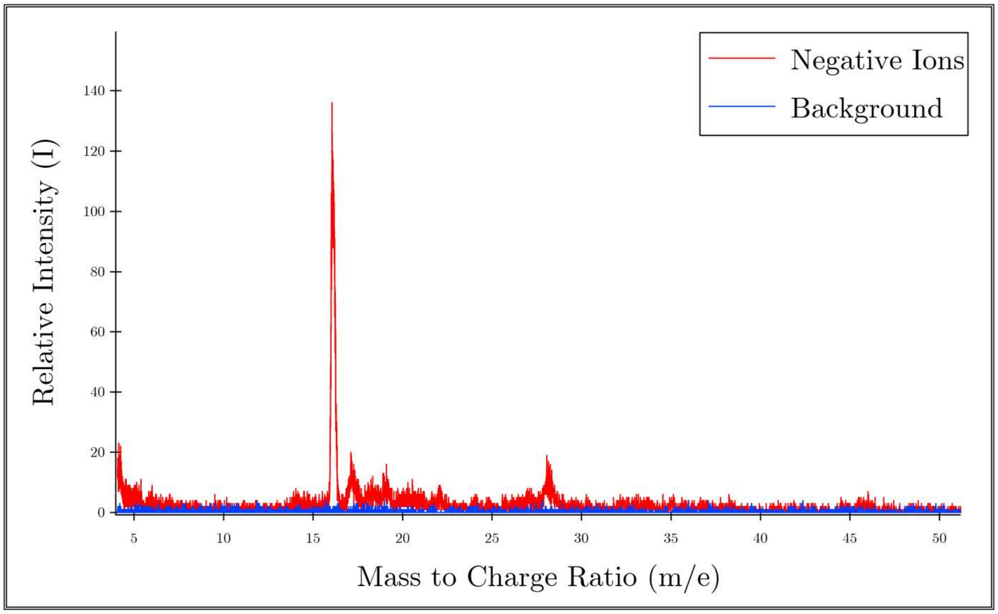

Figure 2.11. First negative ions detected on the NCAT RTOF-MS from electron impact ionization

As mentioned above in the experimental sections, attempts were made to detect ions in the spectrometer from "soft" ionization via CIMS. There was difficulty detecting the negative reagent (acetate) ions. Therefore, in order to verify that reagent ions were being created by alpha particle ionization from polonium-210 radioactive decay, an attempt was made to measure the ion current at the flow tube pinhole exit of the flow reactor. This would at least indicate that acetate ions were being created and available for proton transfer reactions. This was accomplished by connecting a digital volt meter to a BNC feed through connector electrically connected to the pinhole for biasing potential and grounding it to the instrument chassis. The results are shown in Figure 2.12 and one can see not only the proof of ion production in the form of voltage (from the current as it passes thought the 1 MΩ resistance of the multimeter), but also the dependence of the ion production on the flow tube pressure. The optimal operating pressure can easily be extracted from a similar graph when the final instrument parameters are chosen. The dip in voltage at ~15 torr is reproducible, though its cause is presently unknown.

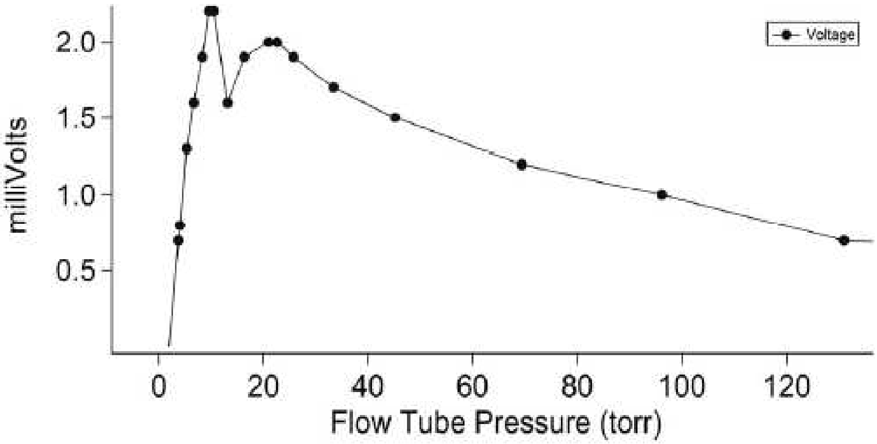

Figure 2.12. Ion current produced at the flow tube/TOF interface from soft ionization (polonium source)

The system was eventually determined to be reasonably sensitive enough to transport soft ions from the flow tube to the time-of-flight source. Only under extreme pressure conditions were ambient ions able to be detected via soft ionization. At approximately $5x10^{-4}$ torr in the TOF source region, the data in Figure 2.13 shows that a reproducible spectrum of ambient oxygen and nitrogen and a slight detection of water vapor could be detected. But this is not sufficient for detection of trace gas concentrations.

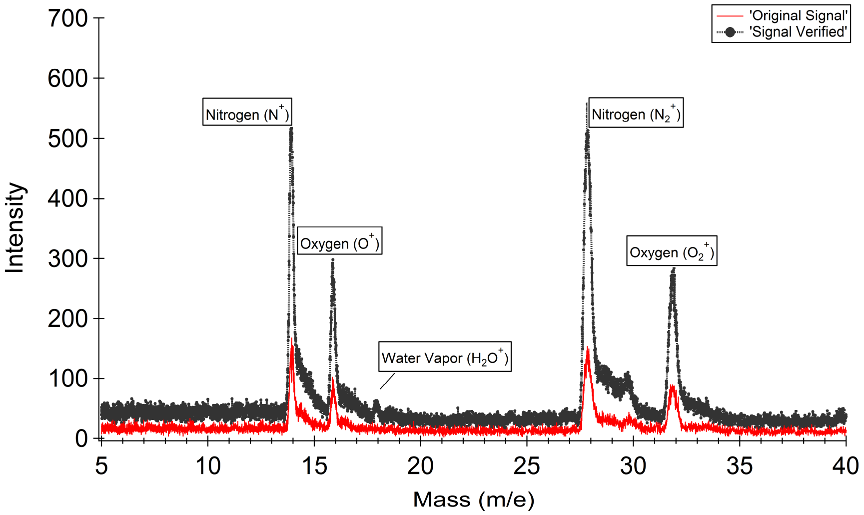

Figure 2.13. Positive ions from soft ionization source

2.6.5. Conclusions. This section provides in detail the technical problems encountered in using the RTOF, lessons learned, and recommendations for improving the system.

Sensitivity for EI ionization is typically in the ppm range (ignoring the sensitivity of the mass analyzer), which is problematic under laboratory conditions and makes measurements impossible under atmospherically realistic concentrations.

2.6.6. Electrical issues and improvements.

2.6.6.1. Repeller plate. There have been several electrical issues associated with the Atom Sciences NCAT RTOF-300 Mass Spectrometer. Many of these have been associated with operating in negative ion mode. Though this system was allegedly constructed to operate in negative ion mode, the needed alterations have shown that his is not the case. One of the first issues dealt with the repeller plate. Initially, the output of Counter 1 (J9, 6602) was connected (via a driver) to both the repeller pulser trigger and to the Start on the TDC. The high voltage output of the repeller pulser follows the +HV input when the trigger is high and it follows the –HV input when the trigger is low. When positive ions are being analyzed, –HV is set to ground potential and +HV is set to a positive, user specified voltage.

In the instrument's initial configuration, in negative ion mode, +HV is set to ground potential and –HV is set to the negative voltage specified by the user. This negative ion case is inappropriate for acquiring mass spectra of negative ions because the repelling voltage (typically -200 V) is on almost all the time. That is, it was necessary for proper operation for the pulse to be a mirror image of positive operation, so that ions are admitted or generated while the voltage is grounded, and thrust into the flight tube during the pulse. In this configuration, however, external ions are prevented from entering the repeller region or constantly entering the flight tube when generated internally. Only during the pulse, when the repeller is grounded, are ions allowed to accumulate.

2.6.6.2. Electrical discharges and the detector. When the X-Y board was damaged for the first time, an analysis of the circuit suggested an issue with the detector assembly. To diagnose these issues, the detector assembly was removed and various resistances were checked. The resistance across each resistor was consistent with the listed in the circuit diagram in Figure 2.14. There was no obvious damage to the detector, no burrs where an arc could take place, and no burn marks due to arcing. There was a slight blemish on the face of the MCP, but it was very small. There were also two capacitors that were not indicated in the circuit diagram. They were class 2 ceramic dielectrics and were 4.7 nF ± 20% (part number 564R60GAD47), and are shown in the revised circuit diagram shown in Figure 2.14. These capacitors should have been able handle 10.5 kV (at atmospheric pressure) before arcing across the leads.

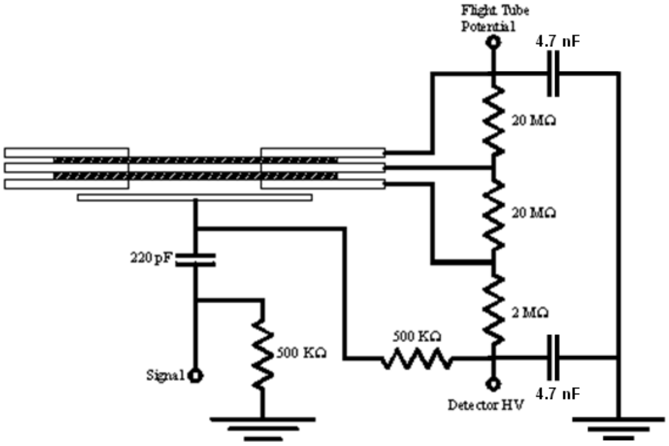

Figure 2.14. The revised circuit diagram for the detector assembly

It was later found, however, that the 4.7 nF capacitors were not appropriate for the voltages that were being applied to them. The detector is always biased positive (1800-2000 V) relative to the flight tube in either ion mode. In positive mode, the flight tube is ~3 kV below ground, making the detector fairly close to ground potential. However, the discharge issues were more prevalent in negative ion mode, because the flight tube is ~3 kV above ground, making the detector voltage ~5 kV above ground potential. Given that these capacitors were inappropriate to begin with, and were later internally altered by arcing, they presented the easiest path to ground. The reason the preamplifiers were damaged was because they were sensitive to any discharge to ground within the system. It is worth noting that damaged preamplifiers are evident by a significant decrease or total loss of signal.

The second time the X-Y board was damaged was, and still is, somewhat mysterious. It occurred during negative ion mode, though no arc was evident. In fact, the preamplifier was undamaged. A postmortem of the board suggested an arc directly to an X-Y plate. This is strange, since the closest elements to the plates inside the instrument are the flight tube and the tube lens. The X-Y plates are biased only a few volts away from the flight tube (indeed, it is biased against it). The tube lens, though not biased against the flight tube, is not likely the cause because it is typically within 500 V of the flight tube. This suggests there could be an issue with the wires between the feedthroughs and the ion optics, though not the cables external to the vacuum system. Though some damage was later noticed on the extraction grids (which are grounded) in the source region, they are too far away from the X or Y plates to have any effect (see Figure 2.14). Since this time, damage to preamplifiers has been very infrequent, though not all together absent. One contributing factor to the discharge issue may be the practice of removing the +15 V supply and the output from the preamplifier while it is not in operation. However, since the X-Y board was damaged without an adequate cause being determined, the instrument has largely been relegated to positive ion mode. Should acetate anion or other negative mode ion chemistry be used, further efforts would be needed to determine the sources of arcing, both internally and externally.

2.6.6.3. Feedthrough mapping. The high voltage feedthroughs were also checked and mapped to elements within the spectrometer. The diagram in Figure 2.15 shows the assignments and their feedthrough numbers in brackets. All elements were found to be independent of each other (>1000 MΩ resistance) except the flight tube to ground, which only read 140 MΩ. It is likely that this reading was due to it being wired to the reflectron and the reflectron feedthroughs still attached.

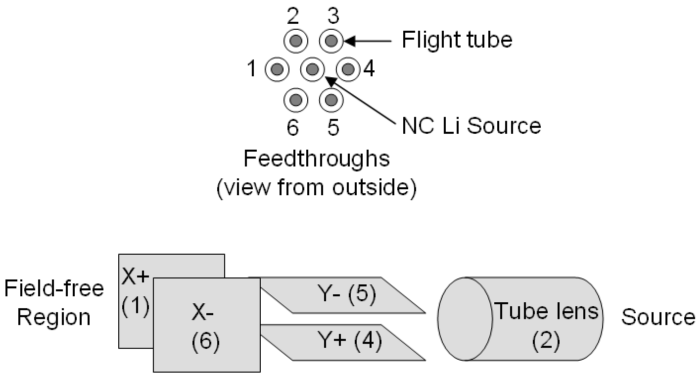

Figure 2.15. The assignments of HV feedthroughs to various elements within the RTOF

2.6.6.4. Detector noise. Since the mass spectrometer's installation, it has been noticed that there are noise spikes in the detection system. These are present at specific masses (or at the same time during each detection cycle), and they are independent of the presence of ions (i.e. they are there when the EII filament is off). The locations and abundances of the noise peaks change with the repeller repetition rate, which are at a minimum at 20 kHz, and suggest a relationship between the detector and repeller. The likely cause is the proximity between the repeller wire and the detector. The repeller feedthrough is in the flight tube region, and the wire goes very close to the detector, goes through the ceramic holding the flight tube, through grounded mesh in the source region, and connects to a screw that holds the repeller plate to the grounded housing of the repeller region. The conflate flange that holds the repeller feedthrough should be moved to the source region, the hole in the grounded mesh should be closed, and the wire should take a much more direct route from the feedthrough to the repeller plate. This would result in much less RF noise from the repeller reaching the detector, since there would be nothing but grounded elements between the two.

2.7. NOAA ESRL Equipment

2.7.1. NI-PT-CIMS. Another instrument used in the efforts of this thesis is the negative ion proton transfer chemical ionization mass spectrometer (NI-PT-CIMS). It is an instrument that was designed at the NOAA Earth Systems Research Laboratory to sample trace organic acids in the troposphere (Figure 2.16). It was described thoroughly by Veres et al. in 2008 (P. Veres et al., 2008). In terms of the work here, it is used in both ground based field measurements and laboratory measurements of important biomass burning products. Those applications and results will be described in the next section. The instrument scheme is shown in Figure 2.16. Ambient air is sampled into the NI-PT-CIMS instrument by 0.25” outer diameter PFA Teflon tubing, which is heated to an external temperature of 75°C to minimize inlet effects. The total inlet flow rate is about 2 slpm. The acetate ion is synthesized by dissociative electron attachment as mentioned above. The sample air is drawn into the flow tube (32 torr) and mixes with the acetate reagent ions. Ion-molecule reactions occur over the entire 12 cm length of the flow tube and the resulting analyte ions are then accelerated through the collisional dissociation chamber (CDC) via an electric field of approximately 25 $V\text{-}cm^{-1}$. The CDC is maintained at 0.15 Torr with a molecular drag pump and molecular collisions in the CDC dissociate weakly bound cluster ions, such as those from the inescapable water vapor $CH_3C(O)O^-(H_2O)_n$. Eliminating clusters is more important here than in the RTOF since the RTOF has much better resolving power than a quadrupole mass spectrometer. An electron multiplier at a pressure less than $7x10^{-5}$ Torr is used to detect the ions.

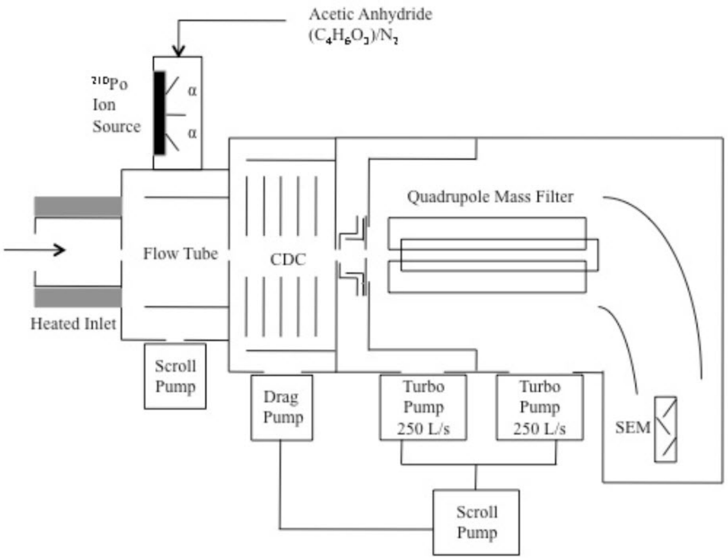

Figure 2.16. NI-PT-CIMS hardware (image courtesy of P. Veres)

2.7.2. Mobile calibration system. It is necessary to zero and calibrate the instrument for quality assurance and to be able to interpret the data in terms of concentration. Figure 2.17 is a schematic diagram of the mobile organic carbon calibration system (MOCCS) (Veres et al., 2010) for the generation and absolute measurements of calibrated VOC mixtures in air that is relatively inexpensive and easy to set up. The MOCCS combines the production of standards using permeation or diffusion sources, quantitative catalytic conversion of carbon containing species to CO_2, and CO_2 measurement. Its effectiveness will be demonstrated in the next chapter where field measurements are calibrated.

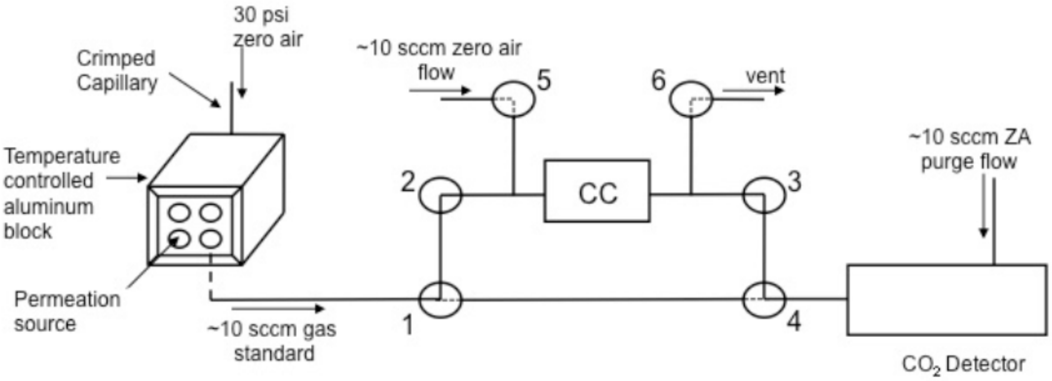

Figure 2.17. Mobile organic carbon calibration system (MOCCS)

2.7.3. Heterogeneous reaction production and delivery system. Both mass spectrometer systems mentioned above can be placed in line with the isocyanic acid gas (HNCO) production and delivery system shown in Figure 2.18 in order to measure heterogeneous (gas-liquid) reactions. A gas phase species is generated in the source by heating and it is then injected into an aqueous solution within the bubbler. Hydrolysis and solubility constants can be extracted from carefully crafted experiment where temperature, flow rate, and solution acidity are varied.

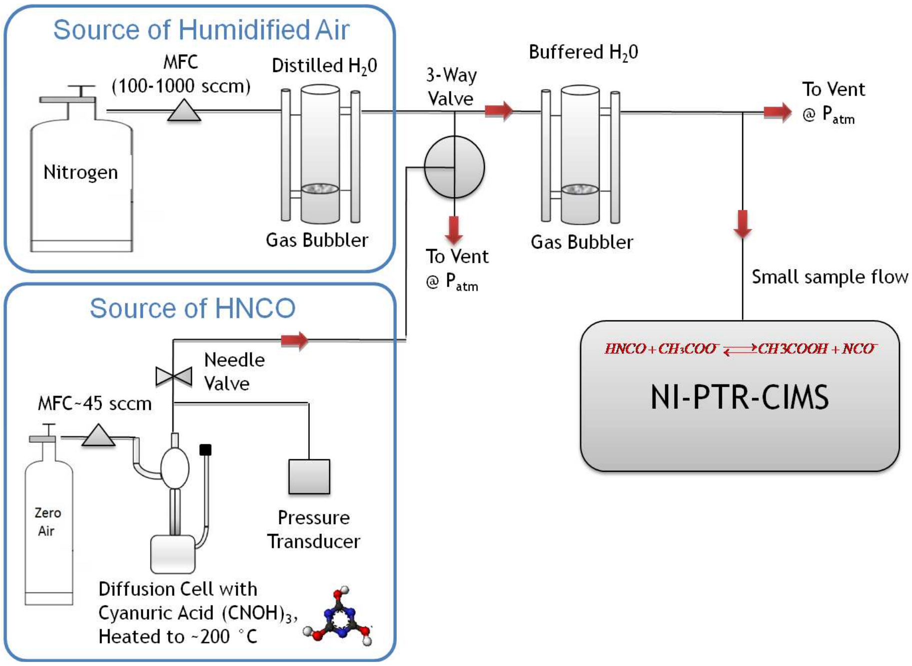

Figure 2.18. Schematic of system built to make the first solubility measurements of HNCO

2.8. NOAA ESRL CSD Experimental Work

2.8.1. CalNex 2010 field campaign. The negative-ion proton-transfer chemical-ionization mass spectrometer (NI-PT-CIMS) described above was deployed in the field to conduct ambient measurements as part of a field study that sought to get a better understanding of the nexus of air quality and climate change. Gas-phase acids (nitric, formic, acrylic, methacrylic, propionic, and pyruvic/butyric acid) were measured using the NI-PT-CIMS in Pasadena, CA as part of the CalNex 2010 regional field campaign and reported by Veres et al.

(2011). Organic acid concentrations ranged from a few parts per trillion by volume (pptv) to several parts per billion by volume (ppbv), with the largest concentrations observed for formic and propionic acids. Figure 2.19 shows the time series measurements from the NI-PT-CIMS over the duration of the campaign in California Institute of Technology (Pasadena, CA). Figure 2.20 shows the diurnal variations of HCl and also shows some night time HONO production.

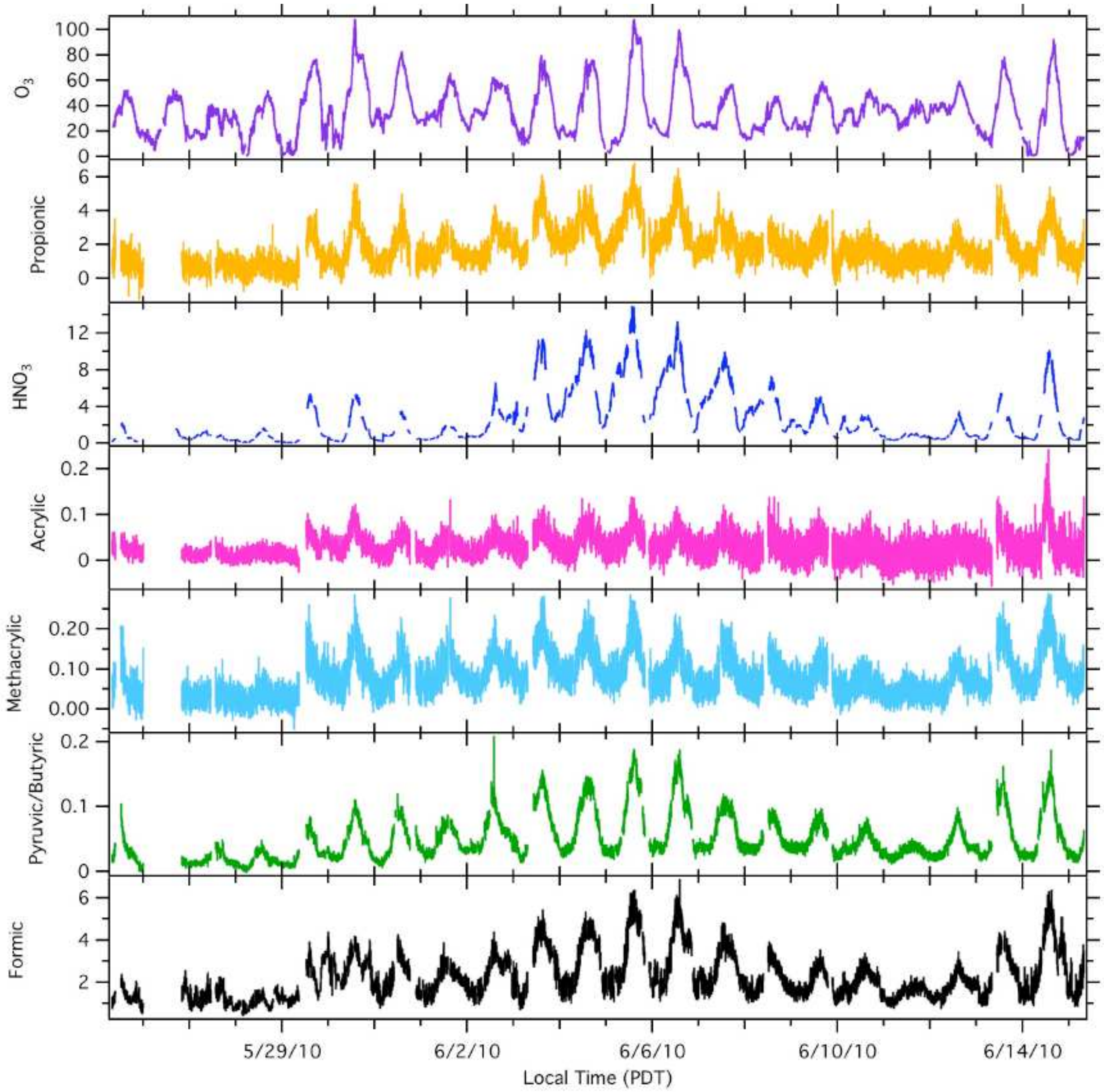

Figure 2.19. Diurnal concentration measurements (ppb) of acids from the CalNex 2010 field campaign

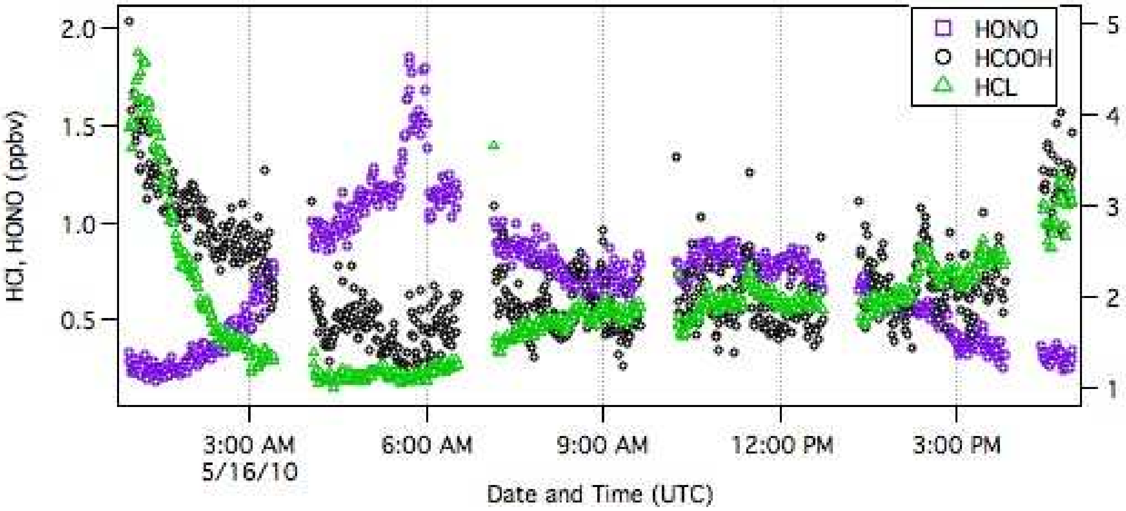

Figure 2.20. Time series measurements of HONO, formic acid, and HCl using the NI-PT-CIMS during 5/16/10

2.8.2. HNCO solubility. HNCO is a moderately weak acid in aqueous solution (pK_a=3.7) (D.J. Belson & A.N. Strachan, 1982) and exhibits relatively slow hydrolysis that is pH-dependent (Jensen, 1958). The partitioning of HNCO to aqueous solution at low-concentration, i.e. Henry's Law solubility, H (M/atm), has apparently not been measured previously. We have measured H for isocyanic acid in an aqueous buffer at pH=3.0±0.1, and room temperature (T=25±1°C) and liquid volume of 25 ml.

Figure 2.21 shows the data for a full experimental sequence where the flow rate is varied. It shows the raw data which first measures the instrument background. Then maximum available concentration of HNCO is measured, followed by a series of (near) saturation and purge sequences that are made at the various flow rates. The linear decay on the log scale is easily noticeable and is the only data used in the calculation. Instrument background data are collected to characterize the minimum instrument signal which is subtracted from the measurement data.

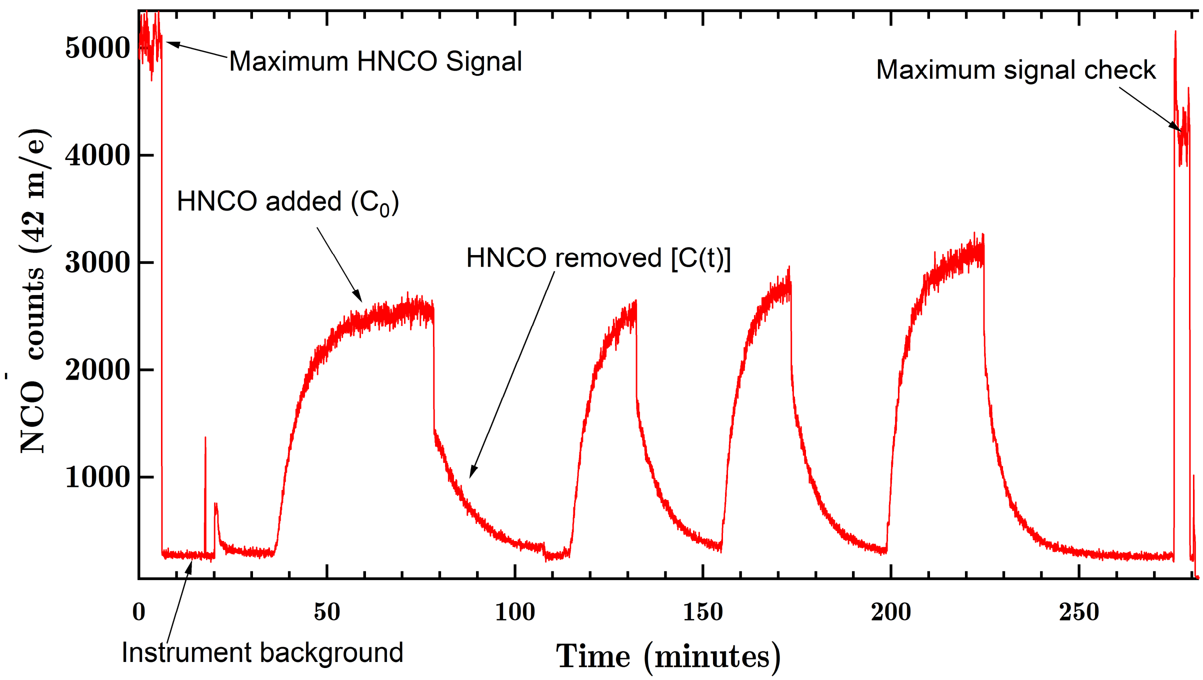

Figure 2.21. HNCO gas stripping experiments; each cycle is at a different (increasing) flow rate

From each cycle, a sample of the log-linear portion of each exponential decay of the HNCO concentration (see Equation 2.20) can be used to extract the slopes at different flow rates from the raw data. Figure 2.22 displays all of the slopes from the various flow rates. These slopes are from the value in parenthesis in Equation 2.32.

The lognormal plot of the relative HNCO concentration against time (Figure 2.22), results in a linear relationship. A linear fit of each cycle produces the hydrolysis rate constant (from the intercept) and Henry's Law constant (from the slope), using Equation 2.20 in section 2.5.2.

The decrease in gas phase HNCO, exiting a saturated liquid sample, was measured for a range of volume flow rates to liquid volumes (Φ/V) (Figure 2.23). For a system in which the mass transfer between the liquid and gas phases is rapid, the relationship in Equation (2.29) holds:

$$\ln\frac{C_0}{C}=\left(\frac{\Phi}{V}\frac{1}{HRT}+k\right)t \tag{2.29}$$

where C_t/C_o is the relative concentration in the gas phase exiting the reactor, Φ is the volumetric flow rate, V is the liquid volume, R is the ideal gas constant, T is temperature, k is the first order loss rate in solution, and t is the time. The slopes of these exponential curves vs. the flow-rate/liq.-volume yield the Henry's coefficient (Figure 2.23).

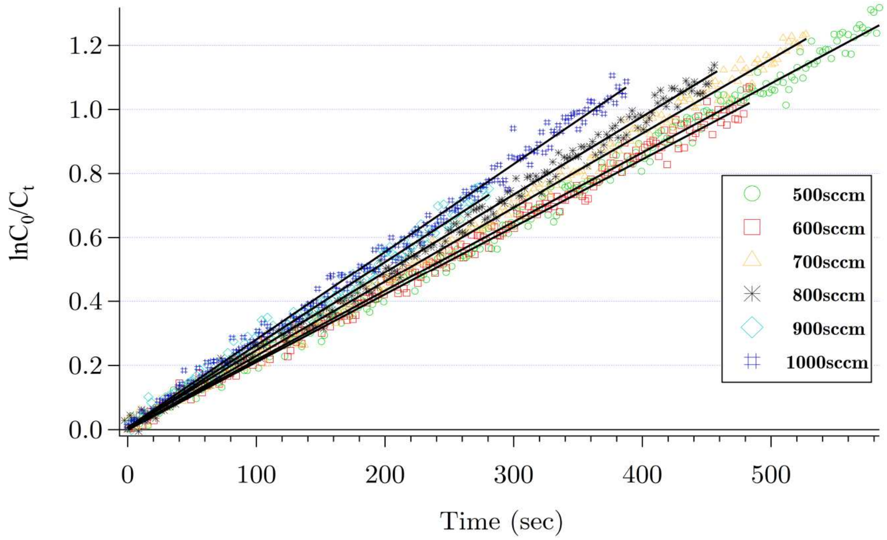

Figure 2.22. Flow rate sensitivity in the gas stripping process

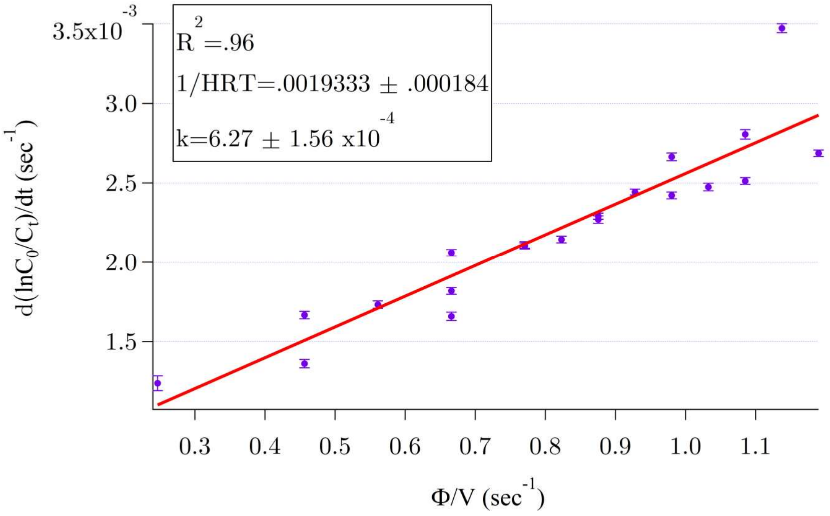

Figure 2.23. Data revealing Henry's Law and hydrolysis rate constants of HNCO at pH=3 and room temperature (T=25±1°C)

The first order loss rate coefficient (k) of HNCO in aqueous solution was also measured. Results show that at a pH of 3.0 ± 0.1 and room temperature (T = 25 ± 1 °C), H was found to be 21.1 ± 2.7 M/atm and k was found to be $6.3 \pm 1.6 \times 10^{-4}$ s^{-1}.

2.8.4. Conclusion. The CalNex results provide direct evidence for rapid photochemical production of organic acids in urban atmospheres. Observations with a fast time response such as with the NI-PT-CIMS are necessary to identify the photochemical production mechanisms responsible for the high organic acid concentrations observed, and then they should be incorporated into existing photochemical models for better accuracy. Organic acid concentrations correlated well with HNO_3 and O_x (odd oxygen $O_x = O_3 + NO_2$) measurements demonstrating that the dominant source of organic acids in Pasadena is the photochemical production from urban emissions.

We measured the Henry's Law solubility of HNCO at pH = 3, and using the expression for solubility of a weak acid, estimate HNCO to be highly soluble at physiologic conditions, pH = 7.4. The HNCO solubility measurement has shown that it is highly soluble in the range of the human body's pH level. If concentrations of HNCO from biomass burning and other sources are significant, there is a great risk for human health effects, since it has been shown that HNCO causes protein carbamylation (Beswick & Harding, 1984) and can cause arthritis and have other negative impacts.

After the solubility measurement was made we were able to make an estimate of the lifetime and published a full study (Roberts et al., 2011) of the potential risks (arthritis, cataracts, and atherosclerosis). People are constantly exposed to smoke from wildfires, tobacco, from biomass burning, or from coal combustion used in cooking and heating (Crutzen & Andreae, 1990). The production of HNCO is expected to increase due to industrial and economic changes.

Given the current levels of exposure in populations that burn biomass or use tobacco, the expected growth in biomass burning emissions with warmer, drier regional climates, and planned increase in diesel SCR controls (Zhao, Hu, Hua, Shuai, & Wang, 2011), it is imperative that we understand the extent and effects of this HNCO exposure.

The results of the experimental work mentioned above in the area of trace gases produced from biomass burning, and isocyanic acid in particular, have lead to an interest in the specific investigation into the lifetime of HNCO given the potential health effects related to it. The next chapter is an exploration into the characteristics of HNCO as it traverses the troposphere through clouds via a 1-dimensional numerical model. This is critical to the research community in not only providing new data for regional and global models, but also in planning future airborne field campaigns. Airborne HNCO measurements have not been conducted at the time of this publication. The lifetimes of HNCO will be reported for various situations, which are necessary given the enormous number of parameters that go into assessing a chemical's risk in the atmosphere.

CHAPTER 3

Cloud Chemistry Modeling—Heterogeneous Uptake of HNCO

3.1. Introduction

In order to adequately describe the aqueous chemistry of HNCO and any modification in its gas phase chemistry in the atmosphere, it is necessary to know how clouds affect the chemistry and transport of these species. A description of clouds, cloud chemistry, cloud microphysics, aerosol interactions, and the modeling method is given in this chapter. It will become evident that chemical processing of HNCO in clouds will be difficult to characterize due to numerous variables involved and the wide range of values that the variables needed to accurately describe the system.

3.2. Clouds

The World Meteorological Organization (WMO) defined a cloud as an aggregate of minute, suspended particles of water or ice, or a combination of both, that are in sufficient concentrations (Holton, Curry, & Pyle, 2003). Clouds are visible accumulations of water droplets or ice crystals that migrate through the Earth's troposphere, moving with the wind. Clouds form when water vapor condenses onto microscopic dust particles known as cloud condensation nuclei (CCN). Varying pressures, temperatures, and relative humidity in the troposphere and at the Earth's surface can cause water to constantly transfer between its gaseous, liquid, and solid states. Clouds, fogs, rain, dew, and wet aerosol particles are forms of this water. Condensed-phase particles play a major role in atmospheric chemistry, atmospheric radiation (reflection and absorption for example), and atmospheric dynamics.

Clouds come in many different forms, and their characteristics reveal the meteorological properties of the atmosphere in which they were born. In the troposphere, four groups of clouds are recognized, depending on the altitude of their bases and their vertical evolution: low level, midlevel, high-level, and clouds with vertical development (see Table 3.1 for the groups and types). These groups are also subdivided depending on their structure. Figure 3.1 is a simplified depiction of where the different clouds are and their structure.

Table 3.1

Major cloud groups and types

Cloud Group	Cloud Type
High clouds	Cirrus Cirrostratus Cirrocumulus
Middle clouds	Altostratus Altocumulus
Low clouds	Stratus Stratocumulus Nimbostratus
Clouds with vertical development	Cumulus Cumulonimbus

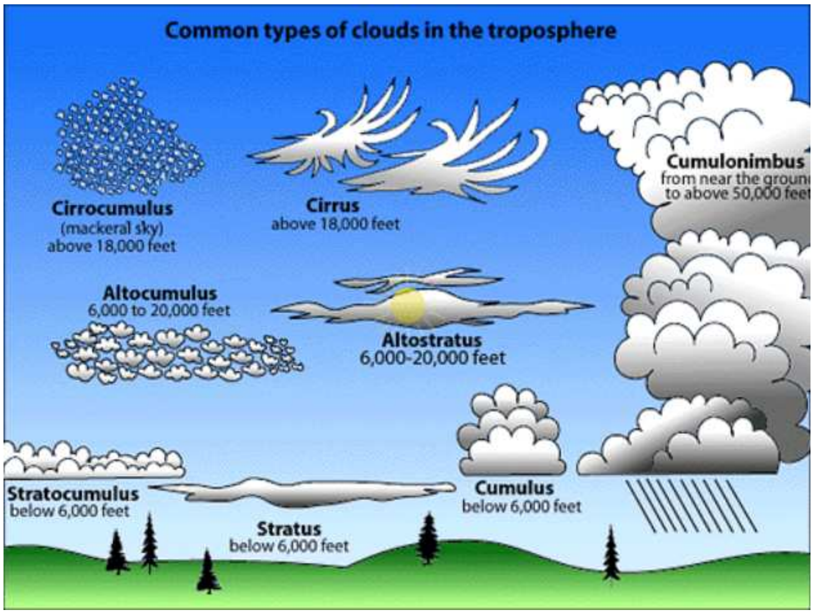

Figure 3.1. Cloud altitudes. Image courtesy of http://scientificmadness.blogspot.com/2011/07/cloud-identification.html

Clouds exist very temporarily; no cloud exists for more than a few hours, and most of the small clouds in the troposphere exist for only a few minutes. But it is difficult to define what water concentration or liquid water content defines a cloud type, so a wide range of droplet sizes constitutes a cloud and ice crystals need to be accounted for as well.

For some scientists, a 50 mm diameter drop represents a ‘drizzle’ droplet likely formed via coalescence; but others define a ‘cloud’ droplet based on its settling velocity (Warner, 1969) for instance, the further that an observer is from falling precipitation, the more it appears to be a ‘cloud’ due to perspective. Many of the higher ‘clouds’ above us, such as cirrus and altostratus are composed mainly of ice crystals and snowflakes that are settling toward the Earth, and would not be considered ‘clouds’ by an observer inside them, but rather a light snowfall.

Some clouds provide a means of transporting constituents found primarily in the boundary layer to the free troposphere if they are part of the convective system. Because clouds scatter solar radiation the actinic flux, and consequently chemical rates for photodissociation, can be altered above, below, and in clouds (Barth et al., 2003). The physics of the interactions between cloud particles can also affect the chemical production and the distribution of chemical species. The behavior of isocyanic acid in clouds is the focus of this modeling work.

3.3. Cloud Chemistry

Even though clouds occupy a small fraction of the total volume of the troposphere, they play a significant role in the chemical processing of the atmosphere, for example, in the global hydrologic cycle (Randall, Harshvardhan, & Dazlich, 1991) and also in influencing atmospheric radiative transfer and the overall albedo (Holloway & Manabe, 1971). Clouds interact with numerous chemical species including the focus of this chapter, isocyanic acid (HNCO). Together with gases and aerosols, clouds make up part of the complex multiphase system (gas, aqueous, surfaces, etc.) that is our atmosphere. Clouds are both engines for the production of new chemical species and as “scrubbers” for particle and trace gas removal (especially HNCO) by wet and direct deposition since they are captured by the surface of cloud and fog droplets and the interior of aerosols (Ravishankara, 1997).

Figure 3.2 is a pictorial overview from of the cloud/particle/trace gas atmospheric system. Isocyanic acid and other trace gases are perpetually forming, reacting, and depositing in the atmosphere. It will be shown later that HNCO does not significantly react in the gas phase chemically or photochemically but it does have condensed phase reactions due to its high solubility.

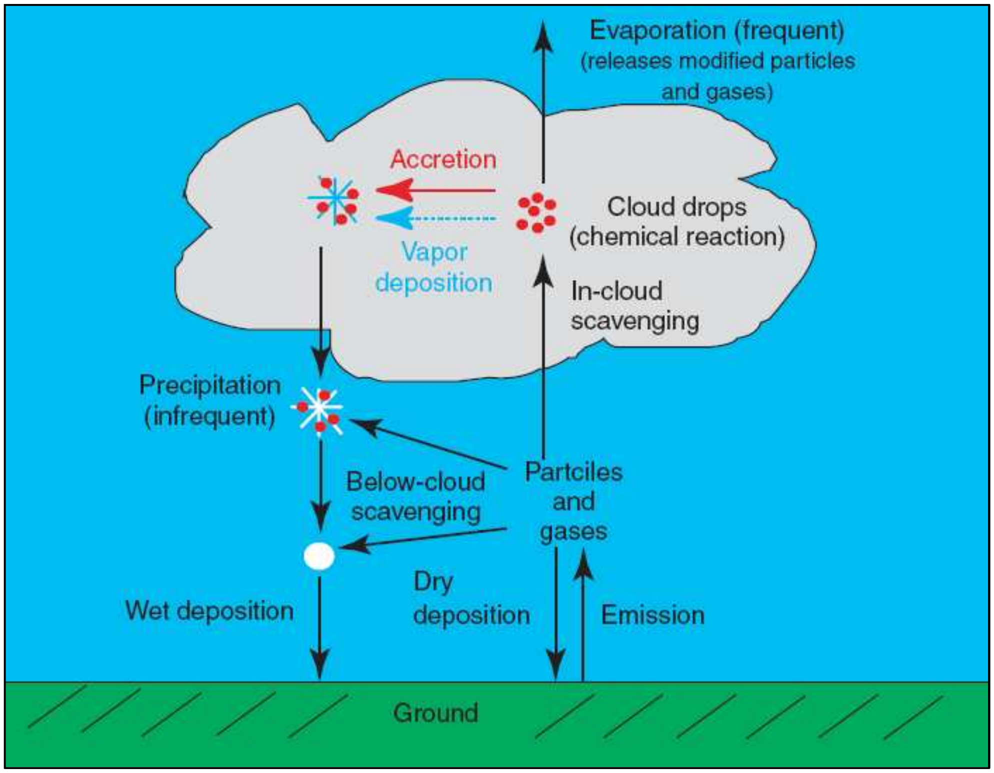

Figure 3.2. A schematic representation of the multiphase cloud-particle-trace gas system in the atmosphere. Included are the sink processes of dry and wet deposition, particle and gas scavenging by cloud drops, chemical reaction, and precipitation formation in a mixed-phase (ice–liquid water) cloud (reproduced from Collett & Herckes, 2003)

Clouds and fogs interact with both aerosol particles and trace gases. The incorporation of particles and gases into cloud drops are key steps in determining the initial chemical composition of the cloud which are necessary in order to determine modeling boundary conditions and cloud composition.

Cloud drops form by condensation of water vapor onto a subset of particles called cloud condensation nuclei (CCN), a process also known as heterogeneous nucleation (Fletcher, 1958). In the absence of CCN, clouds would not readily form since extreme supersaturations would be required for the homogeneous nucleation of water vapor (water to water coalescence).

Particles that have deliquesced (i.e. acquired water from the surroundings via adsorption) are referred to as haze particles. As the humidity increases above what is known as the relative humidity of deliquescence, haze particles can take on additional water as humidity increases in order to maintain equilibrium with the partial pressure of water vapor in the atmosphere. The equilibrium partial pressure of water vapor above a haze drop depends on the drop size and its composition. Increased drop curvature raises the equilibrium water vapor pressure via the Kelvin effect (droplet growth and curvature radius relationship, as shown in equation 3.1). Increased drop solute content such as HNCO lowers the equilibrium vapor pressure by displacement of water molecules near the drop surface. The combined effects of drop curvature and solute content are described in aerosol theory (Danckwerts, 1951) and not described here but have a close relationship.

Droplet growth can be described using an equation developed in 1970 by Fukuta and Walter (Fukuta & Walter, 1970). It was known as the Kelvin effect and accounted for the simultaneous growth and evaporation of what they termed hydrometeors. Essentially the Kelvin effect is the increase in vapor pressure due to an increase in the curved surface competing with the addition of solute that increases the vapor pressure. The governing equation is:

$$\ln\left(\frac{P}{P_0}\right) = \frac{2\gamma V_m}{rRT} \tag{3.1}$$

where P is the vapor pressure, P_0 is the saturated vapor pressure, γ is the surface tension, V_m is the molar volume, R is the gas constant, r is the hydrometeor radius, and T is the temperature.

Activated drops are those that have reached a critical point of supersaturation described by the Kohler theory (Corrigan & Novakov, 1999). Growth of activated drops is limited primarily by the availability of water vapor. Haze particles which do not reach their critical supersaturation will not activate and will stay in equilibrium with the surroundings (Collett & Herckes, 2003).

In most clouds, particles as small as 0.1 micron in diameter can activate and grow into cloud drops (Collett & Herckes, 2003). In other cases, such as particles with low supersaturation values and/or high particle concentrations, the minimum particle size activated may be 0.5 to 1 microns. CCN are typically thought of as being comprised of mainly sulfate particles, sea salt particles, and, potentially nitrate particles. Studies have revealed that many carbonaceous particles are also capable of acting as CCN (Rivera-Carpio et al., 1996). Much more work is needed to understand interactions of carbonaceous particles with fogs and clouds.

3.3.1. Isocyanic acid in cloud chemistry: Atmospheric removal. HNCO is one very interesting carbonaceous species with several sources and known health effects at trace levels and pH levels similar to the human body. Though there is some debate in whether it is organic or inorganic, it is generally and most recently given the inorganic label (Roberts et al., 2010, 2011; Veres et al., 2010).

Trace organics are generally cleaned from the atmosphere by the hydroxyl radical (OH) (Sun & Saeys, 2008). HNCO is essentially stable with respect to OH reactions in the gas phase (Tsang, 1992), with lifetimes on the order of several decades. HNCO is also not expected to be affected by photolysis or photodisintegration due to the fact that it has very low absorption in the visible to near-UV (Brownsword, Laurent, Vatsa, Volpp, & Wolfrum, 1996).

This leads to the conclusion that the relevant loss processes of HNCO is going to be heterogeneous uptake into one of the aqueous phases (aerosols, fogs, clouds, precipitation, and liquid water and deposition surfaces). The cloud chemistry that is involved in HNCO uptake is listed in the series of reactions below, starting with the actual uptake of the gas-phase HNCO into the aqueous phase (cloud):

$$HNCO_{(g)} \rightleftarrows HNCO_{(aq)} \tag{3.2}$$

where it should be noted that this is an equilibrium balanced equation. Once in the cloud, HNCO undergoes ionic dissociation

$$HNCO_{(aq)} \rightleftarrows H_3O^+ + NCO^-. \tag{3.3}$$

From here an equilibrium constant K_{eq} can be expressed as

$$K_{eq} = \frac{[H^+][NCO^-]}{[HNCO\_aq]}. \tag{3.4}$$

This equilibrium expression will be used to calculate the pH of cloud later in this chapter.

The non-equilibrium reactions in the aqueous phase that dictate the loss are:

$$HNCO + H_2O \Rightarrow NH_3 + CO_2 \tag{3.5}$$

$$HNCO + H_3O^+ \Rightarrow NH_4^+ + CO_2 \tag{3.6}$$

$$NCO^- + 2H_2O \Rightarrow NH_3 + HCO_3^- \qquad (3.7)$$

and they collectively govern the rate of hydrolysis of HNCO.

3.4. Cloud Microphysics

3.4.1. Introduction. Cloud microphysics a sub-branch of atmospheric sciences concerned with the many particles that constitute a cloud (Albrecht, 1989). Relative to the cloud as a whole, the individual particles exist on the 'microscale,' and the microscale 'structure' of a cloud, a specification of the number concentrations, sizes, shapes, and phases of the various particles, is important to the behavior and lifetime of the cloud. This scale is where gas phase products like HCNO react. The abilities of clouds to produce rain or snow, generate lightning, and alter the radiation balance of the earth through albedo (Twomey, 1977) is dictated by their microstructures. Cloud physicists, due to the limitation of instrumentation, attempt to characterize the wide range of microstructures theoretically through modeling and simulation (Fowler, Randall, & Rutledge, 1996; Khairoutdinov & Kogan, 2000).

Figure 3.3 is from the cloud microphysics section written by (Lamb, 2003) of the Encyclopedia of Atmospheric Sciences. It shows the range of liquid drops found in clouds (roughly to scale). The terminal fall speeds increase with the size of the species, and the velocities typically determine how the categories are distinguished (though this is obviously not precise). This chapter will be limited to the cloud droplets ~10 μm and smaller.

When only liquid-phase particles are present in a cloud, it is typically called a warm cloud. In the "mixed-phase" region of a cloud, both the liquid and solid phases of water may be present simultaneously. There is a metastable phase where liquid and solid water co-exists and is known as "supercooled" clouds. The relative abundance of each phase in a given cloud depends on the prevailing ambient conditions and the microphysical processes active throughout the lifecycle of the cloud. Warm clouds and supercooled clouds will be described briefly since they are a focus of a portion of the modeling work presented in the following chapters.

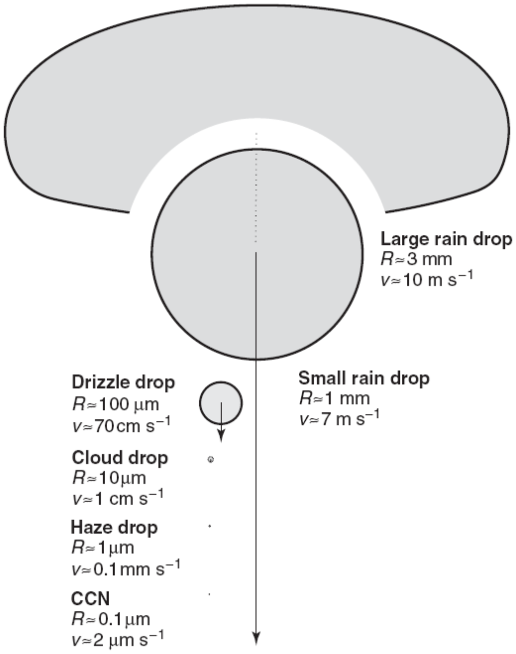

Figure 3.3. Various categories of liquid drops found in clouds. The indicated drop radii (R) are drawn roughly to scale, as are the arrows representing the terminal fallspeeds (v) of the various drop categories. 'CCN' represents a 'cloud condensation nucleus,' a solution droplet that serves as the initial site of condensation. The large raindrop is shown distorted to represent the effect of a large dynamic pressure on its underside (Lamb, 2003)

3.4.2. Water vapor release from biomass burning—Pyro-cumulus clouds. The heated air in a biomass wildfire rises due to convection, sending water vapor released during combustion into the atmosphere. There can be intense updrafts of warm air into cooler air, and horizontal winds which could shape and drive the formation and dynamics of pyro-cumulus clouds.

The moisture content from fresh vegetation contributes significantly to the water vapor in biomass burning emissions (Parmar, Welling, Andreae, & Helas, 2008), and its influence on the cloud microphysics of fire plumes and pyro-cumulus clouds need to be evaluated. This is the focus of one phase of the modeling results mentioned later. Water vapor production from biomass burning is generally considered to have little effect on atmospheric water vapor concentration. On a local scale, however, large open fires can trigger cloud formation and may even lead to thunderstorms (Fromm, Tupper, Rosenfeld, Servranckx, & McRae, 2006). It is not clear what role water vapor released from biomass combustion plays in the atmospheric conditions above the fire (Potter, 2005; Trentmann et al., 2006). This is therefore an attempt to model the interaction of HNCO in clouds under these pyro-cumulus conditions.

Figure 3.4 is a photo of a smoke plume produced from a prescribed fire about 100 minutes after ignition. It depicts the obvious merging and influence on normal cumulus clouds in the lower troposphere. Figure 3.5 (Trentmann et al., 2006) shows the temperature and humidity dependence due to altitude. These will prove to be critical parameters in the model.

Figure 3.4. Photograph of the smoke plume produced from the Quinault prescribed fire at 1250 LT, at about 100 min after the ignition (photo taken by R. Ottmar, reproduced from Kaufman et al., 1996)

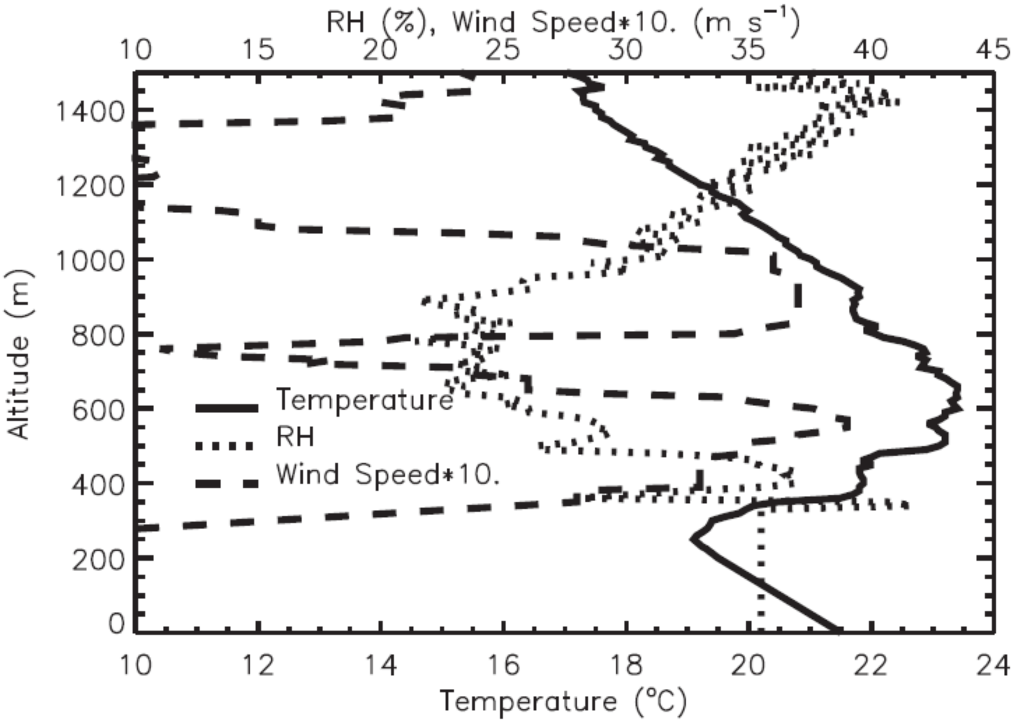

Figure 3.5. Initial atmospheric profiles of the temperature (lower axis), relative humidity (RH) (upper axis), and wind speed (upper axis) up to an altitude of 1.5 km used in the model simulations. Above 320 m, aircraft measurements are used (Trentmann et al., 2006)

3.4.3. Supercooled clouds. Supercooled clouds exist at higher altitudes and lower temperatures in the upper troposphere (Cantrell & Heymsfield, 2005). These are clouds containing pure water droplets at temperatures considerably below the nominal freezing temperature of 0°C. Though the upper troposphere is generally characterized by homogeneous nucleation (Heymsfield & Sabin, 1989), meaning that mostly liquid water or ice constitutes the medium and does not require an aerosol with which to form. However, **heterogeneous** nucleation is where CCN can be the source of nucleation in the presence of ice and water (DeMott et al., 1998). At high enough concentrations such as from a biomass fire, isocyanic acid can be transported to the upper troposphere given that it only reacts in the aqueous phase, thus it needs to be modeled under such conditions.

Figure 3.6, from the Cantrell review (Cantrell & Heymsfield, 2005), is a plot of both calculated nucleation rates for temperatures of upper tropospheric interest, along with actual experimental data from several laboratories. The calculated nucleation rates are in reasonable agreement with the data for temperatures greater than -38°C. At the lower temperatures the Pruppacher's calculation is up to two orders of magnitude lower than the measurements, but at the moment it seems that the theories and their representations in models are adequate to predict homogeneous nucleation rates for water droplets in the atmosphere. Isocyanic acid will be modeled under cirrus cloud conditions in these temperature ranges, but the water content of nuclei in this region can vary and one has to question whether it is truly in a heterogeneous nucleation medium when supercooled.

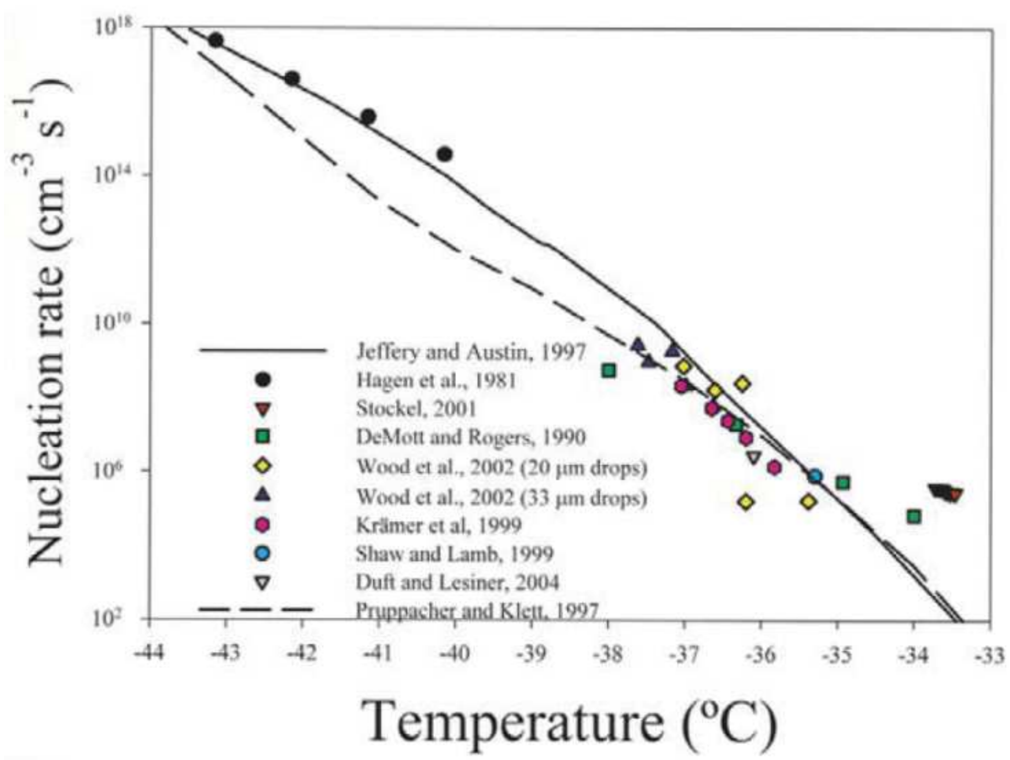

Figure 3.6. Calculated nucleation rates using data from several experiments. All of the data taken from experiments are from suspended or freely falling droplets (reproduced from Cantrell & Heymsfield, 2005)

3.5. The Cloud Box Model

Chemical models are designed to give us a better understanding of atmospheric chemistry, and for predicting the future state of the chemicals such as HNCO in the atmosphere. A model contains different modules to treat processes such as gas-phase chemistry, photolysis, aqueous phase chemistry, and heterogeneous chemistry. In some cases even the emission and deposition of chemical species can be modeled.

The most recent review of the state-of-the-art numerical modeling of cloud microphysics was conducted by Khain et al. (Khain, Ovtchinnikov, Pinsky, Pokrovsky, & Krugliak, 2000). They highlight the problem and limitations in the numerical models and gaps and uncertainty in the field of cloud microphysics. For example, assuming contact nucleus size of 0.3–0.5 microns, a concentration of 10^5 to 10^6 m^3 for nuclei active at -4^oC was deduced. The fact that the droplet size, water content, and acidity have such wide distributions in cloud microphysics makes it difficult to model gas phase species such as HNCO.

The cloud chemical box model used here (Barth, 2006; Barth et al., 2003) is based on the chemical continuity equation (Equation 3.8), which expresses the rate of change of a chemical species concentration. Integration of Equation 3.8 allows the concentration to be modeled forward in time, where C is the species concentration, P is the chemical production rate of C and L is the first order loss of C.

$$\frac{dC}{dt} = P - LC \tag{3.8}$$

Figure 3.7 is modified from the numerical models section in Chipperfield (2003) and it depicts the overall picture of the chemical model and where the continuity equation is the central component. In this work, we are only concerned with the aqueous phase heterogeneous/aqueous chemistry since HNCO does not readily undergo and gas phase chemical reactions or photolysis (Roberts et al., 2011).

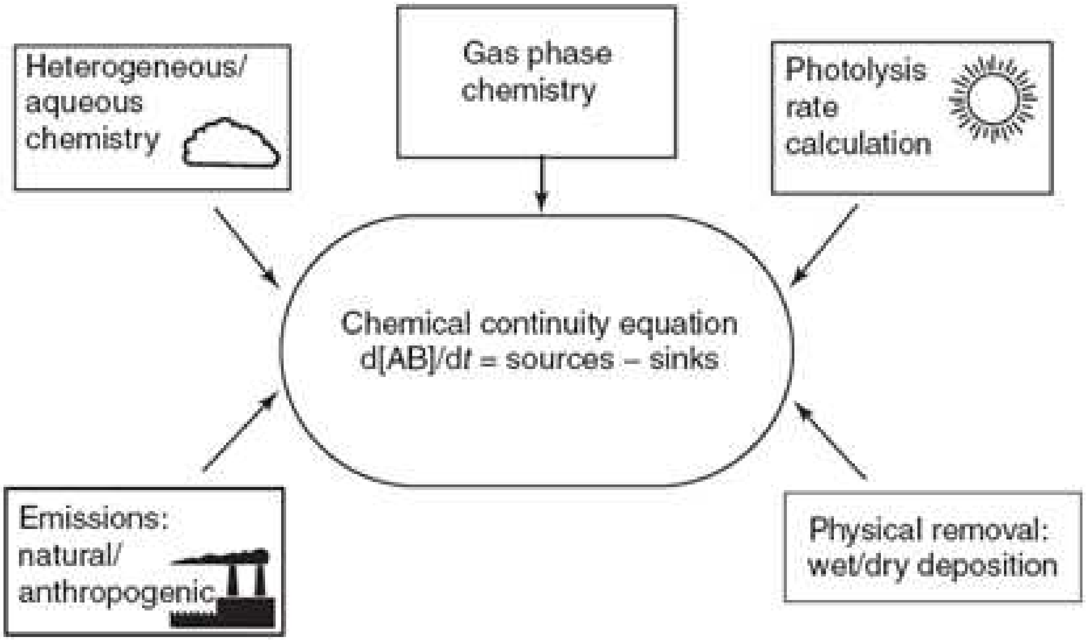

Figure 3.7. Modified components of an atmospheric chemical model (Chipperfield, 2003). A multidimensional model will also include dynamical and radiation modules. These may be combined so that the chemistry is or is not coupled

The model used here for aqueous-phase characterization of HNCO is a modified version of the Barth-EBI (Euler Backward Iterative) method (Barth et al., 2003). Equation 3.9 is the EBI equation and it solves the continuity Equation (3.8)

$$\mathrm{C}_{\mathrm{n+1,i+1}} = \frac{C_n + P_{n+1,i}\Delta t}{1 + L_{n+1,i}\Delta t}. \tag{3.9}$$

In this equation, Δt is duration of each timestep, n is the time step, n+1 is the next time step. C, P, and L are vector ensembles of individual species from Equation 3.8.

According to Barth et al. (2003), since P and L depend on the concentrations of different species, a Gauss-Seidel procedure is followed where current concentrations from the previous time step are used an initial guess to calculate concentrations at the new time step and first iteration. Then the new concentrations are used to calculate P and L for the next time step and iteration. If all the species converge (i.e., the concentration at consecutive iterations are nearly the same) then the species' concentrations have been determined for the current time step, otherwise the process is repeated. The Barth-EBI uses a 0.01% threshold convergence criterion to terminate the iterations for all species.

The next section describes how HNCO and cloud acidity calculations were added to the Barth-EBI model to in order to generate a more accurate cloud modeled representation. Extended details of the calculations and programming involved can be found in the appendices.

3.6. Methods and Results

In order to use the Barth-EBI model for modeling the fate and transport of HNCO in the troposphere, the following steps must be achieved:

1. All relevant reactions in the gas and aqueous phase must be identified
2. The cumulative rate constant must be calculated in each phase
3. The Henry's coefficient and heterogeneous uptake calculations must be made
4. The model FORTRAN code must be modified accordingly
5. Proper input parameters must be chosen and assumptions identified

Appendix A lists the coded species included in the Barth-EBI model. As mentioned earlier in section 3.3.1 when the cloud chemistry was discussed, it was noted that there are not expected to be any gas-phase chemical reactions nor photolysis involved with HNCO. Comparing the rate constants in the Tables 3.2 and 3.3, it is apparent that the reactions occurring in the aqueous phase are much slower and therefore are the rate limiting steps in the process of heterogeneous uptake of HNCO from the gas to condensed phase.

The next step is to identify all of the relevant reactions (both equilibrium and non-equilibrium). It is also shown in section 3.3.1 that the equilibrium processes of HNCO are dissociation (3.3) and partitioning into the aqueous phase (3.2). These equilibrium reactions do not contribute to any loss of HNCO. Three equations associated with the hydrolysis of HNCO (3.5 to 3.7) are the actual loss mechanisms of HNCO in the aqueous phase. Tables 3.2, 3.3, and 3.4 list the gas phase, aqueous phase, and equilibrium reactions (respectively) that are taken into consideration in the code. Table 3.5 lists the additional aqueous phase reactions needed in order to characterize HNCO.

Table 3.2

Gas phase reactions in the Barth-EBI model

Number	**Reaction**	**k_{298} [a]**	**-E/ R**
(G1)	$O_3 + h\upsilon \rightarrow O(1D) + O_2$	4.0 x 10^{-5}	0
(G2)	$O(1D) + M \rightarrow M + O_3$	2.9 x 10^{-11}	-100
(G3)	$O(1D) + H_2O \rightarrow 2OH$	2.2 x 10^{-10}	0
(G4)	$HO_2 + O_3 \rightarrow OH + 2O_2$	2.0 x 10^{-15}	500
(G5)	$OH + O_3 \rightarrow HO_2 + O_2$	6.8 x 10^{-14}	940
(G6)	$HO_2 + OH \rightarrow H_2O + O_2$	1.1 x 10^{-10}	-250
(G7)	$HO_2 + HO_2 \rightarrow H_2O_2 + O_2$	k_a =1.7 x 10^{-11} [b]	-600
		k_b =4.9 x 10^{-32}	-1000
		k_c = 2.24 x 10^{-18}	-2200
(G8)	$H_2O_2 + h\upsilon \rightarrow 2OH$	9.2 x 10^{-6}	0
(G9)	$H_2O_2 + OH \rightarrow HO_2 + H_2O$	1.7 x 10^{-12}	160
(G10)	$NO + O_3 \rightarrow NO_2 + O_2$	1.8 x 10^{-14}	1400
(G11)	$HO_2 + NO \rightarrow OH + NO_2$	8.1 x 10^{-12}	-250
(G12)	$NO_2 + h\upsilon \rightarrow NO + O_3$	9.4 x 10^{-3}	0
(G13)	$OH + NO_2 + M \rightarrow HNO_3 + M$	k_o =2.5 x 10^{-30} $(T/300)^{-4.4}$	
		k_∞ =1.6 x $10^{-11}$$(T/300)^{-1.7}$	
(G14)	$HNO_3 + h\upsilon \rightarrow OH + NO_2$	6.5 x 10^{-7}	0
(G15)	$NO_2 + O_3 \rightarrow NO_3 + O2$	3.2 x 10^{-17}	2500
(G16)	$NO_3 + h\upsilon \rightarrow .92\ NO_2 + .08\ NO + .92\ O_3$	9.4 x 10^{-1}	0
(G17)	$NO_3 + NO \rightarrow 2NO_2$	2.6 x 10^{-11}	-170
(G18)	$NO_3 + NO_2 + M \rightarrow N_2O_5 + M$	k_o =2.2 x 10^{-30} $(T/300)^{-3.9}$	
		k_∞ =1.5 x 10^{-12} $(T/300)^{-0.7}$	

Table 3.2 *(cont.)*

Number	Reaction	k_{298} [a]	-E/R
(G17)	$NO_3 + NO \rightarrow 2NO_2$	2.6×10^{-11}	-170
(G18)	$NO_3 + NO_2 + M \rightarrow N_2O_5 + M$	$k_o = 2.2 \times 10^{-30}\ (T/300)^{-3.9}$ $k_\infty = 1.5 \times 10^{-12}\ (T/300)^{-0.7}$	
(G19)	$N_2O_5 + M \rightarrow NO_3 + NO_2 + M$	$K_{G19} = 2.9 \times 10^{-11}$	11,000
(G20)	N_2O_5 + hυ → $NO_3 + NO_2$	k = k_{G18} / K_{G19} 5.1 x 10-5	 0
(G21)	$CH_4 + OH + O_2 \rightarrow CH_3OO + H_2O$	6.3×10^{-15}	1800
(G22)	$CH_3OO + NO + O_2 \rightarrow CH_2O + NO_2 + HO_2$	7.7×10^{-12}	-280
(G23)	$CH_3OO + HO_2 \rightarrow CH_3OOH + O_2$	5.6×10^{-12}	-800
(G24)	$CH_3OO + HO_2 \rightarrow CH_2O + H_2O + O_2$	2.0×10^{-12}	0
(G25)	$CH_3OO + CH_3OO + O_2 \rightarrow 2CH_2O + 2HO_2$	4.7×10^{-13}	-190
(G26)	CH_3OOH + hυ + O_2 → $CH_2O + OH + HO_2$	8.7×10^{-6}	0
(G27)	$CH_3OOH + OH \rightarrow .7\ CH_3OO + .3\ CH_2O + .3\ OH$	7.4×10^{-12}	-200
(G28)	CH_2O + hυ + 2 O_2 → CO + 2 HO_2	3.6×10^{-5}	0
(G29)	CH_2O + hυ → CO + 2 H_2	5.0×10^{-5}	0
(G30)	$CH_2O + OH + O_2 \rightarrow CO + HO_2 + H_2O$	1.0×10^{-11}	0
(G31)	$CH_2O + NO_3 + O_2 \rightarrow CO + HNO_3 + HO_2$	5.8×10^{-16}	0
(G32)	$CO + OH + O_2 \rightarrow CO_2 + HO_2$	2.4×10^{-13}	0
(G33)	$HCOOH + OH + O_2 \rightarrow CO_2 + HO_2 + H_2O$	4.3×10^{-13}	0

[a] Units for the photolysis frequencies are s^{-1}, for the second-order reaction rate constants are cm^3 $molecules^{-1}$ s^{-1}, and for the third-order reaction rate constants are cm^6 $molecules^{-2}$ s^{-1}.

[b] Here, the rate constant is of the form $k = (k_a + k_b [M]) (1 + k_c[H2O])$ where $[H_2O]$ is the water vapor concentration.

Table 3.3

Aqueous-phase reactions

Number	Reaction	k_{298} [a]	-E/R
(A1)	O_3+hυ+H_2O→H_2O_2+O_2	6.0×10^5	
(A2)	H_2O_2+hυ↔2OH	1.4×10^5	
(A3)	$CH_2(OH)_2+OH+O_2 \rightarrow HCOOH+HO_2+H_2O$	2.0×10^9	1500.
(A4)	$HCOOH+OH+O_2 \rightarrow CO_2+HO_2+H_2O$	1.6×10^8	1500.
(A5)	$HCOO+OH+O_2 \rightarrow CO_2+HO_2+OH^-$	2.5×10^9	1500.
(A6)	$CH_3OO+O_2^-+H_2O \rightarrow CH_3OOH+OH^-+O_2$	5.0×10^7	1600.
(A7)	$CH_3OOH+OH \rightarrow CH_3OO+H_2O$	2.7×10^7	1700.

Table 3.3 *(cont.)*

Number	Reaction	k_{298} [a]	-E/R
(A8)	$CH_3OOH+OH \rightarrow CH_2(OH)_2+OH$	1.9×10^{7}	1900
(A9)	$HO_2+O_2^- \rightarrow HO_2^-+O_2$	1.0×10^{8}	1500
(A10)	$HO_2^-+H^+ \rightarrow H_2O_2$	5.0×10^{10}	1500
(A11)	$OH+OH \rightarrow H_2O_2$	5.2×10^{9}	1500
(A12)	$O_3+O_2^-+H_2O \rightarrow OH^-+2O_2+OH$	1.5×10^{9}	1500
(A13)	$O_3+OH^- \rightarrow HO_2+O_2+OH^-$	3.0×10^{9}	1500
(A14)	$H_2O_2+OH \rightarrow HO_2+H_2O$	2.7×10^{7}	1700
(A15)	$OH+O_2^- \rightarrow OH^-+O_2$	1.0×10^{10}	1500
(A16)	$HCO_3^-+OH \rightarrow CO_3^-+H_2O$	1.0×10^{7}	1500
(A17)	$HCO_3^-+O_2^- \rightarrow CO_3^-+HO_2^-$	1.5×10^{6}	1500
(A18)	$CO_3+H_2O_2 \rightarrow HCO_3+HO_2$	8.0×10^{5}	2800

[a] Units for the photolysis frequencies are s^{-1}, for the second-order reaction rate constants are cm^3 $molecules^{-1}$ s^{-1}. Reaction rates are of the form $k = k_{298} \exp[-E/R(1/T - 1/298)]$.

Table 3.4

Equilibrium coefficients[a]

Number	Reaction	k_{298}	ΔH/R
	Henry's Law Equilibria		
(E1)	$O_3(g) \leftrightarrow O_3(aq)$	1.1×10^{-2}	2300
(E2)	$H_2O_2(g) \leftrightarrow H_2O_2(aq)$	8.3×10^{4}	7400
(E3)	$OH(g) \leftrightarrow OH(aq)$	3.0×10^{1}	4500
(E4)	$HO_2(g) \leftrightarrow HO_2(aq)$	4.0×10^{3}	5900
(E5)	$CH_3OO(g) \leftrightarrow CH_3OO(aq)$	5.0×10^{0}	5600
(E6)	$CH_3OOH(g) \leftrightarrow CH_3OOH(aq)$	3.1×10^{2}	5200
(E7)	$CH_2O(g) \leftrightarrow H_2C(OH)_2(aq)$	3.2×10^{3}	6800
(E8)	$HCOOH(g) \leftrightarrow HCOOH(aq)$	5.4×10^{3}	5700
(E9)	$NO(g) \leftrightarrow NO(aq)$	1.9×10^{-3}	1500
(E10)	$NO_2(g) \leftrightarrow NO_2(aq)$	6.4×10^{-3}	2500
(E11)	$HNO_3(g) \leftrightarrow HNO_3(aq)$	2.4×10^{6}	8700
(E12)	$N_2O_5(g) \rightarrow 2HNO_3(aq)$	1.0×10^{12}	0
(E13)	$NO_3(g) \leftrightarrow NO_3(aq)$	1.8×10^{0}	2000

Table 3.4 *(cont.)*

Number	Reaction	k_{298} [a]	-E/R
(E14)	$CO_2(g)\leftrightarrow CO_2(aq)$	$3.6\text{x}10^{-2}$	2200
	Acid Dissociation Equilibria		
(E15)	$H_2O_2(aq)\leftrightarrow HO_2^-+H^+$	$2.2\text{x}10^{-12}$	3700
(E16)	$HO_2(aq)\leftrightarrow O_2^-+H^+$	$3.5\text{x}10^{-5}$	0
(E17)	$HCOOH(aq)\leftrightarrow HCOO^-+H^+$	$1.8\text{x}10^{-4}$	1500
(E18)	$HNO_3(aq)\leftrightarrow NO_3^-+H^+$	$1.5\text{x}10^{0}$	0
(E19)	$CO_2(aq)\leftrightarrow HCO_3^-+H^+$	$4.5\text{x}10^{-7}$	1000
(E20)	$Cl_2^-(aq)\leftrightarrow Cl^-+Cl(aq)$	$5.3\text{x}10^{-6}$	0

[a] Units for the solubility constants are M atm^{-1}, and units for dissociation constants are M. Coefficients are of the form $k = k_{298} \exp[-\Delta H/R(1/T - 1/298)]$.

Table 3.5

Hydrolysis reactions involving HNCO in the aqueous-phase[a]

Number	Reaction	k298	-E/R
(A1)	$HNCO + H_2O \rightarrow NH_3 + CO_2$		
(A2)	$NCO^- + 2H_2O \rightarrow NH3 + HCO_3^-$	$kI^b = 7.8 \times 10^{-4}\ sec^{-1}$	0
(A3)	$HNCO + H_3O^+ \rightarrow NH_4+ + CO_2$	$kII = 6.0 \times 10^{-2}\ M^{-1}\ sec^{-1}$	1500

[a] Reaction rates are of the form $k = k_{298} \exp[-E/R(1/T - 1/298)]$.
[b] kI is the sum of A1 and A2

In order to model heterogeneous uptake of gas, knowledge of Henry's coefficient characterizing the solubility of HNCO is necessary. However, these measurements have not yet been made experimentally. Instead, equations 3.10 and 3.11 were used to extrapolate measured Henry's coefficient values to values under different conditions. These equations are described in greater detail in Sander (Sander, 1999), but in brief, equation 3.10 is the expression for the effective Henry's coefficient (H_{eff}) as a function of pH is

$$H_{eff} = H^*\left(1+\frac{K_a}{[H^+]}\right), \tag{3.10}$$

where H* is the intrinsic Henry's coefficient, K_a is the dissociation constant (equation 3.4) and $[H^+]$ is the hydrogen ion concentration (in mol L^{-1} or M), which equals 10^{-pH}.

$$H^* = H^{\theta} e^{\left(-\frac{\Delta H}{R}\left[\frac{1}{T}-\frac{1}{T^{\theta}}\right]\right)} \tag{3.11}$$

The intrinsic Henry's coefficient is also described by Sander (Sander, 1999), and mainly describes the temperature dependence. Here $H^{\square}$ is H at standard temperature (298 K), ΔH is the enthalpy of dissolution, R is the gas constant, T is temperature and $T^{\square}$=298 K. After measuring the effective H for isocyanic acid in an aqueous buffer at pH=3.0 and room temperature, as detailed in Chapter 2, the written code was tested to verify that it reproduces the expected decrease in H_{eff} with increasing temperature. As shown in Figure 3.8 where for a given pH, as the temperature increase from 253 K to 298 K H_{eff} decreses which translates to an increase in solubility.

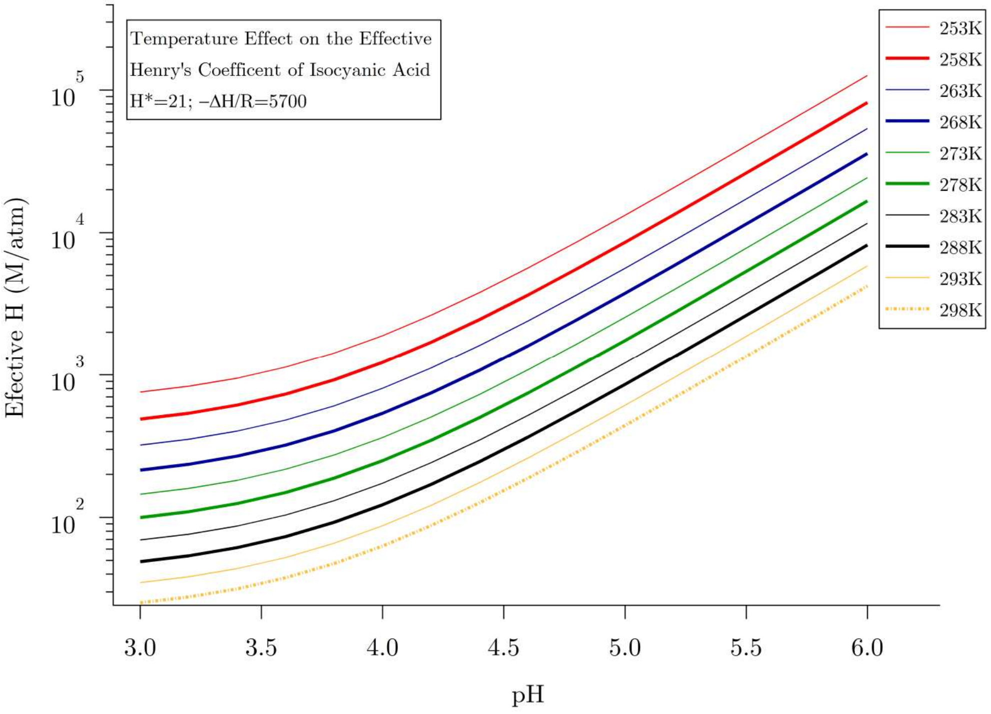

Figure 3.8. Effective H versus pH versus temperature

The next phase of incorporating HNCO into the model is to establish the overall reaction rate of it in solution. Appendix C details the first step to this calculation, where the "family" of aqueous HNCO is defined as:

$$[HNCO\_aqfam] = [HNCO\_aq] + [NCO^-] \tag{3.12}$$

where $[HNCO\_aq]$ is the aqueous HNCO concentration and $[NCO^-]$ is the isocyanate ion concentration. The appendix goes through the calculation to arrive at the fraction or weight of each to the HNCO family. From the rate expression of each reaction (3.5-3.7 and Appendix C), the time derivative (rate of change) of the total $[HNCO\_aqfam]$ can be derived obtaining Equation 3.13:

$$\frac{d[HNCO\_aqfam]}{dt} = -k_1\frac{[H^+]}{[H^+]+K_{eq}}[HNCO\_aqfam] - k_2\frac{[H^+]}{[H^+]+K_{eq}}[HNCO\_aqfam][H^+] - k_3\frac{K_{eq}}{[H^+]+K_{eq}}[HNCO\_aqfam] \tag{3.13}$$

which is entered directly into the code for obtaining the HNCO concentrations. Appendix D shows the portion of the code created to solve equation 3.13. Subsection 3.7.1 is the set of model results analyzed for the static pH case. Subsection 3.7.2 describes the improved results for the case of a dynamic pH that is calculated at each timestep. A contrast and comparison of the two cases is made in the conclusion.

3.6.1. Model output with static pH. As expected, the partitioning and reactivity of isocyanic acid was highly sensitive to the acidity of a cloud due Henry's law and the pH dependant reaction rates. Removal of HNCO was sensitive to the liquid water content due to the volume of liquid in which HNCO can be taken up and reacted. One unanswered question is how certain the extent to which the temperature will have on the system. Therefore this and other sensitivity studies were modeled. The model input parameter unless otherwise noted are:

- Particle size = 10 micron
- Temperature = 20 °C (293K) (ranging from 233K to 293K)
- pH = 4.5 (ranging from 3 to 6)
- Liquid water content 0.05g/kg (air) (ranging from 0.05 to 1.3)
- Pressure = 850 hPa

Figure 3.9 shows the dramatic effect that the prescribed cloud acidity (pH) has on the initial gas phase concentration of 10 pptv HNCO as it traverses a cloud. The different slopes indicate that hydrolysis reactions are occurring much more rapidly, and thus less HNCO will remain at the end of the cloud. These slopes are directly related to the lifetime of HNCO if it were to remain in the cloud continuously. The lifetime estimates are plotted for each pH value in Figure 3.10. It should be noted that there is excellent agreement with these lifetimes and the lifetimes estimated from Roberts et al. (2011) shown in Figure 3.11.

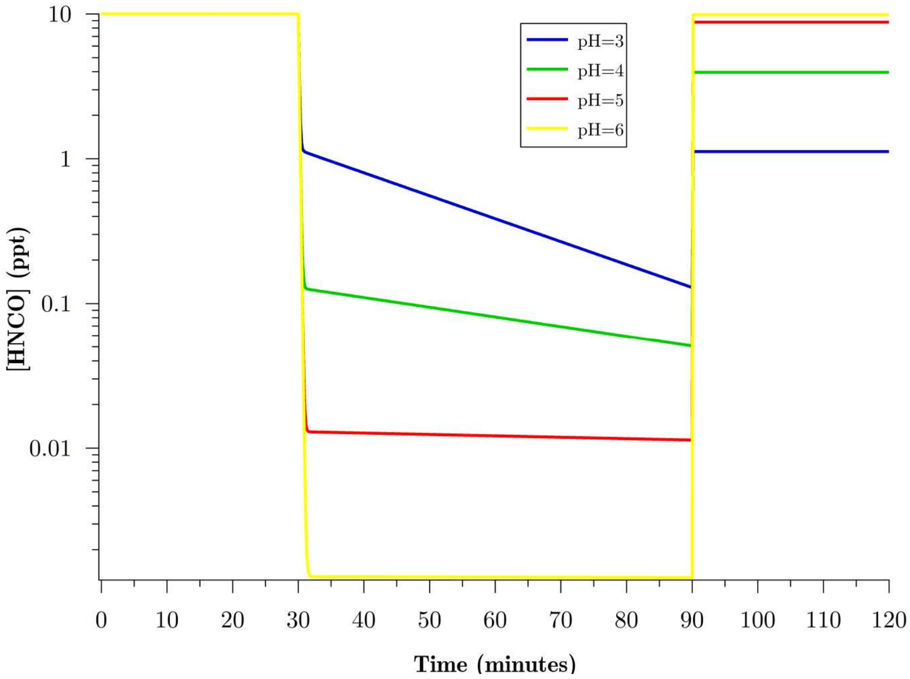

Figure 3.9. The uptake and removal of HNCO in simulated clouds of varying pH, as a function of cloud exposure time

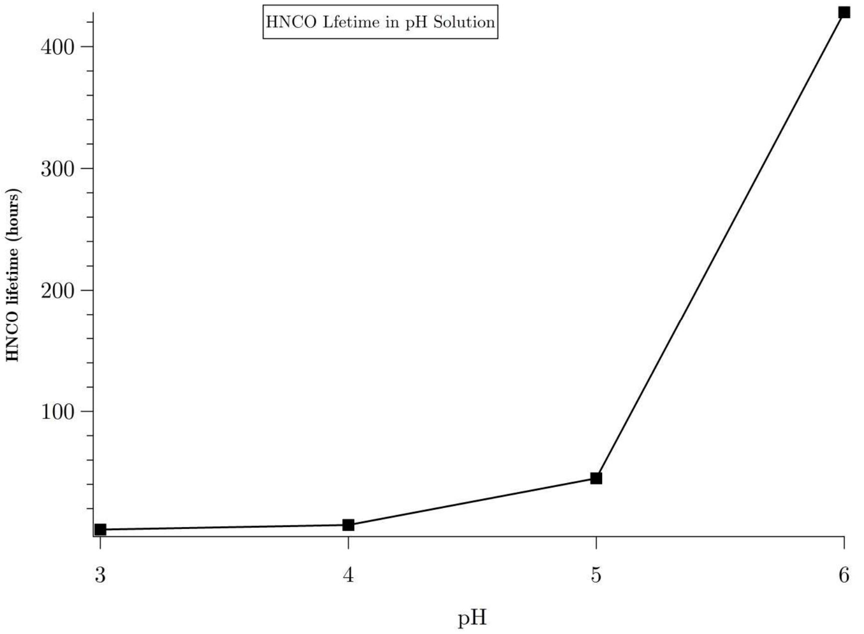

Figure 3.10. HNCO lifetimes versus pH

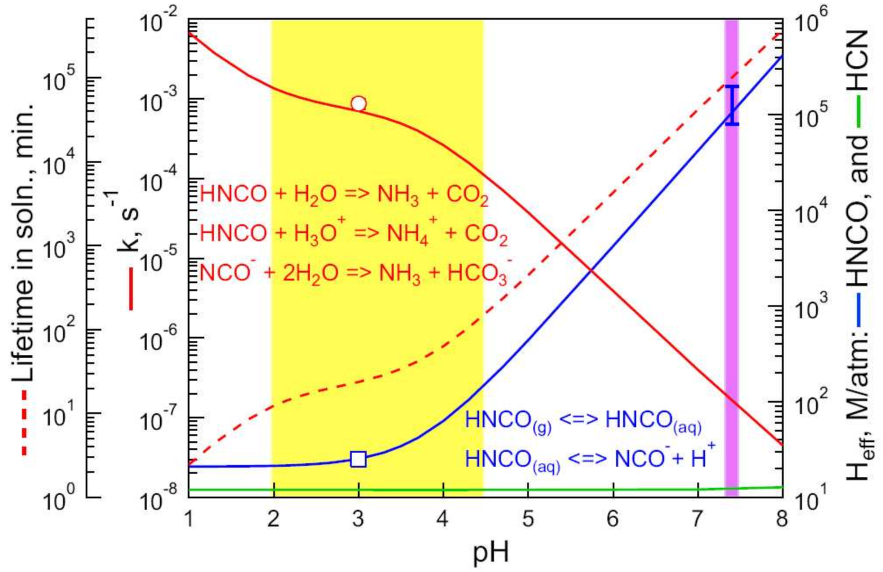

Figure 3.11. Plots of the Henry's Law constant (blue), first order loss rate due to hydrolysis (solid red), and aqueous phase lifetime (dashed red) of HNCO versus pH. Also shown is the Henry's Law constant for HCN (green). The yellow band indicates the range of pHs most characteristic of ambient aerosol, and the pink band indicates physiological pH. Clouds are typically in the pH=3 to 6 range (image from the addendum to Roberts et al., 2011)

Table 3.6 shows the in-cloud reaction rate results extracted from the HNCO concentration sensitivity study in Figure 3.12. The rate constants are obtained by taking a sample from the aqueous phase reaction window (between 30 and 90 minutes) of the simulation. Since the HNCO concentration is decaying exponentially within this reaction window, it is easy to extract the rate constant by simply taking the natural log of the inverse of the selected data. The slope of the resulting data is the rate constant (k) in units of time^{-1}. The in-cloud lifetime tau (τ) is the inverse of τ are plotted in Figure 3.13 versus the concentration. The lifetimes can all be seen to be within statistical agreement with each other with an average of 16.39 ± .29 hours. This method is used in the remainder of the thesis for extracting in-cloud lifetime estimates for HNCO.

Table 3.6

In-cloud reaction rates at different concentrations

Concentration (pptv)	**k(min^{-1})**	**1σ (min^{-1})**
35	0.0010191	$1.74\text{x}10^{-06}$
500000	0.0010098	$5.12\text{x}10^{-07}$
100	0.0010077	$3.89\text{x}10^{-07}$
200	0.0010066	$2.18\text{x}10^{-07}$
100000	0.0010533	$3.38\text{x}10^{-07}$
10000	0.0010059	$3.86\text{x}10^{-07}$

Figure 3.14 is a gas-phase study of HNCO temperature sensitivity in clouds using 100 pptv of HNCO, a water content of .05 g/m^3 and a 10 micron droplet size. It is qualitatively apparent that at increased temperatures, much more HNCO is taken up into the aqueous-phase but is essentially released back into the gas-phase. This indicates that the temperature does not dramatically affect the reaction rate in the condensed phase.

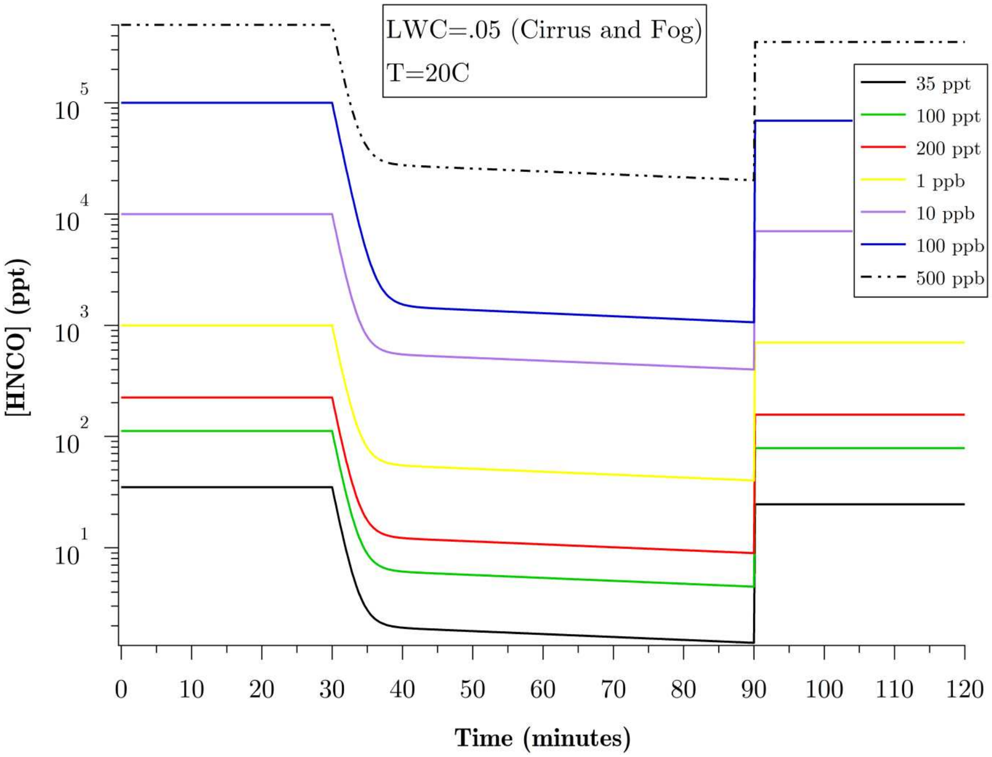

Figure 3.12. Gas-phase cloud processing of HNCO at multiple concentrations, with a LWC of 0.05 g/m^3 at 20 °C and a pH of 4.5

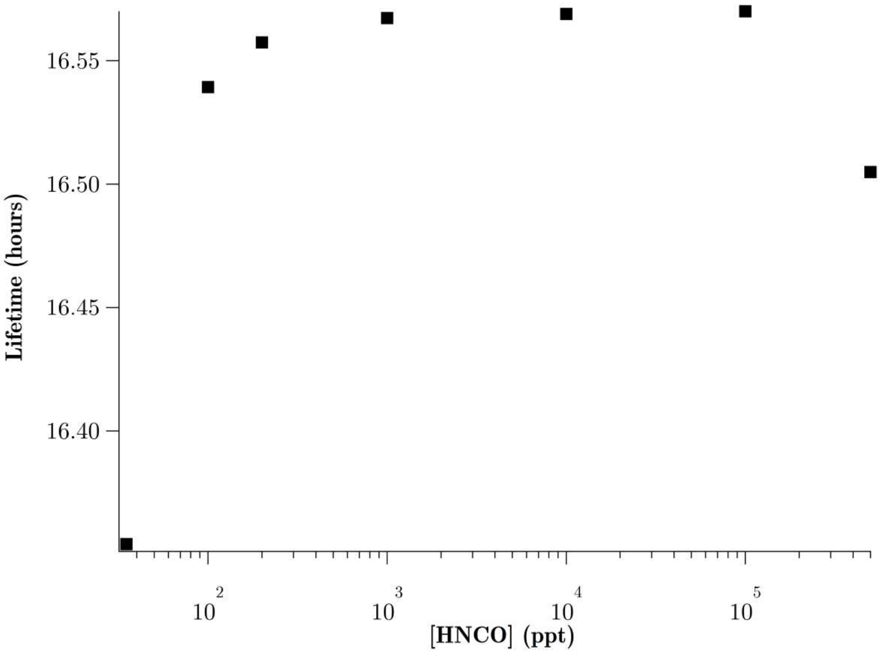

Figure 3.13. In-cloud lifetimes versus concentration

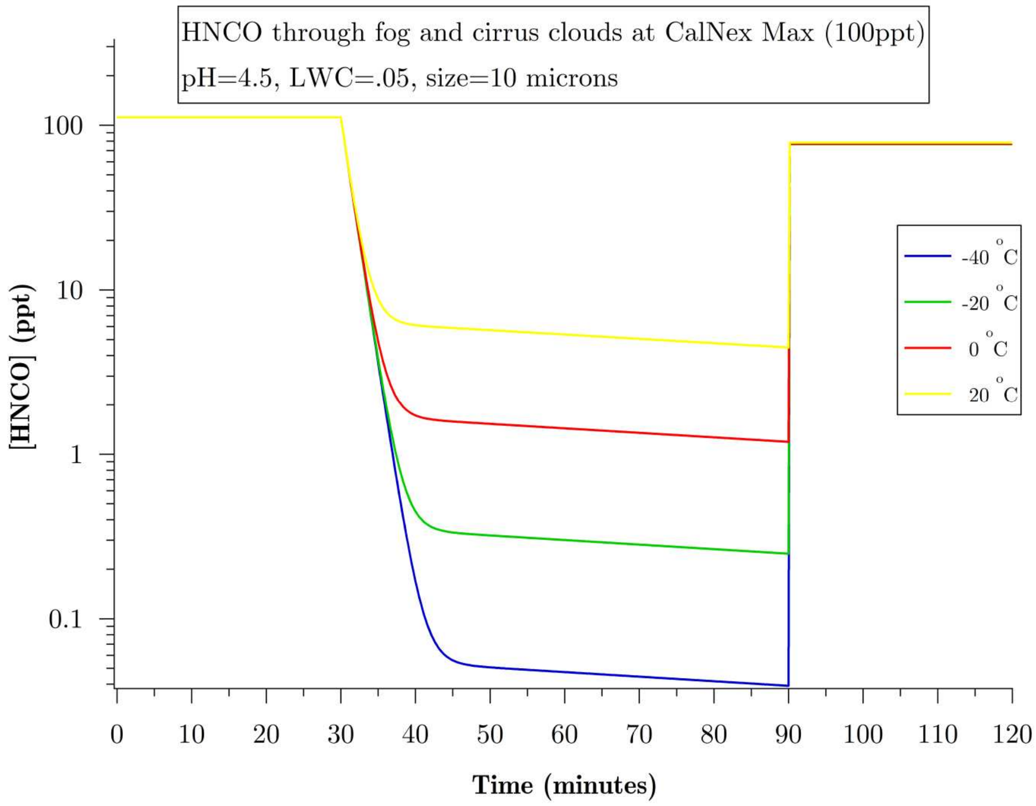

Figure 3.14. Temperature effect on uptake and reaction of HNCO

Figure 3.15 shows the temperature dependence of the lifetime and this is due to the temperature dependence of the effective Henry's law coefficient. There appears to be a small increase with increasing temperature, but it would only be on the order of about 60 minutes.

The liquid water content sensitivity as shown in Figure 3.16 shows two different stages of equilibrium. With increasing LWC, the rate of HNCO uptake is increased and a shorter amount of time elapses before equilibrium is reached. The initial slopes (within the first 10 minutes) associated with condensed-phase chemistry are altered and the rest of the reaction time the slopes remain the same therefore the loss of HNCO should be the same. This is why the final HNCO concentration is essentially the same. This makes sense, in that for a given droplet size, LWC would scale linearly with the number of droplets and, therefore, liquid surface area. Once in solution, though, all conditions relevant to the reaction rate (see Equation 3.13) are consistent.

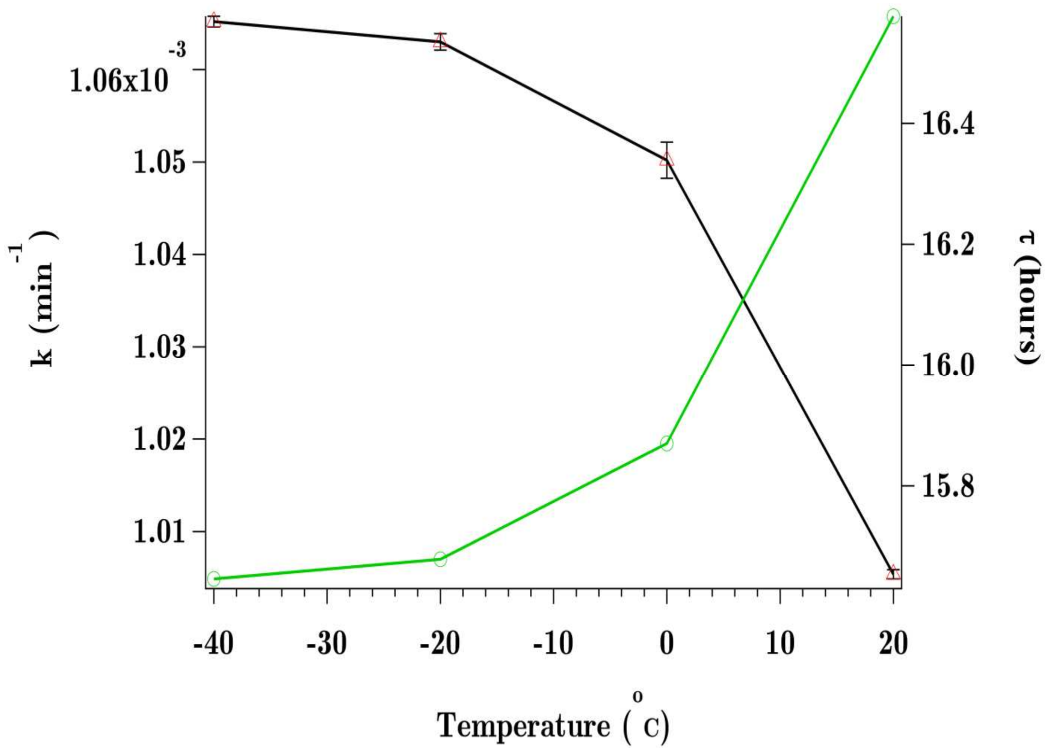

Figure 3.15. Temperature dependence of the HNCO rate constant (black) and lifetime (green)

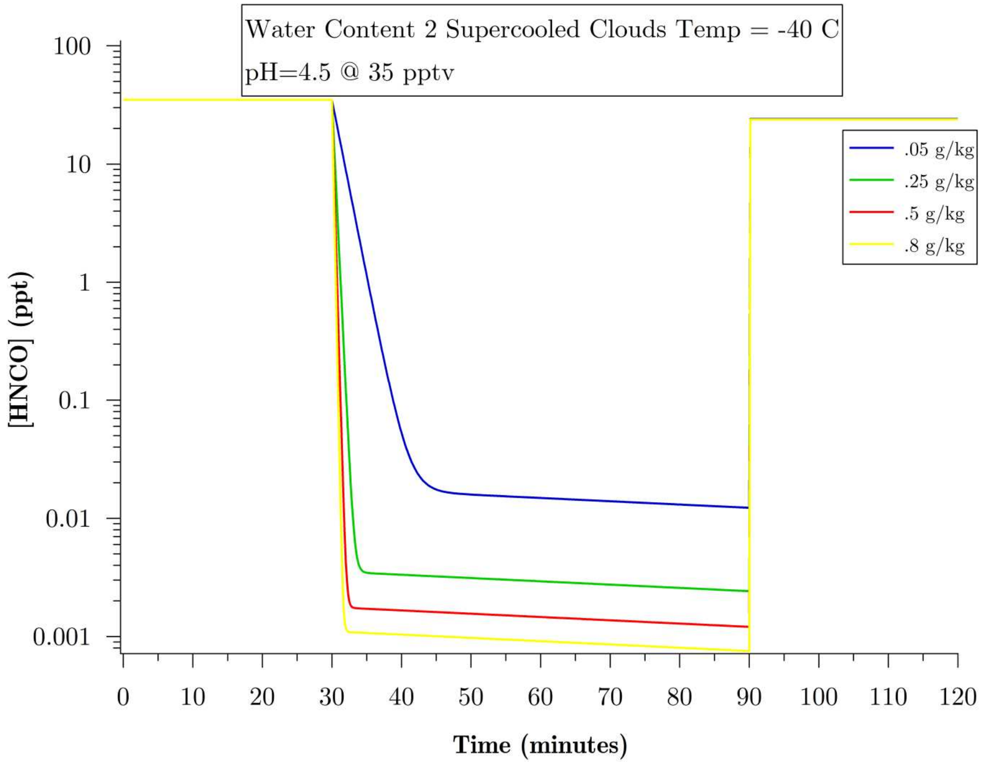

Figure 3.16. Liquid water content sensitivity, saturation times affected

3.6.2. Dynamic pH modeling. The more accurate way to model HNCO in the troposphere is to know the time dependent nature of the acidity (pH) of each cloud that a parcel encounters. The first step in making this calculation is to come up with an expression that accounts for all of the significant ionic (charged) species in the aqueous cloud chemistry. The full charge balance equation used is

$$\begin{aligned}&[H_3O^+]+[NH_4^{\,+}]=2[SO_4^{\,2-}]+[HSO_3^{\,-}]+2[SO_3^{\,2-}]+[NCO^-]+[HCO_3^{\,-}]\\&+[OH^-]+[O_2^{\,-}]+[HO_2^{\,-}]+[CO_3^{\,-}]+[NO_3^{\,-}]+[HCOO^-]\end{aligned} \tag{3.14}$$

It is assumed that the ammonium concentration is approximately equal to one unit of the sulfate ion therefore the final charge balance equation becomes

$$\begin{aligned}&[H_3O^+]=[SO_4^{\,2-}]+[HSO_3^{\,-}]+2[SO_3^{\,2-}]+[NCO^-]+[HCO_3^{\,-}]\\&+[OH^-]+[O_2^{\,-}]+[HO_2^{\,-}]+[CO_3^{\,-}]+[NO_3^{\,-}]+[HCOO^-]\end{aligned} \tag{3.15}$$

where H_3O^+ is hydronium ion concentration which is related to the aqueous phase pH of the cloud.

Each of these ions can be expressed in terms of their acid dissociations and Appendix E contains a definition of each term needed to evaluate the overall acidity in a cloud under equilibrium conditions. The cloud model is initially based on gas-phase reactions and then aqueous phase reactions are modeled due to heterogeneous uptake of gas species into the condensed phase. Equations 3.16 to 3.18 shows the calculation of one of the charged species' $[NH_4^+]$ concentration needed in the charge balance equation. The dissociation equilibrium reaction and the heterogeneous equilibrium reaction is necessary to solve for $[NH_4^+]$.

$$K_{NH_4^+}=\frac{[NH_3(aq)][H^+]}{[NH_4^{\,+}]} \tag{3.16}$$

$$[NH_3(aq)]=H_{NH_3}[NH_3(g)] \tag{3.17}$$

$$[NH_4^+] = \frac{H_{NH_3}[NH_3(g)][H^+]}{K_{NH_4^+}} \tag{3.18}$$

where K_{NH4^+} is the dissociation constant, H_{HN_3} is Henry's coefficient for ammonia and the remaining bracketed terms are the concentrations of each species. The summation of all of the solved equations for the species in the charge balance equation (Appendix E) are added and solved for $[H^+]$ which is the value used to calculate the acidity at each time iteration.

The following section details the model results for numerous sensitivity studies for the behavior of HNCO in clouds using the pH-modified model. Section 3.8 describes the conclusion to not only the HNCO sensitivity but also a contrast of the differences in the static versus dynamic pH calculation.

3.6.2.1. HNCO sensitivity studies. Each sensitivity study was conducted under similar model inputs in order to make independent comparisons of each variable. Unless otherwise noted, the cloud model is a 2-hour process that has an initial 30 minute gas phase start-up time, 1 hour of condensed phase cloud chemistry time, and a 30 minute lag time. The temperature is 277K, pressure is 81.22 kPa, liquid water contend (LWC) is .25 g/m^3, a droplet size of 10 microns, initial pH is 4.5, and initial gas phase concentrations are noted in table 3.7 (note the HNCO mixing ratio is 10 pptv).

Table 3.7

Model input concentrations

Species	Mixing Ratio (ppbv)
H_2	550
O_3	50
H_2O_2	0.5
HO	0.000162
HO_2	0.0162

Table 3.7 *(cont.)*

Species	**Mixing Ratio (ppbv)**
CH_3OO	0
CH_3OOH	0.2
CH_2O	0.5
HCOOH	0
NO	0
NO_2	0.125
HNO_3	0.1
N_2O_5	0
NO_3	0
CO_2	360000
Cl_2^-	1.67×10^{-09}
Cl^-	0.836
Cl	2.51×10^{-08}
CO_3^-	0
HNCO	0.01
CH_4	1700
CO	100

The first model study was of the effect of altitude on the cloud acidity and ultimately the concentration of HNCO. The altitude was modeled by varying both the atmospheric pressure and temperature simultaneously. Table 3.8 shows the values used in generating the plots shown in Figures 3.17 and 3.18. Figure 3.17 shows the pH variation due to altitude and it can be seen that above 20,000 feet (6.1 km) the pH takes on a totally different characteristic. We are not too quick to draw conclusions here due to the fact that the clouds are expected to be supercooled at this point and there could be much more ice content involved and therefore the liquid water content would be much less than .25 g/m^3.

Table 3.8

Altitude sensitivity inputs

Altitude (ft)	Pressure (kPa)	Temperature (K)
2000	94.19	284
4000	87.49	280
6000	81.22	276
8000	75.22	272
10,000	69.64	268
20,000	46.61	249
30,000	30.13	229
40,000	18.82	216
50,000	11.65	216

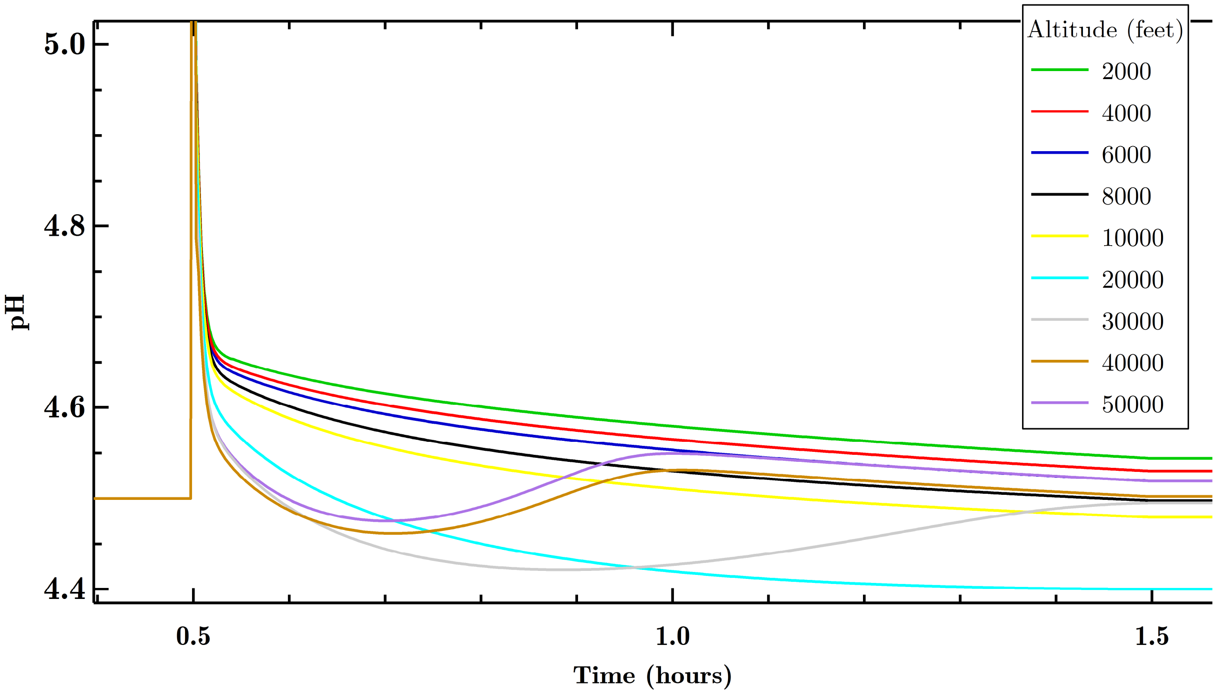

Figure 3.17. Effect of altitude (temperature and pressure differences) on the cloud pH

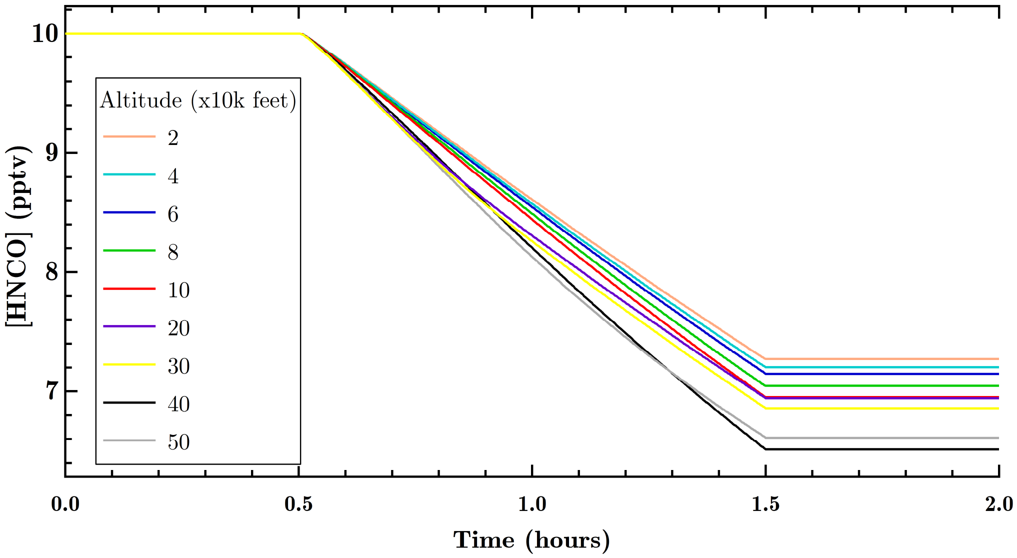

Figure 3.18. HNCO concentration sensitivity due to altitude

An estimate of the in-cloud lifetime of HNCO can be made by taking the inverse natural log of a sample of the data from the cloud interaction portion (between 30 and 90 minutes) of the simulation. This can then be linearly fit and the resulting slope of that fit is the rate constant (k). The inverse of the rate constant is the lifetime which corresponds to the time that it takes for the concentration to drop to approximately 37% (1/e) of the initial concentration. Figure 3.18 is the altitude sensitivity where both the temperature and pressure were varied simultaneously. The constants, lifetimes, and statistics extracted from Figure 3.18 are listed in Table 3.9. It shows that deviations from the normal concentration pattern begin between above approximately 20,000 feet. This can be also seen in the deflection in the lifetime plot (Figure 3.19) at 20,000 feet.

Table 3.9

HNCO rate constants and in-cloud lifetimes

Altitude (x1,000 feet)	**rate constant (min^{-1})**	**error (1σ)**	**lifetime (hours)**	**error (1σ)**
2	0.00089	1.23×10^{-06}	18.7266	0.025881
4	0.000917	1.32×10^{-06}	18.1752	0.026163
6	0.000939	1.38×10^{-06}	17.7494	0.026085

Table 3.9 (cont.)

Altitude (x1,000 feet)	rate constant (min^{-1})	error (1σ)	lifetime (hours)	error (1σ)
8	0.000982	1.54x10^{-06}	16.9722	0.026616
10	0.00102	1.68x10^{-06}	16.3399	0.026913
20	0.001212	2.37x10^{-06}	13.7514	0.02689
30	0.001202	1.07x10^{-06}	13.8658	0.012343
40	0.001057	1.44x10^{-06}	15.7679	0.014424
50	0.001022	1.49x10^{-06}	16.3079	0.023776

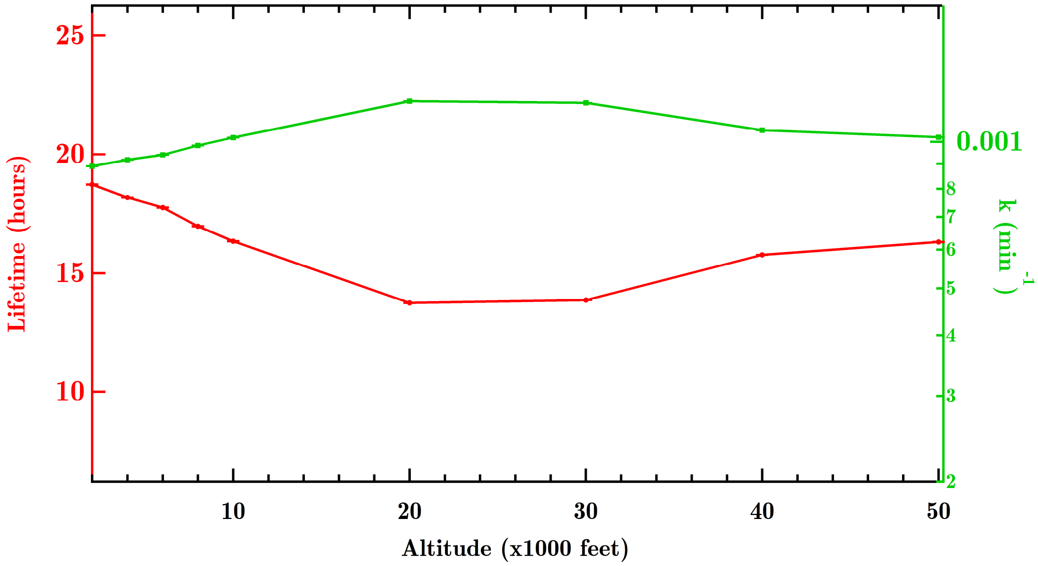

Figure 3.19. HNCO rate constants and in-cloud lifetimes

Finally, the HNCO lifetime dependence on altitude is graphically shown in Figure 3.19. The lifetime appears to decrease with the altitude (approximately 19 to 13 hours) until the 20,000 ft point where it appears to increase. This may or may not be characteristic of altitude given the fact that this inflection happens at the point of freezing and there could be much more ice and less liquid water content. This simulation only varied the temperature and pressure and not water content.

All acid concentrations are going to affect the in-cloud pH primarily due to the fact that acid dissociation will increase the hydronium ion concentration. With this in mind, the HNCO concentration sensitivity was studied under the basic conditions mentioned above. Figure 3.20 shows the higher mixing ratios of HNCO that were explored (500 to 10 ppbv) only to enunciate the exponential decay which is more defined on the linear scale than the lower concentrations. The largest change in lifetime due to HNCO concentration is between 100 pptv and 1 ppbv. The pH sensitivity plot in Figure 3.21 shows the significant dependence of the acidity on the concentration of HNCO. The higher the concentration the higher the acidity but notable at the 1 ppbv level and higher, the pH increases while in the aqueous phase.

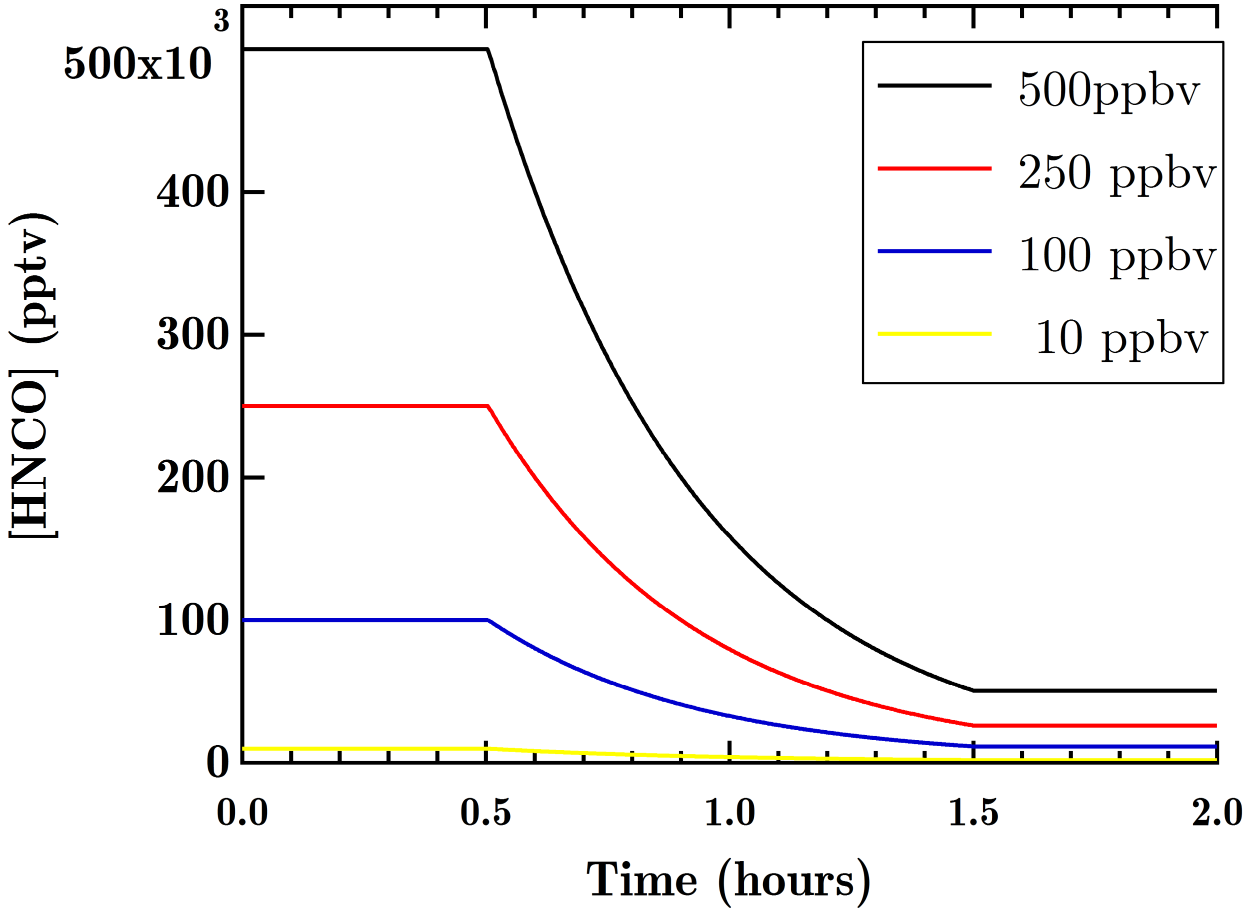

Figure 3.20. HNCO concentration sensitivity

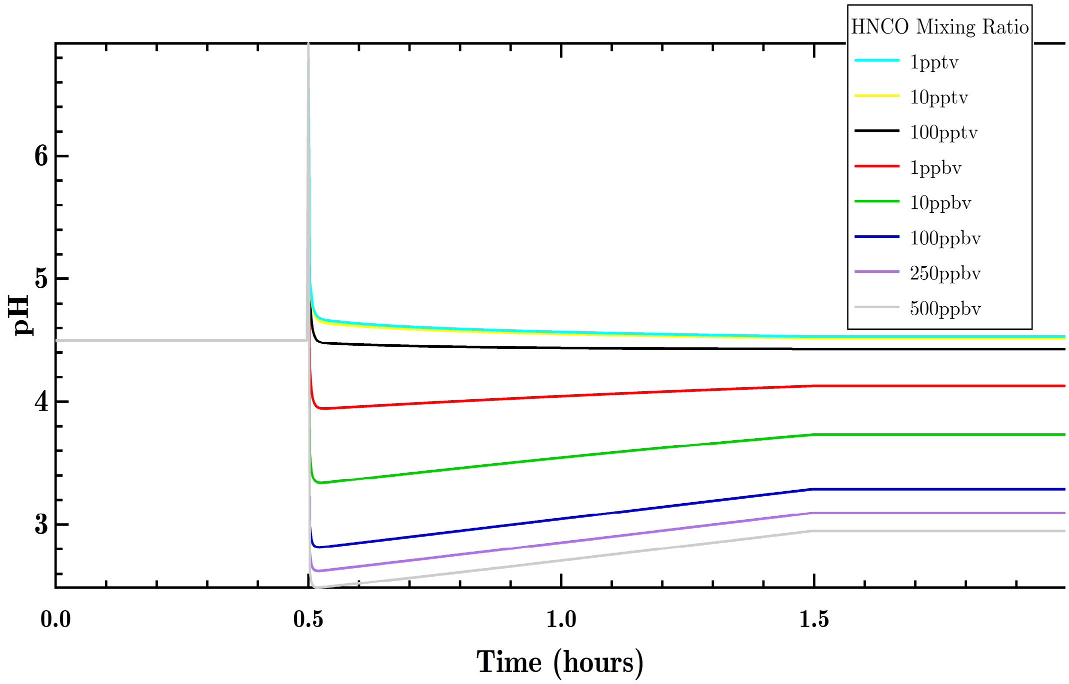

Figure 3.21. Effect of [HNCO] on cloud pH

Table 3.10 lists the concentrations explored which are all potentially realistic from 1 pptv (very clean) to 500 ppbv (extreme contamination such as close to a biomass fire). The lifetimes can also be found in Table 3.10 and the results are shown in Figure 3.22.

Table 3.10

Effect of [HNCO] on its in-cloud lifetime

[HNCO] pptv	**rate constant (min^{-1})**	**error (1σ)**	**lifetime (hours)**	**error (1σ)**
1	0.000909499	$1.46x10^{-06}$	18.3251	0.029417
10	0.000939	$1.38x10^{-06}$	17.7494	0.026085
100	0.00119603	$6.66x10^{-07}$	13.935	0.00776
1000	0.00245318	$4.75x10^{-06}$	6.7939	0.013155
10000	0.00458846	$1.07x10^{-05}$	3.6323	0.00847
100000	0.00609269	$5.66x10^{-06}$	2.73552	0.002541
250000	0.00634958	$2.66x10^{-06}$	2.62485	0.0011
500000	0.00642192	$6.64x10^{-07}$	2.59528	0.000268

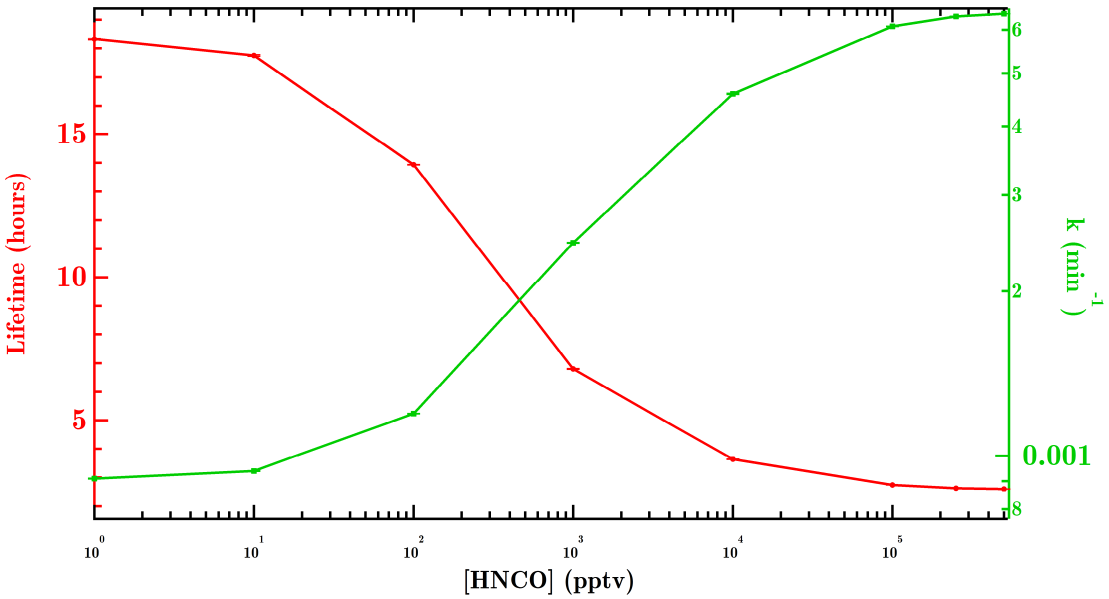

Figure 3.22. HNCO in-cloud lifetime due only to a change in HNCO concentration

The liquid water content was expected to be a critical factor in the uptake of HNCO, just as it was in the static pH case of section 3.7.1 (see Figure 3.16). However, in the dynamic pH case, the results are drastically different. In this case (Figure 3.23) it appears that HNCO reacts less with increasing water content. This is likely due to the pH effect shown in Figure 3.24 as well as the other dissociation chemistry involved in the charge balance equation. Table 3.11 contains the lifetime results and the results are graphed in Figure 3.25. It appears that the relation could be linear but more sample points would be needed. A linear fit to the red trace in Figure 3.25 has an R^2 value of .985.

The sulfate (SO_4^-) and sulfite (HSO_3^-) ion concentrations were expected to have a somewhat significant impact on the cloud acidity and thus affect the pH balance, but as can be seen from Figure 3.26 where reasonable concentrations of each were chosen, no significant change is seen in the HNCO concentration. It should be noted that these values are prescribed and not calculated (i.e. they remain constant), but they are still not expected to reach level that would compete with HNO_3 or HNCO.

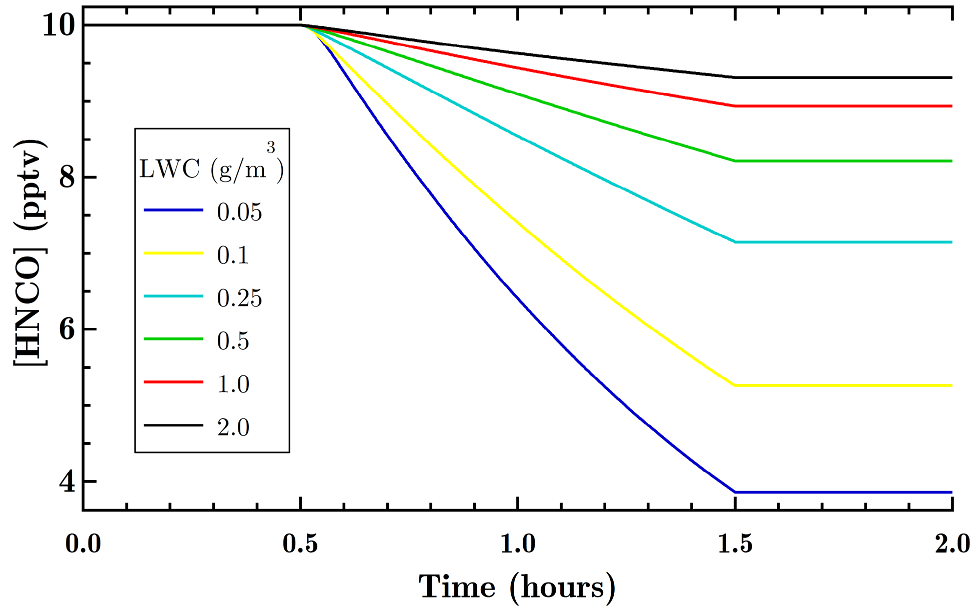

Figure 3.23. Liquid water content sensitivity: Increased amounts of water content reduce the uptake rate of HNCO

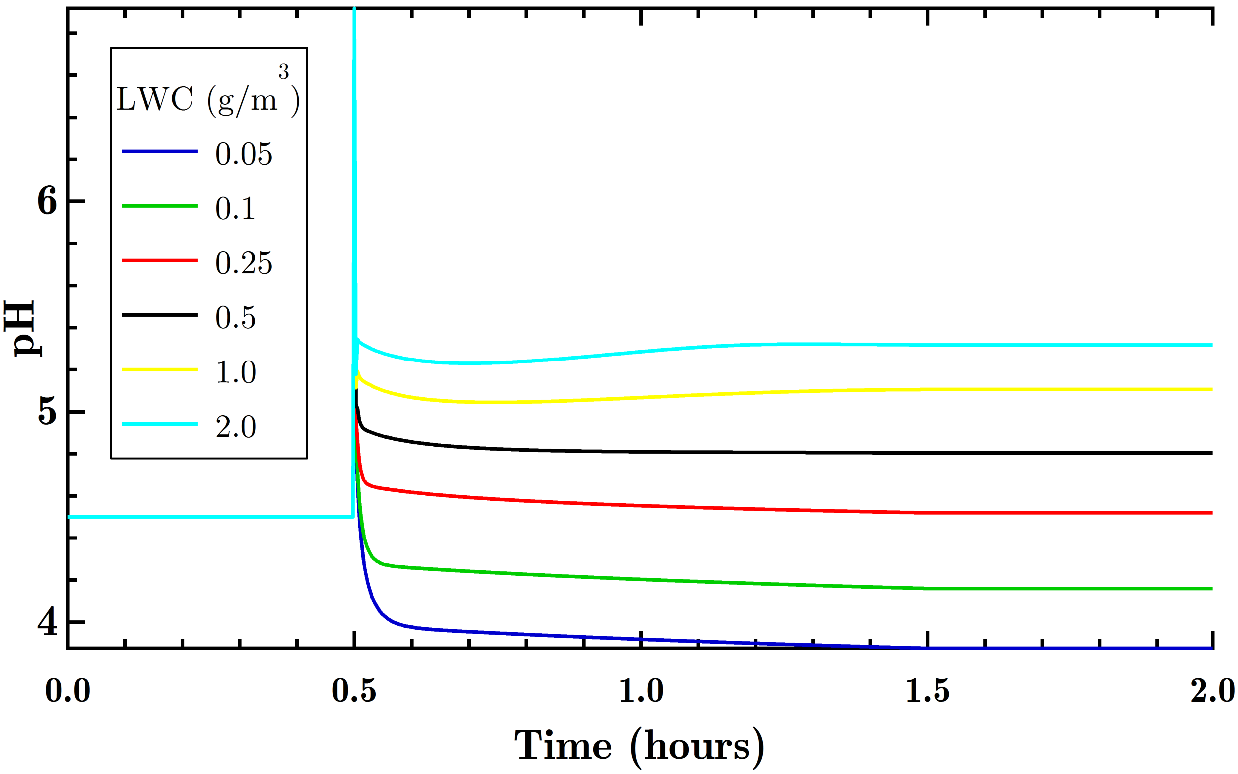

Figure 3.24. pH dependence of the liquid water content of a cloud droplet

Table 3.11

Liquid water content lifetime sensitivity

LWC (g/m^3)	rate constant (min^{-1})	error (1σ)	lifetime (hours)	error (1σ)
0.05	0.00270716	$2.99x10^{-06}$	6.15651	0.0068
0.1	0.00180483	$2.35 x10^{-06}$	9.23448	0.012024
0.25	0.000938558	$1.38 x10^{-06}$	17.7577	0.02611
0.5	0.000553921	$4.59 x10^{-07}$	30.0885	0.024933
1	0.000321	$3.70 x10^{-07}$	51.9211	0.059847
2	0.00020218	$4.62 x10^{-07}$	82.4348	0.18837

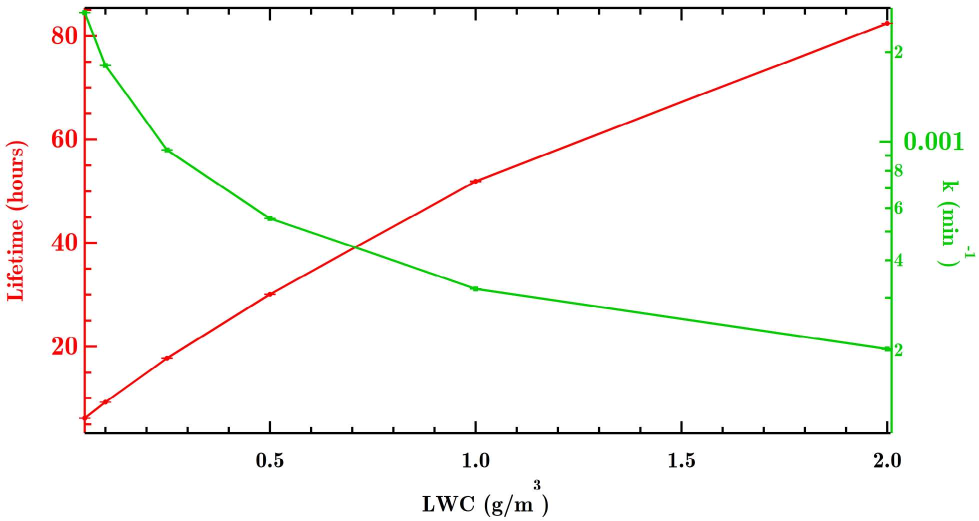

Figure 3.25. Lifetime increases with increasing cloud water content

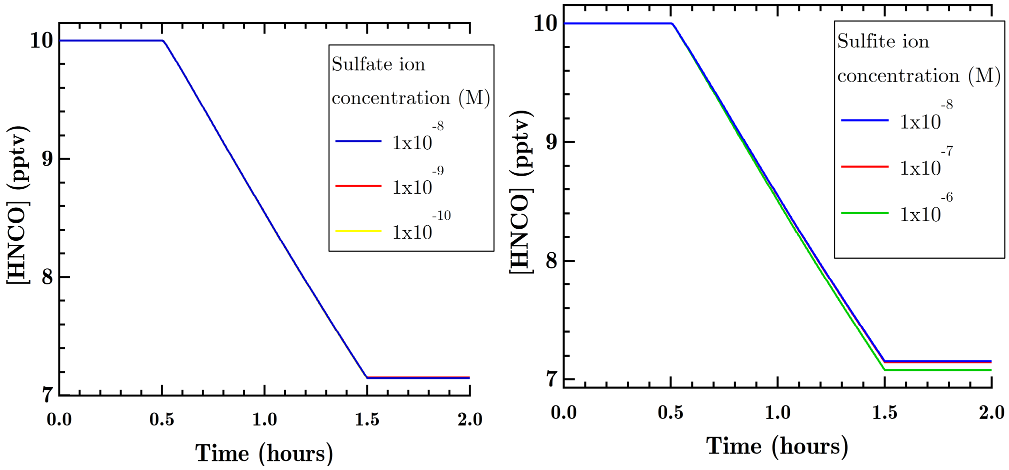

Figure 3.26. Sulfite and sulfate effect on HNCO concentration

Figure 3.27 shows both the pH and HNCO effect by droplet size where the pH increases with size and HNCO mixing ratios decrease. Table 3.12 shows the particle size sensitivity on the in-cloud lifetime of HNCO. The lifetime is apparently increasing as the cloud droplet gets smaller.

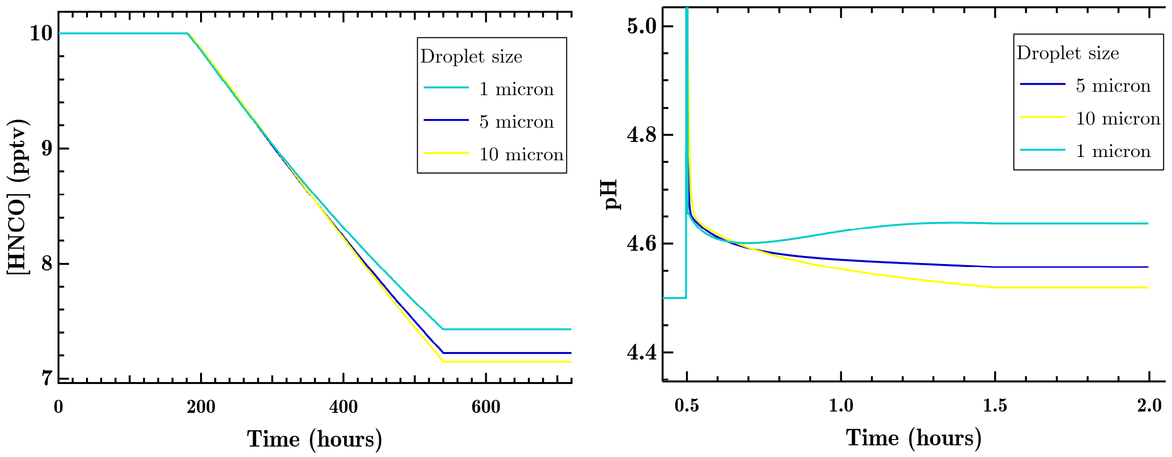

Figure 3.27. Droplet size pH and HNCO sensitivity

Table 3.12

Cloud droplet size effect on HNCO lifetime

Size (microns)	Rate Constant (min^{-1})	Error (1σ)	Lifetime (hours)	Error (1σ)
1	0.000836333	6.68×10^{-07}	19.9283	0.015917
5	0.000911932	7.28×10^{-07}	18.2762	0.01459
10	0.000938558	1.38×10^{-06}	17.7577	0.02611

By far, the most interesting result of these sensitivity studies would have to be that of the effect that nitric acid (HNO_3) has on the overall cloud system. Figure 3.28 shows both the HNCO concentration and pH sensitivity plots that show dramatic differences at different HNO_3 mixing ratios making it the most sensitive of all the parameters studied. It basically dictates the acidity of cloud. Figure 3.29 is the lifetime plot and just a one order of magnitude change in HNO_3 (.1 to 1.0 ppbv) causes the lifetime to change 83%. This is evidence that the gas-phase nitric acid concentration has the largest impact on cloud acidity and thus the rate at which other acids like HNCO will be removed.

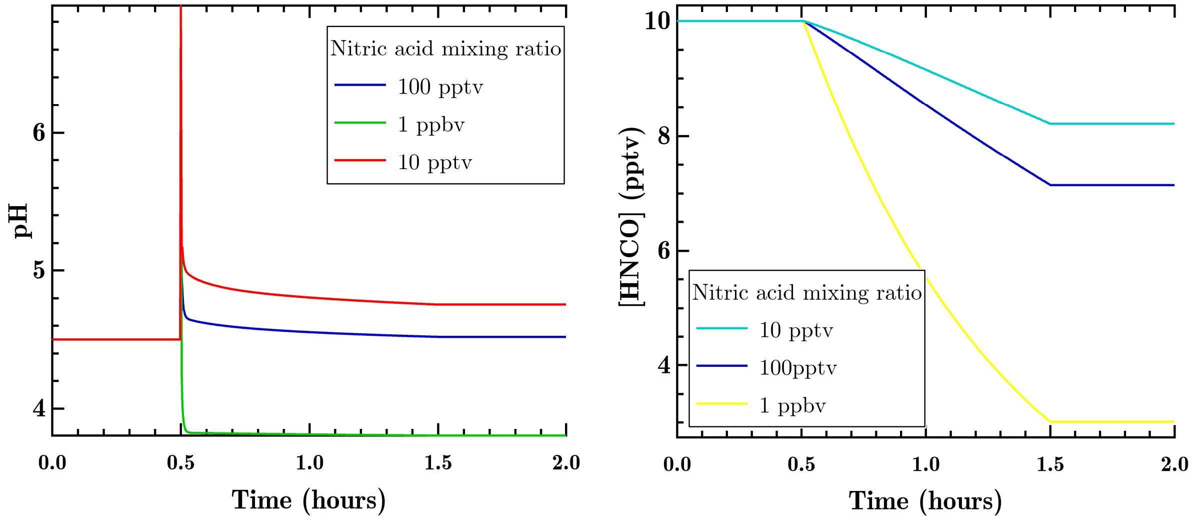

Figure 3.28. [HNO_3] impact on HNCO concentration and cloud pH

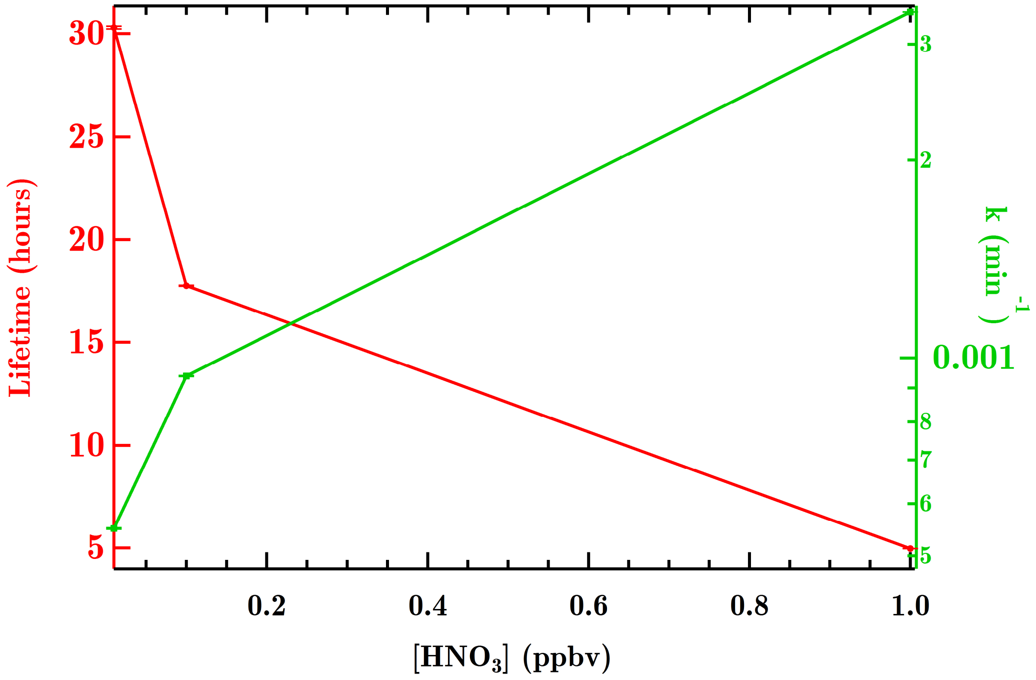

Figure 3.29. Nitric acid effect on the HNCO in-cloud lifetime

3.6.2.2. HNCO scenarios. Finally, some scenarios combining the effects of multiple variables were modeled. The first scenario is of some common cloud types. Table 3.13 contains the characteristics of the lower tropospheric clouds not expected to contain large amounts of ice.

Table 3.13

Data used in modeling different types of clouds

Cloud type	**Altitude (ft)**	**Pressure (kPa)**	**Temperature (K)**	**LWC (g/m^3)**
cumulonimbus	15,000	57.16	259	1.5
cumulus	5000	84.33	278	0.25
stratocumulus	5000	84.33	278	0.5
fog/haze	1000	97.63	286	0.05

Figure 3.30 shows the HNCO concentration as it is traversing different cloud types. Note that this is simulation uses a mixing ration of 100 pptv of HNCO instead of the 10 pptv run in previous simulations in order to model a somewhat contaminated sample. As expected from the earlier observation of liquid water content sensitivity, the fog and haze and cumulus clouds are better at “scrubbing” HNCO out of the troposphere due to their low water content. This is encouraging given that increased levels of HNCO are expected to be produced in the future from pyrolysis of biomass fire, cooking with coal, and urea selective catalytic reduction, and the lower clouds and fog have the potential to remove HNCO significantly, thus reducing the potential human health effects greatly. Table 3.14 shows that the lifetime of 100 pptv of HNCO in fog is only 6 hours whereas it is more than 50 hours for a cumulonimbus cloud. This means that HNCO may not migrate very far from a given source. Combining this with the fact that the lifetime of HNCO decreases with increased concentration. HNCO may not be much of a threat to human health even at small distances from a strong source.

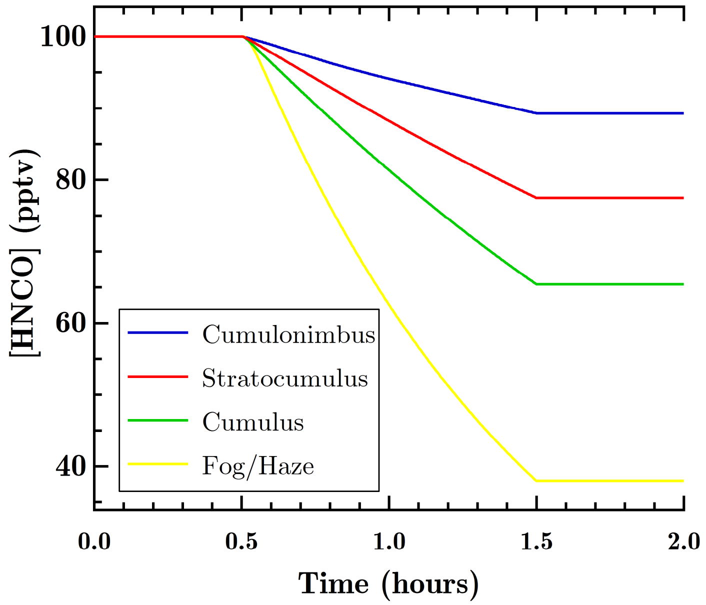

Figure 3.30. Cloud type sensitivity

Table 3.14

HNCO lifetime in different cloud types

Cloud type	rate constant (min^{-1})	error (1σ)	lifetime (hours)	Error (1σ)
cumulus	0.00119074	6.40×10^{-07}	13.9969	0.007523
stratocumulus	0.000719284	2.48×10^{-07}	23.1712	0.007989
fog/haze	0.00275498	7.62×10^{-07}	6.04965	0.001673
cumulonimbus	0.000318995	8.84×10^{-07}	52.2474	0.144788

Lastly, 3 scenarios of different levels of contamination were considered. Table 3.15 shows the concentrations of each case. Given that the values are extremely variable, estimates were taken from multiple sources and some of the biomass concentrations are maximum values for added contrast. The results shown in Figure 3.31 show that the most polluted situation has the shortest in-cloud lifetime. The increased HNO_3 and HNCO concentrations both contribute to higher cloud acidity therefore HNCO will be removed faster.

Table 3.15

Contamination scenarios

Species	Clean (pptv)	Polluted (pptv)	Biomass fire (pptv)
H_2	550	550	550
O_3	50	75	75
H_2O_2	0.5	1	1.7
HO	0.000162	0.000162	0.000162
HO_2	0.0162	0.0162	0.0162
CH_3OO	0	0	0
CH_3OOH	0.2	0.2	0.2
CH_2O	0.5	0.5	0.5
HCOOH	0	3.5	200
NO	0	0	6000
NO_2	0.125	19	1000
HNO_3	0.099998	6.5	40
N_2O_5	0	0	0
NO_3	0	0	0
CO_2	360000	360000	4000000
Cl_2^-	1.67×10^{-09}	1.67×10^{-09}	1.67111×10^{-09}
CL^-	0.835785	0.835785	0.835785062
CLA	2.51×10^{-08}	$2.51E^{-08}$	2.50689×10^{-08}
CO_3^-	0	0	0
HNCO	0.01	0.1	250
CH_4	1700	1700	120000
CO	100	100	125000

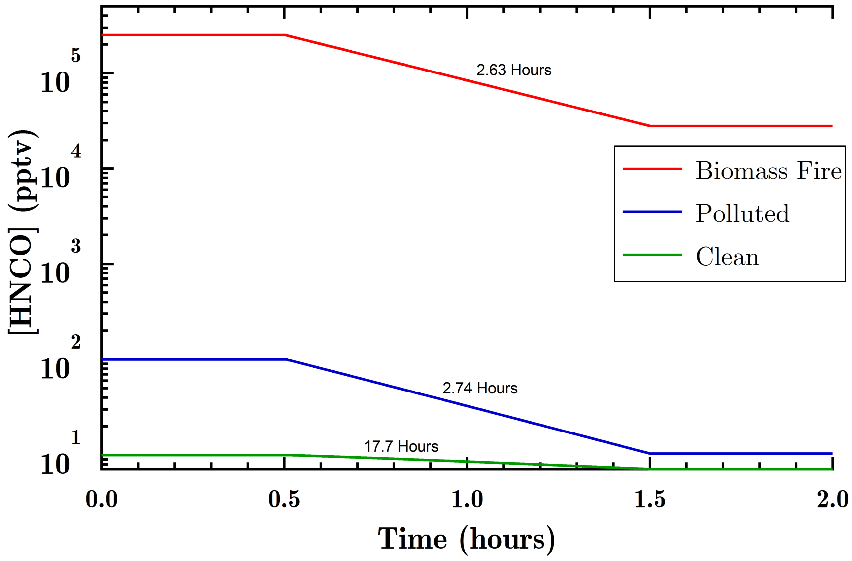

Figure 3.31. HNCO concentrations and in-cloud lifetimes at different levels of contamination

3.7. Conclusions

Given the apparent human health concerns of HNCO exposure due to biomass burning, cooking, diesel engine selective catalytic converters, and tobacco use, the modeling of HNCO in the atmosphere is of the utmost importance. An accurate method at estimating the lifetime is therefore of great interest. The pH of the aqueous medium that HNCO encounters a major factor. At normal physiological pH levels around 7.4, the data shows that the solubility is enormous at a level of 10^5 M/atm. In other words, the HNCO would continuously be absorbed if constantly exposed.

Model results show first that there is a need for the acidity of the condensed phase to be calculated in real-time in order to get realistic values of aqueous-phase concentrations. The initial simulation showed that the concentration of HNCO does not impact the lifetime, since a variability of HNCO concentration over four orders of magnitude only produced a lifetime change of about 1.2%. However, with the addition of the dynamic pH calculation, this was shown to be far from accurate in that over the span of reasonable HNCO concentrations, there is an 86.3% difference between the minimum and maximum concentrations.

The model shows that the elevation, liquid water content, droplet size, and gas-phase nitric and isocyanic acid concentrations are critical in characterizing HNCO in clouds. The in-cloud lifetime of HNCO is estimated to range from approximately 6.156 ± 0.007 to 82.4348 ± 0.188 hours. It is also noteworthy to mention that the lower liquid water content of a cloud such as fog or haze (approximately .05 g/m^3), the better the chance of reducing the HNCO concentration.

The cloud type and liquid water content sensitivity measurements show that HNCO may not be as much of a risk in the troposphere since the lower water content condensed phases are better at removal. It must be noted that this cloud scenario is just one of several mechanisms that could aid in HNCO reduction. In order for the uptake of HNCO to be properly understood, there also needs to be a study into the aerosol chemistry with HNCO as well as surface water interactions.

This work is not a definitive look at HNCO in the troposphere and the potential risks, but meant to be more of a call for further investigations (both theoretically and experimentally) given the potential impact to human health. It is imperative that more studies be conducted in order to be confident of accurate modeling and work towards true HNCO exposure levels that would lead an a responsible risk assessment such as those determined by the U.S. Environmental Protection Agency.

References

Adams, N. G., & Smith, D. (1976). The selected ion flow tube (SIFT); A technique for studying ion-neutral reactions. *International Journal of Mass Spectrometry and Ion Physics, 21*(3-4), 349–359.

Ai, M., & Ohdan, K. (1997). Formation of glyoxylic acid by oxidative dehydrogenation of glycolic acid. *Bulletin of the Chemical Society of Japan, 70*(8), 1995–1999.

Albrecht, B. A. (1989). Aerosols, cloud microphysics, and fractional cloudiness. *Science, 245*(4923), 1227–1230.

Alfarra, M. R., Paulsen, D., Gysel, M., Garforth, A. A., Dommen, J., Prévôt, A. S. H., . . . Coe, H. (2006). A mass spectrometric study of secondary organic aerosols formed from the photooxidation of anthropogenic and biogenic precursors in a reaction chamber. *Atmospheric Chemistry and Physics, 6*, 5279–5293.

Allan, M. (1999). Mass Spectrometry, Historical Perspective. In J. C. Lindon (Ed.), *Encyclopedia of Spectroscopy and Spectrometry* (pp. 1241–1248). Oxford: Elsevier.

Altshuller, A. P. (1991). Estimating product yields of carbon-containing products from the atmospheric photooxidation of ambient air alkenes. *Journal of Atmospheric Chemistry, 13*(2), 131–154.

Andreae, M. O. (1983). Soot carbon and excess fine potassium–long-range transport of combustion-derived aerosols. *Science, 220*(4602), 1148–1151.

Andreae, M. O., & Merlet, P. (2001). Emission of trace gases and aerosols from biomass burning. *Global Biogeochemical Cycles, 15*(4), 955–966.

Ashby, R. A., & Werner, R. L. (1965). Vibration-rotation spectrum of HNCO between 1200-450 cm^{-1}. *Journal of Molecular Spectroscopy, 18*(2), 184–201.

Barth, M. C. (2006). The importance of cloud drop representation on cloud photochemistry. *Atmospheric Research, 82*(1-2), 294–309.

Barth, M. C., Hess, P. G., & Madronich, S. (2002). Effect of marine boundary layer clouds on tropospheric chemistry as analyzed in a regional chemistry transport model. *Journal of Geophysical Research-Atmospheres, 107*(D11).

Barth, M. C., Sillman, S., Hudman, R., Jacobson, M. Z., Kim, C. H., Monod, A., & Liang, J. (2003). Summary of the cloud chemistry modeling intercomparison: Photochemical box model simulation. *Journal of Geophysical Research-Atmospheres, 108*(D7).

Belson, D. J., & Strachan, A. N. (1982). Preparation and properties of isocyanic acid. *Chemical Society Reviews, 11*(1), 41–56.

Beswick, H. T., & Harding, J. J. (1984). Conformational-changes induced in bovine lens alpha-crystallin by carbamylation—relevance to cataract. *Biochemical Journal, 223*(1), 221–227.

Blake, R. S., Monks, P. S., & Ellis, A. M. (2009). Proton-transfer reaction mass spectrometry. *Chemical Reviews, 109*(3), 861–896.

Blake, R. S., Whyte, C., Hughes, C. O., Ellis, A. M., & Monks, P. S. (2004). Demonstration of proton-transfer reaction time-of-flight mass spectrometry for real-time analysis of trace volatile organic compounds. *Analytical Chemistry, 76*(13), 3841–3845.

Bowman, D., Balch, J. K., Artaxo, P., Bond, W. J., Carlson, J. M., Cochrane, M. A., . . . Pyne, S. J. (2009). Fire in the earth system. *Science, 324*(5926), 481–484.

Brownsword, R. A., Laurent, T., Vatsa, R. K., Volpp, H. R., & Wolfrum, J. (1996). Photodissociation dynamics of HNCO at 248 nm. *Chemical Physics Letters, 258*(1-2), 164–170.

Burling, I. R., Yokelson, R. J., Griffith, D. W. T., Johnson, T. J., Veres, P., Roberts, J. M., . . . de Gouw, J. A. (2010). Laboratory measurements of trace gas emissions from biomass burning of fuel types from the southeastern and southwestern United States. *Atmospheric Chemistry and Physics, 10*(22), 11115–11130.

Caldwell, G., Renneboog, R., & Kebarle, P. (1989). Gas-phase acidities of aliphatic carboxylic-acids, based on measurements of proton-transfer equilibria. *Canadian Journal of Chemistry-Revue Canadienne De Chimie, 67*(4), 611–618.

California, S. O. (2001). Determination of Noncancer Chronic Reference Exposure Levels Batch 2B December 2001. from http://oehha.ca.gov/air/chronic_rels/pdf/methyliso.pdf

Calvert, J. G., Yarwood, G., & Dunker, A. M. (1994). An evaluation of the mechanism of nitrous-acid formation in the urban atmosphere. *Research on Chemical Intermediates, 20*(3-5), 463–502.

Cantrell, W., & Heymsfield, A. (2005). Production of ice in tropospheric clouds – A review. *Bulletin of the American Meteorological Society, 86*(6), 795–807.

Chameides, W. L., & Davis, D. D. (1983). Aqueous-phase source of formic-acid in clouds. [Letter]. *Nature, 304*(5925), 427–429.

Chapman, E. G., Kenny, D. V., Busness, K. M., Thorp, J. M., & Spicer, C. W. (1995). Continuous airborne measurements of gaseous formic and acetic-acids over the western north-atlantic. *Geophysical Research Letters, 22*(4), 405–408.

Chebbi, A., & Carlier, P. (1996). Carboxylic acids in the troposphere, occurrence, sources, and sinks: A review. *Atmospheric Environment, 30*(24), 4233–4249.

Chipperfield, M. P. (2003). Numerical Models/Chemistry Models. In J. R. Holton (Ed.), *Encyclopedia of Atmospheric Sciences* (pp. 1414–1428) Oxford: Academic Press.

Christian, T. J., Kleiss, B., Yokelson, R. J., Holzinger, R., Crutzen, P. J., Hao, W. M., . . . Ward, D. E. (2003). Comprehensive laboratory measurements of biomass-burning emissions: 1. Emissions from Indonesian, African, and other fuels. *Journal of Geophysical Research-Atmospheres, 108*(D23).

Collett, J. L., & Herckes, P. (2003). Cloud chemistry. In J. R. Holton (Ed.), *Encyclopedia of Atmospheric Sciences* (pp. 451–459). Oxford: Academic Press.

Corrigan, C. E., & Novakov, T. (1999). Cloud condensation nucleus activity of organic compounds: a laboratory study. *Atmospheric Environment, 33*(17), 2661–2668.

Crutzen, P. J., & Andreae, M. O. (1990). Biomass burning in the tropics—impact on atmospheric chemistry and biogeochemical cycles. *Science, 250*(4988), 1669–1678.

Crutzen, P. J., Heidt, L. E., Krasnec, J. P., Pollock, W. H., & Seiler, W. (1979). Biomass burning as a source of atmospheric gases CO, H_2, N_2O, NO, CH_3CL and CO_2. *Nature, 282*(5736), 253–256.

Danckwerts, P. V. (1951). Absorption by simultaneous diffusion and chemical reaction into particles of various shapes and into falling drops. *Transactions of the Faraday Society, 47*(9), 1014–1023.

de Gouw, J. A., Middlebrook, A. M., Warneke, C., Goldan, P. D., Kuster, W. C., Roberts, J. M., . . . Bates, T. S. (2005). Budget of organic carbon in a polluted atmosphere: Results from the New England Air Quality Study in 2002. *Journal of Geophysical Research-Atmospheres, 110*(D16).

de Gouw, J. A., & Warneke, C. (2007). Measurements of volatile organic compounds in the earths atmosphere using proton-transfer-reaction mass spectrometry. *Mass Spectrometry Reviews, 26*(2), 223–257.

de Gouw, J. A., Warneke, C., Karl, T., Eerdekens, G., van der Veen, C., & Fall, R. (2003). Sensitivity and specificity of atmospheric trace gas detection by proton-transfer-reaction mass spectrometry. *International Journal of Mass Spectrometry, 223-224*, 365–382.

DeMott, P. J., Rogers, D. C., Kreidenweis, S. M., Chen, Y. L., Twohy, C. H., Baumgardner, D., . . . Chan, K. R. (1998). The role of heterogeneous freezing nucleation in upper tropospheric clouds: Inferences from SUCCESS. *Geophysical Research Letters, 25*(9), 1387–1390.

Ennis, C. J., Reynolds, J. C., Keely, B. J., & Carpenter, L. J. (2005). A hollow cathode proton transfer reaction time of flight mass spectrometer. *International Journal of Mass Spectrometry, 247*(1-3), 72–80.

Ferguson, E. E., Fehsenfeld, F. C., Schmeltekopf, A. L., Bates, D. R., & Immanuel, E. (1969). Flowing Afterglow Measurements of Ion-Neutral Reactions *Advances in Atomic and Molecular Physics* (Vol. Volume 5, pp. 1–56): Academic Press.

Finlayson-Pitts, B. J., & Pitts, J. J. N. (2000a) *Chemistry of the Upper and Lower Atmosphere*. San Diego: Academic Press.

Finlayson-Pitts, B. J., & Pitts, J. J. N. (2000b). Kinetics and Atmospheric Chemistry *Chemistry of the Upper and Lower Atmosphere* (pp. 130–178). San Diego: Academic Press.

Finneran, M. (2010, September 24, 2010). *Wildfires: A symptom of climate change.* Retrieved from http://www.nasa.gov/topics/earth/features/wildfires.html

Fishman, J., Watson, C. E., Larsen, J. C., & Logan, J. A. (1990). Distribution of tropospheric ozone determined from satellite data. *Journal of Geophysical Research-Atmospheres, 95*(D4), 3599–3617.

Fisseha, R., Saurer, M., Jaggi, M., Siegwolf, R. T. W., Dommen, J., Szidat, S., . . . Baltensperger, U. (2009). Determination of primary and secondary sources of organic acids and carbonaceous aerosols using stable carbon isotopes. *Atmospheric Environment, 43*(2), 431–437.

Fletcher, N. H. (1958). Size effect in heterogeneous nucleation. *Journal of Chemical Physics, 29*(3), 572–576.

Fornaro, A., & Gutz, I. G. R. (2003). Wet deposition and related atmospheric chemistry in the Sao Paulo metropolis, Brazil: Part 2—contribution of formic and acetic acids. *Atmospheric Environment, 37*(1), 117–128.

Fowler, L. D., Randall, D. A., & Rutledge, S. A. (1996). Liquid and ice cloud microphysics in the CSU general circulation model .1. Model description and simulated microphysical processes. *Journal of Climate, 9*(3), 489–529.

Fromm, M., Tupper, A., Rosenfeld, D., Servranckx, R., & McRae, R. (2006). Violent pyro-convective storm devastates Australia's capital and pollutes the stratosphere. *Geophysical Research Letters, 33*(5).

Fukuta, N., & Walter, L. A. (1970). Kinetics of Hydrometeor Growth from a Vaper-Spherical Model. *Journal of the Atmospheric Sciences, 27*(8), 1160–1172.

Gelencser, A., & Varga, Z. (2005). Evaluation of the atmospheric significance of multiphase reactions in atmospheric secondary organic aerosol formation. *Atmospheric Chemistry and Physics, 5*, 2823–2831.

Ghilarducci, D. P., & Tjeerdema, R. S. (1995). Fate and effects of acrolein. *Reviews of Environmental Contamination and Toxicology, Vol 144, 144*, 95–146.

Graul, S. T., Schnute, M. E., & Squires, R. R. (1990). Gas-phase acidities of carboxylic-acids and alcohols from collision-induced dissociation of dimer cluster ions. *International Journal of Mass Spectrometry and Ion Processes, 96*(2), 181–198.

Hansel, A., Jordan, A., Holzinger, R., Prazeller, P., Vogel, W., & Lindinger, W. (1995). Proton transfer reaction mass spectrometry: On-line trace gas analysis at the ppb level. *International Journal of Mass Spectrometry and Ion Processes, 149-150*, 609–619.

Herzberg, G., & Reid, C. (1950). Infra-red spectrum and structure of the hnco molecule. *Discussions of the Faraday Society* (9), 92–99.

Heymsfield, A. J., & Sabin, R. M. (1989). Cirrus crystal nucleation by homogeneous freezing of solution droplets. *Journal of the Atmospheric Sciences, 46*(14), 2252–2264.

Holloway, J. L., & Manabe, S. (1971). Simulation of climate by a global general circulation model. 1. Hydrologic cycle and heat balance. *Monthly Weather Review, 99*(5), 335–370.

Holton, J. R., Curry, J. A., & Pyle, J. A. (2003) Encyclopedia of Atmospheric Sciences, Volumes 1-6: Elsevier.

Howard, C. J. (1979). Kinetic measurements using flow tubes. *Journal of Physical Chemistry, 83*(1), 3–9.

Husar, R. B., & Shu, W. R. (1975). Thermal analyses of Los-Angeles smog aerosol. *Journal of Applied Meteorology, 14*(8), 1558–1565.

Inomata, S., Tanimoto, H., Aoki, N., Hirokawa, J., & Sadanaga, Y. (2006). A novel discharge source of hydronium ions for proton transfer reaction ionization: design, characterization, and performance. *Rapid Communications in Mass Spectrometry, 20*(6), 1025–1029.

Jensen, M. B. (1958). On the kinetics of the decomposition of cyanic acid. *Acta Chemica Scandinavica, 12*(8), 1657–1670.

Jordan, A., Haidacher, S., Hanel, G., Hartungen, E., Märk, L., Seehauser, H., . . . Märk, T. D. (2009). A high resolution and high sensitivity proton-transfer-reaction time-of-flight mass spectrometer (PTR-TOF-MS). *International Journal of Mass Spectrometry, 286,* 122–128.

Jordan, A., Hansel, A., Holzinger, R., & Lindinger, W. (1995). Acetonitrile and benzene in the breath of smokers and non-smokers investigated by proton transfer reaction mass spectrometry (PTR-MS). *International Journal of Mass Spectrometry and Ion Processes, 148*(1-2), L1–L3.

Kames, J., & Schurath, U. (1995). Henrys law and hydrolysis-rate constants for peroxyacyl nitrates (pans) using a homogeneous gas-phase source. *Journal of Atmospheric Chemistry, 21*(2), 151–164.

Kawamura, K., Steinberg, S., & Kaplan, I. R. (1996). Concentrations of monocarboxylic and dicarboxylic acids and aldehydes in southern California wet precipitations: Comparison of urban and nonurban samples and compositional changes during scavenging. *Atmospheric Environment, 30*(7), 1035–1052.

Keene, W. C., Galloway, J. N., & Holden, J. D. (1983). Measurement of weak organic acidity in precipitation from remote areas of the world. *Journal of Geophysical Research-Oceans and Atmospheres, 88*(NC9), 5122–5130.

Kesselmeier, J., Ciccioli, P., Kuhn, U., Stefani, P., Biesenthal, T., Rottenberger, S., . . . Andreae, M. O. (2002). Volatile organic compound emissions in relation to plant carbon fixation and the terrestrial carbon budget. *Global Biogeochemical Cycles, 16*(4).

Khain, A., Ovtchinnikov, M., Pinsky, M., Pokrovsky, A., & Krugliak, H. (2000). Notes on the state-of-the-art numerical modeling of cloud microphysics. *Atmospheric Research, 55*(3-4), 159–224.

Khairoutdinov, M., & Kogan, Y. (2000). A new cloud physics parameterization in a large-eddy simulation model of marine stratocumulus. *Monthly Weather Review, 128*(1), 229–243.

King, D. S., Fields, C. G., & Fields, G. B. (1990). A cleavage method which minimizes side reactions following fmoc solid-phase peptide-synthesis. *International Journal of Peptide and Protein Research, 36*(3), 255–266.

Kolb, C. E., Cox, R. A., Abbatt, J. P. D., Ammann, M., Davis, E. J., Donaldson, D. J., . . . O'Dowd, C. D. (2010). An overview of current issues in the uptake of atmospheric trace gases by aerosols and clouds. *Atmospheric Chemistry and Physics, 10*(21), 10561–10605.

Kummerlöwe, G., & Beyer, M. K. (2005). Rate estimates for collisions of ionic clusters with neutral reactant molecules. *International Journal of Mass Spectrometry, 244*(1), 84–90.

Lamb, D. (2003). Cloud chemistry. In J. R. Holton (Ed.), *Encyclopedia of Atmospheric Sciences* (pp. 459–467). Oxford: Academic Press.

Lelieveld, J., & Crutzen, P. J. (1991). The role of clouds in tropospheric photochemistry. *Journal of Atmospheric Chemistry, 12*(3), 229–267.

Levine, J. S., Cofer, W. R., Cahoon, D. R., & Winstead, E. L. (1995). Biomass burning—a driver for global change. *Environmental Science & Technology, 29*(3), A120–A125.

Lindinger, W., Hansel, A., & Jordan, A. (1998). On-line monitoring of volatile organic compounds at pptv levels by means of proton-transfer-reaction mass spectrometry (PTR-MS) medical applications, food control and environmental research. *International Journal of Mass Spectrometry and Ion Processes, 173*(3), 191–241.

Mackay, D., Shiu, W. Y., & Sutherland, R. P. (1979). Determination of air-water henrys law constants for hydrophobic pollutants. *Environmental Science & Technology, 13*(3), 333–337.

Madronich, S., & Calvert, J. G. (1990). Permutation reactions of organic peroxy-radicals in the troposphere. *Journal of Geophysical Research-Atmospheres, 95*(D5), 5697–5715.

Madronich, S., Chatfield, R. B., Calvert, J. G., Moortgat, G. K., Veyret, B., & Lesclaux, R. (1990). A photochemical origin of acetic-acid in the troposphere. *Geophysical Research Letters, 17*(13), 2361–2364.

Mahecha, M. D., Reichstein, M., Lange, H., Carvalhais, N., Bernhofer, C., Grunwald, T., . . . Seufert, G. (2007). Characterizing ecosystem-atmosphere interactions from short to interannual time scales. *Biogeosciences, 4*(5), 743–758.

McFarland, M., Albritton, D. L., Fehsenfeld, F. C., Ferguson, E. E., & Schmeltekopf, A. L. (1973). Flow-drift technique for ion mobility and ion-molecule reaction rate constant measurements. III. Negative ion reactions of O[sup -] with CO, NO, H_2, and D_2. *The Journal of Chemical Physics, 59*(12), 6629–6635.

Mirsaleh-Kohan, N., Robertson, W. D., & Compton, R. N. (2008). Electron ionization time-of-flight mass spectrometry: Historical review and current applications. *Mass Spectrometry Reviews, 27*(3), 237–285.

Molina, M. J., Molina, L. T., & Kolb, C. E. (1996). Gas-phase and heterogeneous chemical kinetics of the troposphere and stratosphere. *Annual Review of Physical Chemistry, 47*, 327–367.

Moortgat, G. K., Veyret, B., & Lesclaux, R. (1989). Kinetics of the reaction of HO_2 with $CH_3C(O)O_2$ in the temperature-range 253 K - 368 K. *Chemical Physics Letters, 160*(4), 443–447.

Munson, M. S. B., & Field, F. H. (1966). Chemical ionization mass spectrometry .i. General introduction. *Journal of the American Chemical Society, 88*(12), 2621–2630.

NOAA Earth Systems Research Laboratory, Chemical Science Division. (2009). CalNex 2010: Research at the Nexus of Air Quality and Climate Change, http://www.esrl.noaa.gov/csd/calnex/.

Novakov, & Penner, J. E. (1993). Large contribution of organic aerosols to cloud-condensation-nuclei concentrations. *Nature, 365*(6449), 823.

Pabst, M. A., & Hofer, F. (1998). Deposits of different origin in the lungs of the 5,300-year-old Tyrolean Iceman. *American Journal of Physical Anthropology, 107*(1), 1–12.

Pariat, Y., & Allan, M. (1991). Dissociative electron attachment to methyl acetate: evidence for ion/molecule complexes as intermediates. *International Journal of Mass Spectrometry and Ion Processes, 103*(2-3), 181–192.

Parmar, R. S., Welling, M., Andreae, M. O., & Helas, G. (2008). Water vapor release from biomass combustion. *Atmospheric Chemistry and Physics, 8*(20), 6147–6153.

Penner, J. E., Dickinson, R. E., & Oneill, C. A. (1992). Effects of aerosol from biomass burning on the global radiation budget. *Science, 256*(5062), 1432–1434.

Potter, B. E. (2005). The role of released moisture in the atmospheric dynamics associated with wildland fires. [Article; Proceedings Paper]. *International Journal of Wildland Fire, 14*(1), 77–84.

Radke, L. F., Stith, J. L., Hegg, D. A., & Hobbs, P. V. (1978). Airborne studies of particles and gases from forest fires. *Journal of the Air Pollution Control Association, 28*(1), 30–34.

Randall, D. A., Harshvardhan, & Dazlich, D. A. (1991). Diurnal variability of the hydrologic-cycle in a general-circulation model. *Journal of the Atmospheric Sciences, 48*(1), 40–62.

Ravishankara, A. R. (1997). Heterogeneous and multiphase chemistry in the troposphere. *Science, 276*(5315), 1058–1065.

Rivera-Carpio, C. A., Corrigan, C. E., Novakov, T., Penner, J. E., Rogers, C. F., & Chow, J. C. (1996). Derivation of contributions of sulfate and carbonaceous aerosols to cloud condensation nuclei from mass size distributions. [Article; Proceedings Paper]. *Journal of Geophysical Research-Atmospheres, 101*(D14), 19483–19493.

Roberts, J. M., Veres, P., Warneke, C., Neuman, J. A., Washenfelder, R. A., Brown, S. S., . . . de Gouw, J. A. (2010). Measurement of HONO, HNCO, and other inorganic acids by negative-ion proton-transfer chemical-ionization mass spectrometry (NI-PT-CIMS): application to biomass burning emissions. *Atmospheric Measurement Techniques, 3*(4), 981–990.

Roberts, J. M., Veres, P. R., Cochran, A. K., Warneke, C., Burling, I. R., Yokelson, R. J., . . . de Gouw, J. A. (2011). Isocyanic acid in the atmosphere and its possible link to smoke-related health effects. *Proceedings of the National Academy of Sciences of the United States of America*, *108*(22), 8966–8971.

Sander, R. (1999). Modeling atmospheric chemistry: Interactions between gas-phase species and liquid cloud/aerosol particles. *Surveys in Geophysics, 20*(1), 1–31.

Scott, D. L., Wolfe, F., & Huizinga, T. W. J. (2010). Rheumatoid arthritis. *The Lancet, 376*(9746), 1094–1108.

Slusher, D. L., Huey, L. G., Tanner, D. J., Flocke, F. M., & Roberts, J. M. (2004). A thermal dissociation-chemical ionization mass spectrometry (TD-CIMS) technique for the simultaneous measurement of peroxyacyl nitrates and dinitrogen pentoxide. *Journal of Geophysical Research-Atmospheres, 109*(D19).

Statute Book of the Swedish Work Environment Authority. (2005). *Occupational exposure limit values and measures against air contaminants*. Retrieved from http://www.av.se/dokument/inenglish/legislations/eng0517.pdf.

Streets, D. G., Bond, T. C., Carmichael, G. R., Fernandes, S. D., Fu, Q., He, D., . . . Yarber, K. F. (2003). An inventory of gaseous and primary aerosol emissions in Asia in the year 2000. *Journal of Geophysical Research-Atmospheres, 108*(D21).

Strobel, B. W. (2001). Influence of vegetation on low-molecular-weight carboxylic acids in soil solution—a review. *Geoderma, 99*(3-4), 169–198.

Sun, J. D., & Dent, J. G. (1980). A new method for measuring covalent binding of chemicals to cellular macromolecules. *Chemico-Biological Interactions, 32*(1-2), 41–61.

Sun, W. J., & Saeys, M. (2008). First principles study of the reaction of formic and acetic acids with hydroxyl radicals. *Journal of Physical Chemistry A, 112*(30), 6918–6928.

Takegawa, N., Miyakawa, T., Kawamura, K., & Kondo, Y. (2007). Contribution of selected dicarboxylic and omega-oxocarboxylic acids in ambient aerosol to the m/z 44 signal of an aerodyne aerosol mass spectrometer. *Aerosol Science and Technology, 41*(4), 418–437.

Talbot, R. W., Andreae, M. O., Berresheim, H., Jacob, D. J., & Beecher, K. M. (1990). Sources and sinks of formic, acetic, and pyruvic acids over central amazonia II—Wet season. *Journal of Geophysical Research-Atmospheres, 95*(D10), 16799–16811.

Tanimoto, H., Aoki, N., Inomata, S., Hirokawa, J., & Sadanaga, Y. (2007). Development of a PTR-TOFMS instrument for real-time measurements of volatile organic compounds in air. *International Journal of Mass Spectrometry, 263*(1), 1–11.

Trentmann, J., Luderer, G., Winterrath, T., Fromm, M. D., Servranckx, R., Textor, C., . . . Andreae, M. O. (2006). Modeling of biomass smoke injection into the lower stratosphere by a large forest fire (Part I): Reference simulation. *Atmospheric Chemistry and Physics, 6*, 5247–5260.

Tsang, W. (1992). Chemical kinetic data-base for propellant combustion—reactions involving CN, NCO, and HNCO. *Journal of Physical and Chemical Reference Data, 21*(4), 753–791.

Tsigaridis, K., & Kanakidou, M. (2007). Secondary organic aerosol importance in the future atmosphere. *Atmospheric Environment, 41*(22), 4682–4692.

Twomey, S. (1977). Influence of pollution on shortwave albedo of clouds. [Note]. *Journal of the Atmospheric Sciences, 34*(7), 1149–1152.

Veres, P., Gilman, J. B., Roberts, J. M., Kuster, W. C., Warneke, C., Burling, I. R., & de Gouw, J. A. (2010). Development and validation of a portable gas phase standard generation and calibration system for volatile organic compounds. *Atmospheric Measurement Techniques, 3*(3), 683–691.

Veres, P., Roberts, J. M., Burling, I. R., Warneke, C., de Gouw, J. A., & Yokelson, R. J. (2010). Measurements of gas-phase inorganic and organic acids from biomass fires by negative-ion proton-transfer chemical-ionization mass spectrometry. *Journal of Geophysical Research-Atmospheres, 115*.

Veres, P. R., Roberts, J. M., Cochran, A. K., Gilman, J. B., Kuster, W. C., Holloway, J. S., . . . de Gouw, J. A. (2011). Evidence of rapid production of organic acids in an urban air mass. *Geophys. Res. Lett., 38*(17), L17807.

Veres, P. R., Roberts, J. M., Warneke, C., Welsh-Bon, D., Zahniser, M., Herndon, S., & de Gouw, J. A. (2008). Development of negative-ion proton-transfer chemical-ionization mass spectrometry (NI-PT-CIMS) for the measurement of gas-phase organic acids in the atmosphere. *International Journal of Mass Spectrometry, 274*(1-3), 48–55.

Vicente, A., Alves, C., Monteiro, C., Nunes, T., Mirante, F., Evtyugina, M., . . . Pio, C. (2011). Measurement of trace gases and organic compounds in the smoke plume from a wildfire in Penedono (central Portugal). *Atmospheric Environment, 45*(29), 5172–5182.

Viidanoja, J., Reiner, T., & Arnold, F. (1998). Laboratory investigations of negative ion molecule reactions of formic and acetic acids: implications for atmospheric measurements by ion-molecule reaction mass spectrometry. *International Journal of Mass Spectrometry, 181*, 31–41.

Warneke, C., Bahreini, R., Brioude, J., Brock, C. A., de Gouw, J. A., Fahey, D. W., . . . Veres, P. (2009). Biomass burning in Siberia and Kazakhstan as an important source for haze over the Alaskan Arctic in April 2008. *Geophysical Research Letters, 36.*

Warneke, C., & de Gouw, J. A. (2001). Organic trace gas composition of the marine boundary layer over the northwest Indian Ocean in April 2000. *Atmospheric Environment, 35*(34), 5923–5933.

Warneke, C., de Gouw, J. A., Lovejoy, E. R., Murphy, P. C., Kuster, W. C., & Fall, R. (2005). Development of proton-transfer ion trap-mass spectrometry: On-line detection and identification of volatile organic compounds in air. *Journal of the American Society for Mass Spectrometry, 16*(8), 1316–1324.

Warneke, C., Kuczynski, J., Hansel, A., Jordan, A., Vogel, W., & Lindinger, W. (1996). Proton transfer reaction mass spectrometry (PTR-MS): propanol in human breath. *International Journal of Mass Spectrometry and Ion Processes, 154*(1-2), 61–70.

Warner, J. (1969). Microstructure of cumulus cloud II. Effect on droplet size distribution of cloud nucleus spectrum and updraft velocity. *Journal of the Atmospheric Sciences, 26*(6), 1272–1282.

Whitaker, T. (2004). North Carolina A&T University RTOF-300 Reflectron Time-of-Flight Mass Spectrometer. *Atom Sciences, Instrumentation Manual*.

Wight, C. A., & Beauchamp, J. L. (1980). Acidity, basicity, and ion-molecule reactions of isocyanic acid in the gas-phase by ion-cyclotron resonance spectroscopy. *Journal of Physical Chemistry, 84*(20), 2503–2506.

Yang, L. M., Ray, M. B., & Yu, L. E. (2008). Photooxidation of dicarboxylic acids, Part II: Kinetics, intermediates and field observations. *Atmospheric Environment, 42*(5), 868–880.

Zhao, Y. G., Hu, J., Hua, L., Shuai, S. J., & Wang, J. X. (2011). Ammonia Storage and Slip in a Urea Selective Catalytic Reduction Catalyst under Steady and Transient Conditions. *Industrial & Engineering Chemistry Research, 50*(21), 11863–11871.

Appendix A

FORTRAN Code Definitions of Cloud Model Species Calculated

H2O = water vapor
O3 = ozone
HO = hydroxyl radical
2011 = methyl peroxy radical = CH3O2
CH2O = formaldehyde
NO = nitric acid
HNO3 = nitric acid
NO3 = nitrate radical

H2 = hydrogen
H2O2 = hydrogen peroxide
HO2 = hydro peroxy radical
h011 = methyl hydroperoxide (CH3OOH)
a011 = formic acid = HCOOH
NO2 = nitrogen dioxide
N2O5 = dinitrogen pentaoxide
CO2 = carbon dioxide

Appendix B

Heterogeneous Uptake, Dissociation, and Hydrolysis of HNCO

$$[HNCO]_{(g)} \rightleftarrows [HNCO]_{(aq)}$$

$$[HNCO]_{(aq)} \rightleftarrows H_3O^+ + NCO^-$$

$$K_{eq} = \frac{[H^+][NCO^-]}{[HNCO\_aq]}$$

$$HNCO + H_2O \Rightarrow NH_3 + CO_2$$
$$HNCO + H_3O^+ \Rightarrow NH_4{}^+ + CO_2$$
$$NCO^- + 2H_2O \Rightarrow NH_3 + HCO_3^-$$

Appendix C

Calculation of the Aqueous-phase Reaction Rate Expression for HNCO Family

$$[HNCO\_aqfam] = [HNCO\_aq] + [NCO^-]$$

$$f\_HNCO = \frac{[HNCO\_aq]}{[HNCO\_aqfam]}$$

$$f\_NCO^- = \frac{[NCO^-]}{[HNCO\_aqfam]}$$

$$[NCO^-] = \frac{K_{eq}[HNCO\_aq]}{[H^+]}$$

$$[HNCO\_aqfam] = [HNCO\_aq] + \frac{K_{eq}[HNCO\_aq]}{[H^+]}$$

$$f\_HNCO = \frac{[HNCO\_aq]}{[HNCO\_aq] + \dfrac{K_{eq}[HNCO\_aq]}{[H^+]}} = \frac{1}{1 + \dfrac{K_{eq}}{[H^+]}} = \frac{[H^+]}{[H^+] + K_{eq}}$$

$$f\_NCO^- = \frac{\dfrac{K_{eq}[HNCO\_aq]}{[H^+]}}{[HNCO\_aqfam]} = \frac{\dfrac{K_{eq}[HNCO\_aq]}{[H^+]}}{[HNCO\_aq] + \dfrac{K_{eq}[HNCO\_aq]}{[H^+]}} = \frac{\dfrac{K_{eq}}{[H^+]}}{1 + \dfrac{K_{eq}}{[H^+]}} = \frac{K_{eq}}{[H^+] + K_{eq}}$$

$$\frac{d[HNCO\_aqfam]}{dt} = -k_1[HNCO\_aq] - k_2[HNCO\_aq][H^+] - k_3[NCO^-]$$

$$= -k_1\frac{[H^+]}{[H^+] + K_{eq}}[HNCO\_aqfam] - k_2\frac{[H^+]}{[H^+] + K_{eq}}[HNCO\_aqfam][H^+] - k_3\frac{K_{eq}}{[H^+] + K_{eq}}[HNCO\_aqfam]$$

Appendix D

FORTRAN Code Calculating HNCO Aqueous-phase Hydrolysis

```
c tony
c HNCO_aqfam
          if (iwhich(it) .eq. 16) then
           do i=1,iend
            k1 =7.8E-04
            k2 =6.0E-02
            k3 =5.5E-09
            Keq = 2.0E-04
            f_HNCO = 1./(1.+(Keq/hion))
            f_NCOM = Keq/(hion+Keq)
             rk = k1*f_HNCO + k2*f_HNCO*hion + k3*f_NCOM
            rate(i,j,k,ir)= rk
           end do
          endif
```

Appendix E

Charge Balance Equation Definitions of Terms

$$K_{NH_4^+} = \frac{[NH_3(aq)][H^+]}{[NH_4^+]}$$

$$[NH_3(aq)] = H_{NH_3}[NH_3(g)]$$

$$[NH_4^+] = \frac{H_{NH_3}[NH_3(g)][H^+]}{K_{NH_4^+}}$$

$$K_{H_2SO_4} = \frac{[SO_4(aq)]2[H^+]}{[H_2SO_4]}$$

$$[H_2SO_4(aq)] = H_{H_2SO_4}[H_2SO_4(g)]$$

$$[SO_4^{2-}] = \frac{K_{H_2SO_4}H_{H_2SO_4}[H_2SO_4(g)][H^+]}{2[H^+]}$$

$$K_{SO_2} = \frac{[HSO_3^-][H^+]}{[SO_2(aq)]}$$

$$[SO_2(aq)] = H_{SO_2}[SO_2(g)]$$

$$[HSO_3^-] = \frac{K_{SO_2}H_{SO_2}[SO_2(g)]}{[H^+]}$$

$$K_{HSO_3^-} = \frac{[SO_3^{2-}][H^+]}{[HSO_3^-(aq)]}$$

$$[HSO_3^-(aq)] = \frac{K_{SO_2}[SO_2(aq)]}{[H^+]}$$

$$[SO_3^{2-}] = \frac{K_{HSO_3^-}K_{SO_2}[SO_2(aq)]}{[H^+][H^+]} = \frac{K_{HSO_3^-}K_{SO_2}H_{SO_2}[SO_2(g)]}{[H^+]^2}$$

$$K_{HNCO} = \frac{[NCO^-][H^+]}{[HNCO(aq)]}$$

$$[HNCO(aq)] = H_{HNCO}[HNCO(g)]$$

$$[NCO^-] = \frac{K_{HNCO}H_{HNCO}[HNCO(g)]}{[H^+]}$$

$$K_{CO_2} = \frac{[HCO_3^-][H^+]}{[CO_2(aq)]}$$

$$[CO_2(aq)] = H_{CO_2}[CO_2(g)]$$

$$[HCO_3^-] = \frac{K_{CO_2}H_{CO_2}[CO_2(g)]}{[H^+]}$$

$$[OH^-] = H_{OH}[OH^-(g)]$$

$$K_{HO_2} = \frac{[O_2^-][H^+]}{[HO_2(aq)]}$$

$$[HO_2(aq)] = H_{HO_2}[HO_2(g)]$$

$$[O_2^-] = \frac{K_{HO_2} H_{HO_2}[HO_2(g)]}{[H^+]}$$

$$K_{H_2O_2} = \frac{[O_2^-][H^+]}{[H_2O_2(aq)]}$$

$$[H_2O_2(aq)] = H_{H_2O_2}[H_2O_2(g)]$$

$$[HO_2^-] = \frac{K_{H_2O_2} H_{H_2O_2}[H_2O_2(g)]}{[H^+]}$$

$$K_{HCO_3^-} = \frac{[CO_3^{2-}][H^+]}{[HCO_3^-(aq)]}$$

$$[HCO_3^-(aq)] = \frac{K_{CO_2} H_{CO_2}[CO_2(g)]}{[H^+]}$$

$$2[CO_3^-] = \frac{K_{HCO_3^-} K_{CO_2} H_{CO_2}[CO_2(g)]}{[H^+]^2}$$

$$K_{CO_2} = \frac{[HCO_3^-][H^+]}{[CO_2(aq)]}$$

$$[CO_2(aq)] = H_{CO_2}[CO_2(g)]$$

$$[HCO_3^-] = \frac{K_{CO_2} H_{CO_2}[CO_2(g)]}{[H^+]}$$

$$K_{formic} = \frac{[HCO_3^-][H^+]}{[CO_2(aq)]}$$

$$[CO_2(aq)] = H_{CO_2}[CO_2(g)]$$

$$[HCOO^-] = \frac{K_{CO_2} H_{CO_2}[CO_2(g)]}{[H^+]}$$

Appendix F

Dynamic pH Calculation FORTRAN Code

```
subroutine getaqph(t, aspec, ph, qca, rhoair)
   implicit none
   include ‘chem_params.inc’

c Input parameters
   real t            ! temperature (K)
   real qca               ! CW mixing ratio (g/kg)
   real aspec(naq)        ! (molec/cm3)
   real ahion, hion
   real na                !Avogadro’s#
   real lwc               ! liquid water content (cm3 H2O / cm3 air)
   real rhoair            ! density of water kg/cm3
   real fact             !temperature correction factor

c Output parameter
   real ph

c aqueous concentrations
   real nh4p, so4a, hncoa, hso4a, hso2a, so2a, co2a, co3a, hco3a,
  _ho2a, h2o2a, hcooa, oha, o2a, no3a, hso3a, so3a, hno2a, hno3a

c missing types from chems_params.inc for aspec()
   real kso3a, khco3a, kco3a, khso3a, ko2a, kso2a

c dissociation constants
   real dso4a, diso, dh2so4, dhnh3, dhso4m, dhso3m, dw, dso2, dco2,
  _ dho2, dh2o2, dh2co3, dhco3m, dhno2, dhcooh, dh2so3, dhno3,
  _ dnh3

c Fractions
   real f_ncom    ! fraction of HNCO(a) + HNCO- that is NCO- in terms of [H!+]
   real f_nh4p, f_hso4m, f_so4m, f_hso3m, f_so3m, f_hco3m, f_co3m,
  _f_ohm, f_o2m, f_ho2m,  f_no2m, f_no3m, faa, f_hcoom

c because these fractions depend on H+, the calculation will be iterated
c  to determine H+ and pH
   if(qca .lt. 1.e-12) return
   na = 6.022e23

c Aqueous family concentrations
c Static concentrations and converted concentrations molecules/cm^3 to mol/L (M)
   lwc = rhoair*qca * 1.e-6            !1.e-6 converts g H2O to m3 H2O

   so4a = 6.1E-9                    !already in mol/L (M) about 100ppb
   hso3a = 1.0E-7                     !From S and Pandis graph  (too high?  about 10ppm?)
   hncoa = aspec(khncoa)  *1000./ (na * lwc)
```

```
      co2a = aspec(kco2a) *1000./ (na * lwc)
      oha = aspec(koha)  *1000./ (na * lwc)
      ho2a = aspec(kho2a) *1000./ (na * lwc)
c      o2a = aspec(ko2a)  *1000./ (na * lwc)
      h2o2a = aspec(kh2o2a)  *1000./ (na * lwc)
c      co3a = aspec(kco3a)  *1000./ (na * lwc)
      hno2a = aspec(kno2a)  *1000./ (na * lwc)
      hcooa = aspec(kfaa)  *1000./ (na * lwc)
c      hco3a = aspec(khco3a)  *1000./ (na * lwc)
      hno3a = aspec(khno3a)*1000./ (na * lwc)
c ----------------------------------------------------------------------
      write(*,’(1p,(8e12.4))’) aspec(khncoa)
      write(*,’(1p,(8e12.4))’) hion, ahion, hncoa

c use initial guess of pH for this case
c      if(so4a.eq.0. .and. hncoa .eq.0.) return
      if (hno3a.eq.0.) return
c Dissociation constants
      fact = (1./t) - 1./298.        !temperature correction
c using prefix “d” to denote dissociation constant to distinguish from “k” terms in chems_params.inc
c      dh2so4 = 1.e3*exp(0.*fact)  !same as SO3*H2O <-> H+ + HSO4-
c      dhso4m = 1.e-2*exp(2720.*fact)
c      dh2so3 = 1.3e-2*exp(1960.*fact)
c      dhso3m = 6.6e-8*exp(1500.*fact)
      diso = 3.47e-4*exp(-1510.*fact)   !Renamed HNCO dissociation constant since khnco exists in chems
      dw = 1.e-14*exp(-6710.*fact)
      dho2 = 3.5e-5*exp(0.*fact)
      dh2o2 = 2.2e-12*exp(-3730.*fact)
      dh2co3 = 4.35e-7*exp(0.*fact)     !coefficient not found yet
      dhco3m = 4.69e-11*exp(-1760.*fact)
      dhno2 = 6.92e-4*exp(6.7*fact)         !from pKa 3.16 da Silva et al.
      dhcooh = 1.8e-4*exp(-1510.*fact)  !-20 (ref. Pandis table vs. -1500 in original code
      dnh3 = 1.7e-5*exp(-450.*fact)         !Barth et al 2006
      dhno3 = 15.4*exp(0.*fact)         !Barth et al 2006

  5   continue
      hion = 10.**(-ph)

c Local fractions defined
c      f_nh4p=dnh3/(hion+dnh3)
c      f_hso4m=1/(hion/dh2so4 + 1. + dhso4m/hion)
c      f_so4m = 1./((hion*hion/dh2so4*dhso4m) + (hion/dhso4m) + 1.)
c      f_hso3m = 1./((hion/dh2so3) + 1. + (dhso3m/hion))
c      f_so3m = 1./((hion*hion/dh2so3*dhso3m) + (hion/dhso3m) +1. )
      f_hco3m = 1./((hion/dh2co3) + 1. + (dhco3m/hion))
      f_co3m = 1./((hion*hion/dh2co3*dhco3m) + (hion/dhco3m) + 1.)
      f_ncom = diso/(hion + diso)
      f_ohm = dw/(hion + dw)
      f_o2m = dho2/(hion + dho2)
      f_ho2m = dh2o2/(hion + dh2o2)
      f_no2m = dhno2/(hion + dhno2)
```

```
      f_hcoom = dhcooh/(hion + dhcooh)
      f_no3m = dhno3/(hion + dhno3)

c Full case [H+] = -[NH4+] + [HSO4-] + 2[SO4=] + [HSO3-] + 2[SO3=] + [HCO3-]+ 2[CO3=] + c
            [NCO-] + [OH-] + [O2-] + [HO2-] + [NO2-] + [HCOO-]+ [NO3-]

cq assume NH4+ = SO4=  (i.e. sulfate aerosol is NH4HSO4)
c assume Na+ = Cl-    (i.e. NaCl aerosol)
c assume HSO3- dominates S(IV) (which it does for pH of most cloudwater)
c
c assume aspec(kso4)  = SO4= entirely (all SO4 is in drops)
c        aspec(khno3a) = NO3- (all HNO3 in drops is NO3- and not HNO3(a))
c other species gotten by dissociation equilibrium:
c aspec(kso2) = concentration of S(IV) family, so HSO3- = f_hso3 * aspec(kso2)
c  where f_hso3 = HSO3/S(IV)  =  K1*H+ / (H+*H+ + K1*H+ + K1*K2)
c aspec(kfa) = concen of HCOOH(a) + HCOO-, so HCOO- = f_fo * aspec(kfa)
c  where f_fo = K1/(H+ + K1)
c NEED TO ADD so4 and so3a and fractions
c Full case [H+] = [HSO4-] + [SO4=] + [HSO3-] + 2[SO3=] + [HCO3-]+ 2[CO3=] +
c                        [NCO-] + [OH-] + [O2-] + [HO2-] + [NO2-] + [HCOO-]+ [NO3-]

c Full case [H+] = [SO4=] + [HSO3-] + [HCO3-]+ 2[CO3=] +
c                        [NCO-] + [OH-] + [O2-] + [HO2-] + [NO2-] + [HCOO-]+ [NO3-]

c      ahion = f_hso4m*so3a + f_so4m*so3a +f_hso3m*so2a + f_so3m*so2a +
      ahion = so4a + hso3a + .
     _f_hco3m*co2a + 2.*f_co3m*co2a + f_ncom*hncoa + f_ohm*koha +
c      ahion = f_hco3m*co2a + 2.*f_co3m*co2a + f_ncom*hncoa + f_ohm*koha +
     _f_o2m*ho2a + f_ho2m*h2o2a + f_hcoom*hcooa +
     _f_no3m*hno3a

      ph = -alog10(ahion)

      if(ph .lt. 0. .or. ph .gt. 10.) then
       write(*,*) ‘pH = ‘, ph, ‘ stopping program’
       write(*,’(1p,(8e12.4))’) ahion, so4a, hso3a, f_ncom*hncoa,
     _ f_hco3m*co2a, f_ohm*koha,
     _ f_o2m*ho2a, f_ho2m*h2o2a, f_co3m*co2a,
     _ f_hcoom*hcooa, f_no3m*hno3a
       stop
      endif
      if(abs(hion-ahion) .gt. 0.001*hion) go to 5
      write(*,*) ‘pH = ‘, ph
      write(*,’(1p,(8e12.4))’) ahion, so4a, hso3a, f_ncom*hncoa,
     _ f_hco3m*co2a, f_ohm*koha,
     _ f_o2m*ho2a, f_ho2m*h2o2a, f_co3m*co2a,
     _ f_hcoom*hcooa, f_no3m*hno3a

      return
        end
```